THE MECHANISM OF NUCLEATE POOL BOILING HEAT TRANSFER TO SODIUM AND THE CRITERION FOR STABLE BOILING

Isaac Shai

January 1967

DSR 76303-45

Engineering Projects Laboratory
Department of Mechanical Engineering
Massachusetts Institute of Technology

Contract No. AT(30-1)3357,A/3

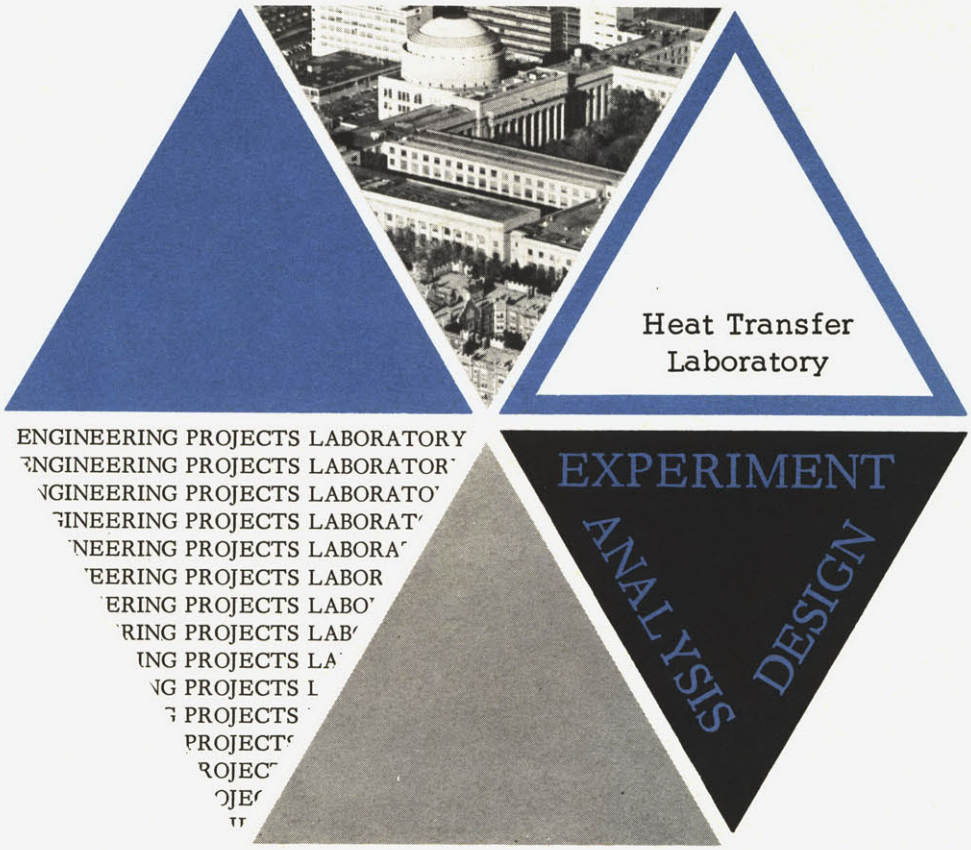

DSR 76303-45

MECHANISM OF NUCLEATE POOL BOILING HEAT TRANSFER TO SODIUM AND THE CRITERION FOR STABLE BOILING

Isaac Shai

Atomic Energy Commission
Contract AT(30-1)3357, A/3

ABSTRACT

A comparison between liquid metals and other common fluids, like water, is made as regards to the various stages of nucleate pool boiling. It is suggested that for liquid metals the stage of building the thermal layer plays the most significant part in transfer heat from the solid. On this basis the transient conduction heat transfer is solved for a periodic process, and the period time is found to be a function of the degree of superheat, the heat flux, and the liquid thermal properties.

A simplified model for stability of nucleate pool boiling of liquid metals has been postulated from which the minimum heat flux for stable boiling can be found as a function of liquid-solid properties, liquid pressure, the degree of superheat, and the cavity radius and depth.

Experimental tests with sodium boiling from horizontal surfaces containing artificial cavities at heat fluxes of 20,000 to 300,000 BTU/ft^{2}hr and pressures between 40 to 106 mm Hg were obtained.

At relatively low heat fluxes, convection currents have significant effects on the period time of bubble formation. An empirical correlation is proposed, which takes into account the convection effects, to match the experimental results.

Some recorded temperature variations in the solid close to the surface during stable nucleate boiling are presented.

TABLE OF CONTENTS

LIST OF FIGURES

NOMENCLATURE

a	constant in Equation (1)
A	constant in Equation (C-4)
b	constant in Equation (1)
b^*	empirical constant in Equation (22)
B	constant in Equation (C-4)
c	constant in Equation (1)
c	specific heat
c_1, c_2	constants in Equation (A-8a)
c_3, c_4	constants in Equation (A-8b)
g	gravity acceleration
h	empirical constant in Equation (30)
h_{fg}	latent heat of vaporization
I	function of β, Equation (12)
J	function of β, Equation (14)
k	thermal conductivity
K	function of β, Equation (21)
ℓ	cavity depth
L	relaxation length
M	molecular weight
n	positive integer
p	pressure
p_{vr}	vapor pressure in equilibrium with the liquid along curvature interface

q	Laplace variable defined by Equation (A-12)
q	instantaneous heat flux at the solid-liquid interface
q_o	average heat transfer per unit area per unit time
r	cavity radius
R	bubble radius
$\dot{R}$	rate of bubble growth
s	complex Laplace variable
t	time
T	absolute temperature
$T_{w\ ext.}$	extrapolated wall temperature
x	axial position in the boiler plate
y	axial position in the liquid
Y	dimensionless parameter, Equation (D-5)
Z	dimensionless variable, Equation (16)
Z_o	dimensionless parameter, Equation (E-5)
α	thermal diffusivity
β	ratio of thermal properties, Equation (A-12)
β^*	parameter in Equation (D-1)
γ	ratio of thermal properties, Equation (A-12)
ϵ	ratio of thermal properties, Equation (A-12)
φ	dimensionless time, Equation (17)
η	dimensionless critical distance, Equation (23)
θ	$(T - T_{sat})$
$\theta_w(0,0)$	the maximum surface temperature difference before bubble grows

$\theta_w'(0,0)$	the temperature gradient at the surface before bubble grows
$\theta_w''(0)$	the second derivative of temperature with respect to position, before bubble grows (not function of position)
μ	dynamic viscosity
ρ	density
σ	surface tension
C^*	coefficient in Equation (D-4)
τ	the waiting time
τ^*	dimensionless time, Equation (D-6)
φ	contact angle
$\phi(\beta^*)$	a function defined by Equation (D-1)

Subscripts

cr	the critical position and time for which the minimum temperature is equal to $\theta_w(0,0)$
d	condition at bubble departure
ℓ	liquid
sat	saturation conditions at the liquid pressure
v	vapor
w	boiler plate

1. INTRODUCTION

The study of heat transfer in pool boiling was primarily performed with non-metallic fluids.

In recent years with the developments of nuclear reactors, the application of liquid metals as a coolant has become important because of their high boiling point. Although none of the designed reactors are based on boiling liquid metals, it is of interest to consider the conditions of boiling in the case of loss of coolant during regular operation.

In previous works of pool boiling with liquid metals (1), (2), (3), (4), (5), and others, it was found that during boiling there exist significant temperature fluctuations close to the heating surface. At low pressures of the order of 1 psi and at heat fluxes below 100,000 BTU/ft^{2}hr, these fluctuations were not regular and were accompanied by a big audible "bump." Also, the data obtained were quite scattered. Noyes (3), Marto (5), and others concluded that these scattering in the data are due to the effects of the conditions of the heating surface.

Using the fluid properties, Krakoviak (6) theoretically explained why such "bumps" should be expected. Recently, Marto (5) established a criterion combining the properties of the liquid and boiler material (including cavity size) which predicts which surface fluid combination at a given heat flux and pressure will have stable nucleate boiling. His criterion is based on the mechanism of heat transfer to a growing

bubble and the surface behaviour suggested for water by Moore (7) and Bonnet (8).

In non-metallic fluids there exist two basic hypothesis for the mechanism of heat transfer in nucleate pool boiling:

I. The mechanism of a microlayer of superheated liquid at the base of a growing bubble evaporates with heat fluxes from the metal surface higher than the average heat flux. (7) (8), (9)

II. The mechanism of builing a thermal layer by transient conduction heat transfer which transfers heat to the growing bubble. The thermal layer is carried away from the surface after the bubble departure. In this mechanism high heat fluxes from the solid surface exist when the thermal layer is built. (10), (11)

The recent work of Cooper (9) with toluene boiling on glass shows that probably the two mechanisms co-exist. The combined properties of the fluid and the solid will determine which one of the two mechanisms plays the most significant role in each case.

The purpose of the present work is to establish the dominant mechanism of heat transfer in nucleate pool boiling with alkali metals, in particular sodium, based on theoretical analysis and experimental results. After the mechanism of heat transfer has been established, a model for the behaviour of an active cavity can be adopted. From this model a criterion is developed combining all the important parameters of the liquid-solid combination. This criterion predicts the minimum heat flux for stable boiling under the operating conditions.

2. MECHANISM OF POOL BOILING

2.1 Introduction

By nature nucleate pool boiling is a nonequilibrium phenomena, where a heated solid transfers heat to the fluid adjacent to the surface and forms bubbles from active cavities. In spite of the nonequilibrium, it is possible to consider a quasi-steady state process when the formation of bubbles and their departure occur in a periodic fashion. The exact details of each part of a full cycle are quite complicated, but it has become common to divide the full cycle into several distinct stages.

I. Building a superheated thermal layer in the liquid near the heated surface

II. Establishing the conditions for bubble growth from an active cavity in thermal and mechanical equilibrium.

III. Bubble growth.

IV. Bubble departure accompanied by a removal of the thermal layer.

The cycle is repeated when cold liquid comes in contact with the solid surface.

Although the various stages are interrelated, it is worthwhile to analyze each one separately to discover the main factors governing each part.

2.2 The Various Stages of Nucleate Pool Boiling

2.2.1 Thermal Layer

The creation of a thermal layer in the liquid is a process of transient conduction heat transfer, when two bodies initially at different temperatures are brought in contact. The time required to build

the thermal layer and the temperature history of the two bodies are functions of the physical properties of both the fluid and the solid as well as the solid surface conditions, the fluid pressure, and the average heat flux transferred from the solid. More detail analysis is given in (2.3).

2.2.2 Initiation of Bubble Growth

A bubble starts to grow from an active cavity, which is a cavity filled with vapor or gas. In this state the new born bubble is in thermodynamic and mechanical equilibrium with the superheated liquid adjacent to the surface. The degree of superheat is a function of the cavity mouth size as well as the fluid pressure and properties. The mathematical formulation of the superheat is given in Appendix C.

2.2.3 Bubble Growth

This part is the most complicated one, since the shape of the growing bubble is not well defined; furthermore, the temperature and the pressure fields around the bubble are not simple.

In order to analyze this stage, several models were adopted, most of which consider a spherical bubble.

One common model considers the growth of a bubble by heat conduction from the thermal layer around the growing bubble and evaporation taking place in the interface between the liquid and the vapor. (11)(12)

More recently the experiments of Moore and Mesler (7), Bonnet, et al., (8), Cooper and Lloyd (9), and others show that a more important factor in bubble growth may be the evaporation of a superheated microlayer which is formed between the solid surface and the growing bubble.

This process is accompanied by a large temperature drop in the solid surface and a quick recovery when the surface dries out. It is visualized that as the bubble grows rapidly the viscous effects very near the solid surface cause this small layer of liquid to be left on the surface under the bubble. The rate of growth of a bubble in one component liquid is controlled by three different mechanisms acting simultaneously, which are as follows: The inertia of the displaced liquid, the heat conduction in the liquid, and the rate of vaporization in the interface. Which one of these will provide the greatest resistance for growth rate will depend on the properties of the liquid, its pressure, and the degree of superheat.

2.2.4 Bubble Departure

The bubble will depart from the surface when the bouyancy force will overcome the surface tension force and the inertia force due to the resistance of flow which in turn is related to the rate of growth. (13)

2.2.5 The Various Stages as Regards to Liquid Metals

As was emphasized before, in all the above-mentioned stages, the physical properties of the liquid are very important. In comparison with common liquids, for example water, liquid metals have much greater thermal conductivity. It therefore would not be surprising to obtain quite different behaviour of liquid metals during the various stages of pool boiling.

First, the degree of superheat will be much greater in liquid metals than in water for the same pressure and cavity size. This can be easily seen from Equation (C-13) of Appendix C, since the degree of superheat

is the function of the absolute boiling temperature squared, and these values are much higher in liquid metals than in any common liquids.

Second, for the same cavity size, pressure, and heat flux, the time required to build the thermal layer as well as its thickness will be much greater in liquid metals than in other liquids.

Third, the rate of bubble growth in liquid metals will be mostly controlled by the inertia terms and vaporization rates rather than by heat conduction. This provides much greater growth rates, or shorter growth time (see Appendix D). Finally, the bubble size at the departure is greater in liquid metals than in water, which means that each cavity influences a greater area.

From what has been said above, it becomes obvious that the period (or frequency) of bubble formation and departure in pool boiling of liquid metals will be almost solely controlled by the first stage of boiling, namely, the formation of a thermal layer. In this stage most of the heat is transferred from the solid to the liquid, and, therefore, a more detailed analysis of this part of the boiling will provide the necessary information to understand the behaviour of liquid metals boiling.

2.3 Detailed Analysis on the Formation of Thermal Layer

2.3.1 Remarks

In general, any heating surface consists of randomly distributed cavities of various sizes, which make any treatment a two-dimensional one. To simplify the problem, we assume that heat conduction in the liquid that flows to the heating after bubbles leave can be treated as a one-dimensional problem.

The recent work of Copper (9) for boiling toluene on glass shows that the surface temperature drops twice in a boiling cycle. The first temperature drop, Figure 1, is due to evaporation taking place from a superheated microlayer during bubble growth, and the second temperature drop is due to cold liquid coming to the surface after bubble departure. As discussed in paragraph 2.2.5, the time for bubble growth and departure in liquid metal is very short compared with the waiting time before the next bubble forms. We shall therefore consider here only the effect of cold liquid coming to the surface and ignore completely any effects during bubble growth. This means that the temperature profile in the solid before the bubble starts to grow is the same as after bubble departure and cold liquid comes to the surface.

2.3.2 Mathematical Formulation

After a bubble and its influenced thermal layer have left the surface, cold liquid at saturation temperature comes in contact with the solid surface. To solve the transient heat conduction, we shall use the following assumptions:

I. The problem is one dimensional.

II. The liquid is semi-infinite and stagnant.

III. Constant liquid and solid properties.

IV. No interfacial thermal resistance between the solid and the liquid.

V. The liquid is at saturation temperature.

VI. The temperature profile in the solid is a parabolic function up to a certain length (X = L) from the surface, where the temperature gradient becomes equal to the average gradient

during a full cycle. Beyond this point the gradient is constant with time and position. (See Figure 2.)

The implication of assumption VI is:

$$\theta_\omega(x,0) = a + bx + cx^2 \qquad 0 \leq x \leq L \tag{1}$$

where $$\theta = T - T_{sat.} \tag{2}$$

$$\left.\begin{aligned} a &= \theta_\omega(0,0) \\ b &= \theta_\omega'(0,0) \\ c &= \frac{\theta_\omega''(0)}{2} \end{aligned}\right\} \tag{3}$$

and

$$\frac{\partial \theta_\omega(L,0)}{\partial x} = \frac{q_o}{k_\omega} = \text{constant} \tag{4}$$

also $\theta_\omega'(x,0) = b + 2cx$. Set $x = L$ and with Equations (3) and (4) find

$$L = \frac{q_o/k_\omega - \theta_\omega'(0,0)}{\theta_\omega''(0)} \quad . \tag{5}$$

The energy equations for the solid and the liquid:

$$\frac{\partial^2 \theta_\omega}{\partial x^2} = \frac{1}{\alpha_\omega} \frac{\partial \theta_\omega}{\partial t} \tag{6a}$$

$$\frac{\partial^2 \theta_\ell}{\partial y^2} = \frac{1}{\alpha_\ell} \frac{\partial \theta_\ell}{\partial t} \tag{6b}$$

with the initial conditions at t = 0

$$0 \leq x \leq L \qquad \theta_\omega(x,0) = \theta_\omega(0,0) + \theta_\omega'(0,0)x + \theta_\omega''(0)\frac{x^2}{2} \tag{7a}$$

$$0 \leq y \qquad \theta_\ell(y,0) = 0 \tag{7b}$$

and the boundary conditions

$$t>0\,, \quad x=L \qquad k_\omega \frac{\partial \theta_\omega(L,t)}{\partial x} = q_o = \text{constant} \tag{8a}$$

$$y \to \infty \qquad \theta_\ell(\infty,t) = 0 \tag{8b}$$

$$t>0\,, \quad x=0\,, \quad y=0$$

$$\theta_\ell(0,t) = \theta_\omega(0,t) \tag{9a}$$

$$-k_\ell \frac{\partial \theta_\ell(0,t)}{\partial y} = k_\omega \frac{\partial \theta_\omega(0,t)}{\partial x} \tag{9b}$$

By solving simultaneously Equations (6) with the initial and boundary conditions, and using the Laplace transformation, we find the temperature history in the liquid and in the solid. Full solution is given in Appendix A.

The simplified solutions (A-16c and (A-16d) are given below:

$$\theta_\omega(x,t) = \theta_\omega(x,0) + \alpha_\omega t\, \theta_\omega''(0) - \frac{\theta_\omega(0,0)}{1+\beta} \operatorname{erfc}\left(\frac{x}{2\sqrt{\alpha_\omega t}}\right) +$$

$$+ \frac{\beta\, \theta_\omega'(0,0)}{1+\beta}\left[2\sqrt{\frac{\alpha_\omega t}{\pi}}\, e^{-\frac{x^2}{4\alpha_\omega t}} - x \operatorname{erfc}\left(\frac{x}{2\sqrt{\alpha_\omega t}}\right)\right] +$$

$$+ \frac{\alpha_\omega\, \theta_\omega''(0)}{1+\beta}\left[x\sqrt{\frac{t}{\pi\alpha_\omega}}\, e^{-\frac{x^2}{4\alpha_\omega t}} - \left(t + \frac{x^2}{2\alpha_\omega}\right)\operatorname{erfc}\left(\frac{x}{2\sqrt{\alpha_\omega t}}\right)\right] \tag{10a}$$

$$\theta_\ell(y,t) = \frac{\beta}{1+\beta}\left\{\theta_\omega(0,0)\operatorname{erfc}\left(\frac{y}{2\sqrt{\alpha_\ell t}}\right) + \theta_\omega'(0,0)\left[2\sqrt{\frac{\alpha_\omega t}{\pi}}\, e^{-\frac{y^2}{4\alpha_\ell t}} - \gamma y \operatorname{erfc}\left(\frac{y}{2\sqrt{\alpha_\ell t}}\right)\right] +\right.$$

$$\left. + \alpha_\omega \theta_\omega''(0)\left[\left(t + \frac{y^2}{2\alpha_\ell}\right)\operatorname{erfc}\left(\frac{y}{2\sqrt{\alpha_\ell t}}\right) - y\sqrt{\frac{t}{\pi\alpha_\ell}}\, e^{-\frac{y^2}{4\alpha_\ell t}}\right]\right\} \tag{10b}$$

These solutions contain three undetermined terms as $\theta_\omega(0,0)$, $\theta_\omega'(0,0)$, and $\theta_\omega''(0)$. It will be shown in Appendix C that $\theta_\omega(0,0)$ is a function of the cavity size and the pressure only. The other two terms will be evaluated in Appendix B by using the conditions of a periodic process.

2.3.3 Periodic Behaviour of the Phenomena

As was mentioned before, stable boiling is a quasi-steady state process in which all the temperature variations occur in a periodic way within the relaxation length L. This cycling behaviour requires that the temperatures and the temperature gradients will be the same after each full cycle. Furthermore, the average heat flux at the surface must be equal to the constant heat flux far away from the surface where no variations of temperature occur during the cycle.

Applying these three requirements to the temperature distribution in the solid (Equation 10a) will give us the periodic time $\mathcal{T}$ as a function of measurable values. (See Appendix B.)

$$\sqrt{\mathcal{T}} = \frac{\theta_\omega(0,0)\sqrt{k_\ell \rho_\ell c_\ell}}{q_0} I(\beta) \tag{11}$$

where $$I(\beta) = \frac{6\pi + 6\pi\beta^2 + 7\pi\beta + 16\beta}{3\sqrt{\pi}(1+\beta)(\pi\beta+4)} \tag{12}$$

The time $\mathcal{T}$ is, in general, the waiting time required to build the thermal layer. Since $I(\beta)$ is not a strong function of properties (see Table 1), this time is a function of the liquid properties as well as the cavity geometry, the heat flux, and the pressure and almost

independent of solid physical properties. In the case of liquid metals, this time is much longer than the bubble growth time; therefore, it is the period time for bubble formation.

Equation (11) can be easily tested by varying one or more of its parameters. For example, one can use a given cavity size and vary the pressure while the heat flux is kept constant or alternatively vary the heat flux while the pressure is kept constant. Moreover, different cavity sizes can be used together with variation in pressures and heat fluxes.

Another quantity can be derived from the analysis of transient heat conduction together with the cycling behaviour. This quantity is the relaxation length L within which the temperature variations occur and beyond which the temperature profile remains unaltered during all the stages of stable boiling.

Using Equations (B-7), (B-8), and (B-10) in the definition of L Equation (5), we find

$$L = \frac{q_o/k_\omega - \theta_\omega'(0,0)}{\theta_\omega''(0)} = \sqrt{\alpha_\omega \tau}\, J(\beta) \tag{13}$$

where $$J(\beta) = \frac{3\pi\beta - 2\pi + 16}{3\sqrt{\pi}(1+\beta)(\pi-2)} \tag{14}$$

$J(\beta)$ is a very weak function of β as shown in Table 1. This value is greater than 1.55 for any β, which makes $\frac{L}{\sqrt{\alpha_\omega t}} > 1.55$ as was pointed out in Appendix A.

Rearranging Equation (13) with the help of Equation (11), we find L as a function of the degree of superheat and the heat flux

$$L = \frac{\theta_\omega(0,0)\sqrt{k_\ell \rho_\ell c_\ell \alpha_\omega}}{q_o} I(\beta) J(\beta) \tag{15}$$

Equation (15) provides some limitation on the minimum thickness of the heating solid of the pool. If the thickness of the heating solid is smaller than the calculated one from this equation, variation in temperature will occur at every point of the solid during the transient period, and the above analysis would not hold.

Finally, it is of interest to find out what kind of temperature variations should be expected at any distance within the relaxation length.

Defining now two dimensionless variables

$$Z = \frac{X}{2\sqrt{\alpha_\omega t}} \tag{16}$$

$$\varphi = \frac{t}{\tau} \tag{17}$$

then Equation (10a) can be written with the help of (B-7) and (B-8) and (7-a)

$$\theta_\omega(Z,\varphi) = \frac{\theta_\omega(0,0)}{1+\beta}\left\{1+\beta-\operatorname{erfc} Z + \frac{2(2+\beta)}{\pi\beta+4}\varphi^{1/2}\left[\sqrt{\pi}\,Z\left(\frac{1+\beta}{\beta}-\operatorname{erfc} Z\right)+e^{-Z^2}\right]+\right.$$

$$\left.+\frac{\pi-2}{\pi\beta+4}\varphi\left[\left(1+2Z^2\right)\left(1+\beta-\operatorname{erfc} Z\right)+\frac{2Z}{\sqrt{\pi}}e^{-Z^2}\right]\right\} \tag{18}$$

The maximum temperature variation will occur at the surface where $Z = 0$.

$$\theta_\omega(0,\varphi) = \frac{\beta\,\theta_\omega(0,0)}{1+\beta}\left[1+\frac{2(2+\beta)}{\beta(\pi\beta+4)}\varphi^{1/2}+\frac{\pi-2}{\pi\beta+4}\varphi\right] \tag{19}$$

Equation (19) shows that for large values of β the temperature variations at the surface will approach zero. This is the case for fluids of very low thermal conductivity in contact with solid material of high thermal conductivity. For the case of liquid metals where β is of the order of 2, we would expect large temperature variations at the surface, even at so-called stable boiling.

The variations of heat flux at the surface can also be found from Equation (10a)

$$q = k_\omega \frac{\partial \theta_\omega(0,\varphi)}{\partial X} = \frac{K q_0}{1+\beta}\left[1 + \frac{\beta(\pi\beta+4)}{\pi(2+\beta)}\varphi^{-1/2} + \frac{2\beta(\pi-2)}{\pi(2+\beta)}\varphi^{1/2}\right] \qquad (20)$$

where $$K = \frac{3\pi(1+\beta)(2+\beta)}{6\pi + 6\pi\beta^2 + 7\pi\beta + 16\beta} \qquad (21)$$

Equations (18), (19), and (20) are plotted in Figures (3) and (4), respectively.

3. STABILITY OF NUCLEATE POOL BOILING

3.1 General Considerations

Boiling from a heated surface in a pool is taking place by heterogeneous nucleation (14) from active cavities in the solid surface. Those cavities which have trapped vapor and a size corresponding to the liquid superheat are called active cavities. During the various stages of boiling, some active cavities may become de-active if all the trapped vapor condenses, and only those cavities which succeed in maintaining vapor remain active cavities. If under certain conditions all the active cavities in the surface become de-active, the boiling will stop, and the heat will transfer by natural convection only. Since the heat transfer coefficient for boiling is much higher than that for natural convection, it should be expected to have a temperature rise in the heating solid when boiling stops. This temperature rise increases the liquid superheat and might activate smaller cavities (see Equation (C-10)) which in turn when boiling resumes will re-activate even larger cavities. This phenomena causes fluctuation of temperatures between the boiling point and the natural convection point for a given heat flux, and it is called unstable boiling, or bumping.

As will be shown later, stability of boiling of ordinary fluids exists almost always. On the other hand, several investigators (2), (3), (5) have reported unstable behaviour of liquid alkali metals during boiling. Prior to these observations no one had observed these instabilities.

3.2 Stability Criterion Obtained by Marto (5)

Marto was the first who attacked analytically the stability problem. He considered the case of a right cylindrical cavity filled with vapor immediately after a bubble has departed and cold liquid comes in contact with the surface. He assumed that at that moment the surface temperature was cooled down to the coming liquid temperature. By solving the energy equation for the penetrating liquid into the cavity while condensation takes place in the liquid-vapor interface, he found the conditions when condensation will stop.

His criterion for stability states that if a cavity is deep enough, such that the penetration distance of the liquid into the cavity is smaller than the cavity depth, then the cavity will be an active cavity from which stable boiling exists. On the other hand, if the cavity depth is smaller than that distance, the cavity will be de-activated, and boiling will stop. Any re-entry type cavity will be stable because the liquid-vapor interface must pass a point of infinite radius of curvature.

Since Equation (21) of Marto (5) involves some experimental constants which were obtained with water boiling from stainless steel (15) and could not be applied to other surfaces or different liquids, it would be more convenient to re-write Marto's criterion in the following approximate form:

$$\ell > \frac{4}{\pi} \frac{(T_v - T_{sat.})^2 \sqrt{k_\ell \rho_\ell c_\ell} \sqrt{k_w \rho_w c_w}}{b^* q_o \rho_v h_{fg.} (1 + \sin \varphi)} \qquad (22)$$

where φ is the contact angle;

δ^* is an experimental value, taken as $\delta^* = 20$;

ℓ is the cavity depth.

In reaching Equation (22) Marto assumed that the surface temperature drops during evaporation taking place from a superheated microlayer, and the temperature recovery starts after the bubble leaves the surface. Recently, Cooper (9) showed that for toluene boiling on glass the surface temperature drops when the bubble grows, but the temperature recovery starts and is almost completed before the bubble leaves the surface. This means that during this time, condensation cannot take place.

A second temperature drop occurs when the cold liquid comes in contact with the surface, (See Figure (1)). In this second temperature drop, the surface temperature does not drop down as low as the saturation temperature (see Equation (19)), and, therefore, the rate of condensation will be much smaller than is considered in Marto's analysis. Furthermore, as is shown by Kroger (16) a thermal resistance to condensation plays a significant role in liquid metals which tends to reduce further the rate of condensation, or the penetrating distance by the liquid.

3.3 A New Criterion for Stable Boiling of Alkali Metals

This criterion analysis is based on the model adopted in Chapter 2.

We shall consider a cylindrical cavity of radius-to-length ratio, such that the resistance to heat transfer radially in the cavity will be an order of magnitude smaller than the resistance to heat transfer

in the solid along the cavity, or $\ell \geqslant 10$ r for liquid metals. This choice of cavity geometry allows us to assume that the liquid temperature distribution in the cavity is the same as the temperature distribution in the cavity walls. The liquid temperature in the cavity is therefore given by Equation (18), which describes the temperature variation in the solid at any distance from the surface during the waiting time. At the same time the vapor temperature in the cavity is kept constant at $T_v = T_w$ (0, 0), Appendix C. Here T_v is the saturation temperature corresponding to p_v in the cavity.

As long as the liquid temperature at the liquid-vapor interface will be below the vapor temperature, condensation of vapor will proceed, and the liquid-vapor interface will penetrate into the cavity. The condensation will stop when the liquid temperature at the interface reaches the vapor temperature, T_v.

From this consideration it follows that the condensation will stop after the liquid travels a distance X_{cr} from the solid surface if during the waiting time, the minimum temperature at that point will be equal to the vapor temperature.

By equating to zero, the derivitive of Equation (10a) with respect to time, we get a relation between the distance from the solid surface and the time when the minimum temperature in a cycle occurs. Furthermore, by equating Equation (18) to the liquid superheat, we get another relation between the same quantities.

From these two relations we can find the two unknowns as functions of the relaxation length L and the solid-liquid properties. The mathematical treatment is given in Appendix E.

This critical distance was found to be

$$X_{cr.} = \eta(\beta)\, L \tag{23}$$

where $\eta(\beta)$ is a function of the liquid-solid properties. Values for η are given in Table (1) and Figure (5). Now, if a cavity has a depth of

$$\ell > X_{cr.} \quad , \tag{24}$$

it will always contain vapor; namely, it is an active cavity.

Combining Equations (15), (23), and (24), we get

$$\ell > \frac{\theta_\omega(0,0)\sqrt{k_\ell \rho_\ell c_\ell \alpha_\omega}}{q_o}\, \eta(\beta)\, I(\beta)\, J(\beta) \tag{25}$$

Re-arrange Equation (25) and solve for the heat flux

$$q_o > \frac{\theta_\omega(0,0)\sqrt{k_\ell \rho_\ell c_\ell \alpha_\omega}}{\ell}\, \eta(\beta)\, I(\beta)\, J(\beta) \tag{26}$$

Equation (26) means that any cylindrical cavity for any liquid-solid combination under a given pressure has a critical heat flux below which boiling will not be stable and above which stable boiling will exist. For alkali metals with small cavities at low pressures, this heat flux may be very high, which practically cannot be achieved.

3.4 The Variables Affecting Stable Boiling

3.4.1 Cavity Geometry

The cavity geometry is presented by the term $\frac{\theta_\omega(0,0)}{\ell}$. From Equation (C-13) it follows that $\theta_\omega(0,0) \propto \frac{1}{r}$; therefore, the minimum heat flux required for stable boiling is proportional to $\frac{1}{r\ell}$. The greater the cavity radius the smaller the heat flux, or the greater the cavity

depth the smaller the heat flux (keeping the ratio of $\ell > 10\gamma$). It should be emphasized here that any re-entry-type cavity does not obey Equation (26), since T_v would not remain constant when the interface liquid-vapor passes through the point of infinite radius of curvature.

3.4.2 Fluid Properties and Pressure

The effect of fluid properties on the minimum heat flux for stable boiling is given in quite complicated terms $\theta_\omega(0,0)\sqrt{k_\ell \rho_\ell c_\ell}\,\eta(\beta) I(\beta) J(\beta)$. As was said before (see Table (1)), $I(\beta)J(\beta)$ are very weak functions of β and, therefore, may be considered as constants. Although $\eta(\beta)$ is a strong function of β, it varies very little for values of $\beta > 1.5$, which is the range for most of the fluid-solids combinations. The greatest effect of fluid properties is therefore presented by the term $\theta_\omega(0,0)\sqrt{k_\ell \rho_\ell c_\ell}$. From Equation (C-13) it follows that $\theta_\omega(0,0) \propto \frac{T_{sat.}^2}{B P_{sat.}}$. For fluids of high saturation temperature and high thermal conductivity, as is the case for alkali metals, the minimum heat flux for stable boiling is much higher than for water. On the other hand, as the saturation pressure increases, the term $\frac{T_{sat.}^2}{B P_{sat.}}$ decreases, which in turn tends towards the decrease of the minimum heat flux.

3.4.3 Solid Properties

Solids of higher thermal diffusivity will tend to increase the minimum heat flux since $q_o \propto \sqrt{\alpha_\omega}\,\eta(\beta)$. This is due to the fact that in metals of higher α the temperature fluctuation on the surface will penetrate deeper into the solid than in metals of low α. This conclusion is opposite to what was concluded by Marto (5), but it is in agreement with Equation (22) which is a modified equation of Marto.

3.4.4 Comparison Between Equations (22) and (26)

Although the modified Marto prediction (Equation (22)) differs in form from the present prediction (Equation (26)), the effect of the various variables is in very good agreement.

3.5 Stability for Fluids of Low Thermal Conductivity

In reaching the criterion for alkali metals, Equation (26), it was assumed that the fluid has high thermal conductivity. This assumption allows us to simplify Equation (C-12) to Equation (C-13). For the case of fluids of low thermal conductivity, this assumption does not hold; therefore, the values of $\eta(\beta)$ are not correct. In order to examine the case of fluids of low thermal conductivity, Equation (19) together with Equation (C-12) should be used. From these two equations, it can be easily shown that for fluids of low thermal conductivity boiling from a metal surface, the solid temperature will never fall below the vapor temperature, and stability is secured.

4. DESCRIPTION OF EQUIPMENT

The experimental tests were performed in the same apparatus built and used by Marto (5).

A schematic diagram of the apparatus is given in Figure (6), a partial assembly of equipment is given in Figure (7), and the entire heat transfer facility is shown in Figure (8).

The main components of the equipment are described below.

4.1 Boiler Condenser

The boiler-condenser combination forms a vertical cylinder of 2-1/2-inch I.D. and 40-inch length. The boiler part is ended with a boiler plate at the bottom, and at the top the condenser is ended with a thick plate through which four inlets or outlets are provided.

Two probes were installed in two of the four inlets by means of a Conax packing gland with a teflon sealant. One probe serves as a sensor for the minimum sodium level (see 4.7) and contains the thermocouple for measuring the liquid temperature. The other probe is described in paragraph 4.8. The two other inlets are used for filling sodium and controlling the pressure.

The boiler is a 2-1/2-inch schedule 40, stainless steel 316 pipe, 1-foot long. It consists of two parts: The upper one is a continuation of the condenser pipe passed through the vacuum chamber cover and is welded to the cover. This part is ended with a flange 5-inch O.D. x 1/8-inch thick. The second part of the boiler is shown in Figure (9). The bottom of this part is the boiler plate from which sodium boils. Details about the various boiler plates will be given in Chapter 5. A

nickel pipe 2-1/2-inch I.D. x 3 inches long was welded to the boiler plate. (See Figures (9) and (10).)

The extension of the nickel pipe was a 2-1/2-inch x 6 -inch long schedule 40, stainless steel 316 pipe. This pipe is ended with a flange 5-inch O.D. x 1/8-inch thick to match the upper boiler part. The two flanges were welded together to form the boiler. Each time a different plate surface was tested, the weld of these flanges was ground off, and a new set of the second boiler part was welded instead.

The condenser section is a vertical, 28-inch length of 2-1/2-inch schedule 40 stainless steel 316 pipe with eighteen copper fins, 18-inch long x 1-1/4-inch wide x 1/16-inch thick, silver soldered on the outside. It is welded directly to the boiler pipe just above the vacuum chamber cover. An outer jacket of mild steel which has the dimensions of 6-inch O.D. x 5-3/4-inch I.D. x 28-1/4-inch long is fitted over this condenser pipe to channel the air flow over the copper fins. A 120 CFM centrifugal type air blower is attached to the inlet of this condenser cover by a flexible connector. The air enters at the top of the condenser through a horizontal 4-inch diameter x 3-inch long mild steel tube and is pre-heated by a coil of Chromel "A" resistance wire wrapped around Transite insulation. The air passes over the copper fins and leaves at the bottom of the condenser through a horizontal 4-inch diameter x 3-inch long mild steel tube which is attached by a flexible connector to a 6-inch galvanized duct that leads to the main M.I.T. exhaust system. Flexible connectors between the air blower and condenser inlet and between the galvanized duct and condenser outlet are made of asbestos cloth interwoven with aluminum thread. The condenser is shown in Figures (11) and (12).

4.2 Main Heater

The heater consists of three tantalum 10 percent tungsten filaments fastened in series between four tantalum clamps. The filaments are .010-inch thick x 1-inch wide x 4-inch long. They are fabricated by corrugating a .010 x 3 x 4-inch foil along the 4-inch axis with an internal angle of 30 degrees. An overhead photograph of the heater is shown in Figure 13.

The filaments operate near 4000 ^{o}F (the melting point of tantalum 10 percent tungsten is approximately 5300 ^{o}F) and require the use of a high vacuum system to prevent complete oxidation during operation. In general, the heater is quite reliable, but there were several occasions when one of the filaments cracked due to oxidation embrittlement caused by the coarse grain structure of tantalum. These failures usually took place after operation at high power levels in a poor vacuum (i.e., a vacuum greater than one micron).

Each filament is held in place by pressing it between two 1/4-inch thick tantalum clamps which are machined to fit the filament corrugations. This assembly is riveted together by placing a piece of tantalum wire, 1/16-inch diameter x 5/8-inch long, through a .0635-inch diameter drilled hole and by peening over the edges of the wire. This method of attachment insures a good electrical contact at all times and facilitates dismantling.

The tantalum clamps are fastened to 1/8-inch thick molybdenum electrodes using No. 10-32 x 3/4-inch long tantalum screws with hex. hd. nuts. These molybdenum pieces are bolted to "L" shaped molybdenum

electrodes with 3/8-inch diameter x 1-inch long stainless steel cap screws with hex. hd. nuts. The "L" shaped electrodes are slotted vertically to allow for adjustment of the overall height of the filaments and are in turn bolted to 3/8-inch thick horizontal copper bus bars as shown in Figure 10.

Vertical copper electrodes are silver soldered to the underside of the horizontal bus bars. They are fabricated by silver soldering a 1/2-inch pipe inside a 1-inch pipe (Figure 10). Cooling water from the laboratory supply line flows up the inside of the 1/2-inch pipe and down and out the annulus. These electrodes are electrically insulated from the vacuum chamber base plate by means of Teflon collars which are pressed between stainless steel flanges, silver soldered to the electrodes, and between the base plate (Figure 10). In order to prevent the Teflon from outgassing at high temperature operation, however, water-cooled copper coils are locally installed within grooves machined in the underside of the base plate.

High temperature electrical insulators made of aluminum oxide and also of Lava are used to channel the current so that the three filaments are connected in series. A DC power supply rated at 1000 amps, 15 volts is connected through flexible copper leads to the vertical copper electrodes.

To increase the thermal efficiency of the heater as much as possible, eleven concentric radiation shields are used. They are 12 inches high with diameters varying on the half inch from 8 inches to 13 inches. The innermost shield is made of .010-inch thick molybdenum while all

the rest are made of .019-inch thick stainless steel 304. In addition, fifteen horizontal radiation shields of stainless steel 304, .019-inch thick x 3-inch wide x 6-inch long are placedbeneath the filaments.

4.3 High Vacuum System

The boiler and heater are contained within a 14-inch O.D. x 1/8-inch thick x 18-inch long stainless steel 316 vacuum chamber. This vessel is fabricated by heliarc welding 3/4-inch thick x 16-3/4-inch diameter flanges to the top and bottom of the cylinder and by bolting to these flanges 3/4-inch thick x 16-3/4-inch diameter plates. Twelve 1/2-inch diameter x 2-inch long stainless steel hex. hd. cap screws with hex. hd. nuts are used with each flange. A single 14-1/4-inch O.D. "O" ring, which is made of copper, provides a vacuum seal. The copper "O" rings are silver soldered from .072-inch diameter wire. Three Conax multiple thermocouple glands with Lava sealants are used to provide vacuum seals for all the thermocouples in the test section. These glands are heliarc welded to the vacuum chamber cover at positions 90 degrees apart on an 11-1/2-inch diameter circle. The Teflon collars which were previously described, provide excellent seals for the main heater copper electrodes. A vacuum better than 10^{-5} mm Hg is generally attainable with this system. The entire vacuum chamber is covered with 1-1/2 inches of Fiberfrax thermal insulation to cut down heat losses during operation, and the unit is raised and lowered using two hydraulic jacks and a steel support ring.

The high vacuum line consists of a horizontal, 4-inch schedule 40 stainless steel pipe welded to the wall of the vacuum chamber at a

point 11 inches above the base plate. This pipe is bolted to a National Research Corporation 4-inch flexible connector which in turn is bolted to a 4-inch stainless steel 316 90-degree elbow. Both flanges use standard neoprene gaskets for vacuum seals. The elbow is bolted to a National Research Corporation type HS4-750 diffusion pump using a neoprene "O" ring. A Welsh Duo-Seal type 1402 B mechanical pump, connected directly in series with the diffusion pump, is used as the roughing and backing pump. No cold trap or separate roughing lines are used.

4.4 Helium Cover Gas Line

In order to maintain the sodium as free of oxides as possible, helium is used as a cover gas. The helium is dried and filtered by flowing through a molecular sieve bed (1/16-inch diameter pellets of an alkali metal alumino silicate from Linde Co. were packed firmly within a 2-inch diameter x 10-inch long stainless steel 304 cylinder) at liquid nitrogen temperatures. The entire helium gas line is 1/4-inch stainless steel 316 tubing, and all valves are Hoke type TY440.

A Cenco-Magavac mechanical vacuum pump is connected to this helium system through a standard ice trap where the 1/4-inch stainless steel pressure tubing is joined to a series of 1/4-inch copper coils.

A large stainless steel 316 pressure tank is attached to the helium system above the condenser section. It is an 8-inch schedule 5 pipe, 18 inches long, with welded caps at both ends. Six brass baffles are silver soldered on the inside of the tank, and water-cooled copper coils are soft soldered on the outside. The tank is used both as a reservoir to damp any pressure fluctuations during boiling and also as a cold trap

for sodium vapors. All breakable joints utilize stainless steel Parker Triple-lok or Swagelok fittings, and all permanent joints utilize stainless steel Parker Braze-lok fittings.

4.5 Sodium Fill System

Sodium is stored in a stainless steel 316 tank, 4-1/2-inch O.D. x 6 inches high. This tank is flanged at the top and is sealed with a 4-1/2-inch I.D. x 0.139-inch thick Viton "O" ring. A steel sheathed, 0.260 diameter Calrod heater is wrapped around the tank and is covered with a 1/2-inch thick coating of Thermon cement to provide a good thermal bond. This heater is rated at 1.25 KW and receives power through a 1 KVA variac. Thermal insulation consists of a 1/2-inch thick inner layer of Fiberfrax alumina-silica fibers and a 1/2-inch thick outer layer of standard fiberglas strips.

The sodium fill line is fabricated entirely from 3/8-inch diameter stainless steel 316 tubing. This line goes from the fill tank through a 3/8-inch diameter x 12-inch long Anaconda flexible stainless steel tubing and into the vapor space through the condenser top. Briskeat heating tapes are wrapped around the entire length of the line and are covered with the same type of thermal insulation used on the fill tank. Sodium is filtered before entering the boiler by passing through a flanged stainless steel cup, 1-1/2-inch O.D. x 3 inches long, which is packed with fine grade stainless steel wool. This filter is kept at a temperature near 350 ^{o}F. All valves are Hoke type Ty445, and all breakable joints utilize either Parker Triple-lok or Swagelok fittings.

4.6 Containment and Safety Equipment

Since the boiler section operates within the 14-inch O.D. vacuum chamber, this chamber acts as a primary source of containment for any sodium leakage.

In addition, the entire heat transfer apparatus is enclosed inside a 5 x 5 x 8-foot high enclosure shown in Figures 7 and 8. This enclosure is fabricated by bolting 20-gage steel sheets to an all-welded framework of 1-1/2 x 1-1/2 x 3/16-inch angle irons (Figure 7). Rubber weather stripping is used between the sheets and framework to provide a pressure-tight seal in the event that an inert atmosphere is necessary. A plexiglass window, 22 x 16 x 1/4 inch, is attached to the top half of the front side of the enclosure. Just beneath this window is a 5 x 4-1/2-foot hinged door. All valve handles are extended through the enclosure skin to permit operation from the outside. The enclosure is vented through a 6-inch duct to exhaust any possible fumes.

Safety equipment includes an Ansul MET-L-X fire extinguisher, a safety helmet, safety glasses, a methyl methacrylate face shield, and asbestos lined leather gloves.

4.7 Safety Controls

In order to safely operate the apparatus, a semi-automatic control system is utilized. This system monitors the sodium level within the boiler, the condenser air flow rate, the main electrode cooling water flow rate, and the main vacuum system pressure. If the sodium level drops beneath a prescribed value and if there is a loss of air flow, loss of vacuum, or loss of water circulation, then this system activates

a buzzer and one of four control panel lights. The system is semi-automatic because although detection is automatic, control of the equipment is manual. A master stop button on the control panel is used to shut off the main power supply in the event of an emergency. An electrical wiring diagram for this control circuit is shown in Figure (14).

Each sensing device operates an electrical relay which controls a common buzzer and an individual light. The sensor for the air flow rate is a mercury switch attached to a butterfly valve inside the air duct. When the flow of air is turned on or off, the butterfly valve opens or closes the mercury switch. The sensor for the sodium level utilizes the vertical thermocouple probe described earlier. A 110-volt DC power supply is connected to this probe which is electrically insulated from the condenser by means of a Conax electrode gland with a Teflon sealant. The sodium level acts as a switch, making or breaking contact when the level is above or below the probe tip. The sensors for both the water flow rate and the high vacuum system utilize standard pressure diaphragms attached to micro-switches. As the water pressure (or vacuum) changes, the diaphragm moves, thereby opening or closing the micro-switch.

4.8 Instrumentation

Six platinum-platinum 10% rhodium "Ceramo" type thermocouples are used in the boiler test plate. These thermocouples are 1/16-inch O.D., inconel sheathed, magnesium oxide insulated, and werespecially calibrated at either 1200, 1400, 1600, and 1800 ^{o}F or 1400, 1600, 1800, and

2000 °F by the Thermo Electron Engineering Corporation to an accuracy better than 1 °F. A 1/16-inch O.D., stainless steel sheathed, Chromel-Alumel, "Ceramo" type thermocouple is used in a vertical probe to measure the liquid temperature. In the last few runs, two Chromel-Alumel thermocouples wereadded to the boiler plate, and another one was located in the second vertical probe to measure the vapor temperature. These thermocuples were 0.040-inch O.D., inconel sheathed, magnesium oxide insulated, and grounded at the end. They were calibrated at 1200, 1300, and 1400 °F by Conax.

The above-mentioned thermocouples are connected through a Leeds and Northrup 16-pole rotary switch to a Leeds and Northrup, type K precision potentiometer with an external standard cell, battery, and galvanometer. The reference junction for these thermocouples was chosen at room temperature, and this reference value was recorded for each data point by means of a 30-gage Chromel-Alumel glass insulated thermocouple which was read against an ice junction.

In order to record the temperature of all the above-mentioned thermocouples, two Leeds and Northrup milivolt potentiometers, Cat. No. 8690, were used connected to a Recording Oscillograph 5-124 by Consolidated Electrodynamics Corp. This recorder has various chart speeds of 0.25, 1, 4, 16, and 64 inch per second and can record 18 points.

The two Chromel-Alumel thermocouples, placed in the liquid and in the vapor, were connected through a selecting switch to one of those potentiometers. The other potentiometer was connected, through a switch, in parallel with the type K Leeds and Northrup potentiometer.

These two potentiometers provided a reference temperature level, and only the temperature variations were recorded. The arrangement of these two potentiometers makes it possible to record, at the same time, any temperature variations in the boiler plate together with either the liquid or the vapor temperature. To record the various temperatures in the boiler plate, the main rotary switch was used while the recorder was in operation. All other thermocouples in the apparatus were used to obtain operational information. They were all 30-gage iron-constantan, glass insulated thermocouples and were connected directly to a Minneapolis-Honeywell, Brown Electronik, 20-point recorder which has a range of 0-1000 ^{o}F.

The second vertical probe, shown in Figure (15), serves two purposes. First, it contains the thermocouple to measure the vapor temperature. Second, it acts like a switch in a 1-1/2-volt loop. Whenever the sodium liquid level touches the probe, the loop is closed, and a signal is fed to the Recording Oscillograph. By this arrangement we can record on the same chart the temperature variations and the changes of liquid level. The probe is housed in three inconel bellows which permit its position to be changed without breaking the seal at the top.

Pressure in the helium line was measured by an open-end manometer and a Marsh compound pressure gage. The pressure in the vapor space of the condenser was recorded by a Taylor high temperature volumetric pressure transducer which had been previously calibrated against the manometer down to a pressure of 40 mm Hg.

The main heater voltage drop was recorded by a 0-25-volt DC voltmeter, and the main current was determined by observing the voltage drop

across a National Bureau of Standards shunt. This voltage drop across the shunt was recorded by a 0-50 MV millivolt meter. For the shunt, 50 MV equalled 1000 amps. All other heater power supplies were monitored using variacs and ammeters in each circuit.

The pressure in the high vacuum system was determined with two thermocouple gages and one ionization gage. All three gages were connected to a National Research Corporation, type 710 B gage control. The vacuum was monitored from 1 mm Hg down to 10^{-6} mm Hg.

A phonograph crystal cartridge is taped directly to the high vacuum line to pick up vibrations in the test section. Because the crystal is limited to temperatures below approximately 140 ^{o}F, the pickup is positioned about 2 inches from the vacuum chamber wall and is locally cooled by flowing water through copper coils which are soldered to the vacuum line. The noise created during boiling is directly transmitted to this cartridge, and the electrical signal is fed to an oscilloscope for observation.

5. EXPERIMENTAL PROCEDURE

5.1 General

In order to confirm the theory presented in Chapter 2 from which the stability criterion was developed (Chapter 3), the test surfaces must contain a pre-described cavity.

Initially some of Marto's (5) surfaces were re-run for the purpose of getting acquainted with the apparatus and the operation methods. Also, it was of interest to see how a surface containing re-entry type cavities would behave after cleaning and re-installing. The experimental procedure consists of the following steps: preparation of the test surface, preparation of the system, operating the system, and reducing the data.

5.2 Preparation of Test Surfaces

There were mainly three types of boiler plates which were used in this experiment.

5.2.1 Surfaces for Repeating Marto's Work

These boiler plates were made of nickel "A" discs of 2-9/16-inch diameter x 0.750-inch thick, with six holes of 1/16-inch diameter, Figure 16, containing removable thermocouples for temperature measurements. One plate had twelve re-entry-type cavities (runs 27, 28 of Marto). These cavities were fabricated by drilling a hole of 0.0145-inch diameter x 0.025-inch deep in the test surface. A plug, 0.015-inch diameter x 0.015-inch long, which was tappered on one end with a 45-degree bevel, was press fitted into the hole in the test surface so that the top of the plug was flush with the top of the surface. This plug had

a 0.004-inch diameter hole drilled along its longitudinal axis to provide a mouth for the cavity. (See Figure 17.)

The other two plates were coated by porous discs. The coating procedure was as follows: The test plate was lapped to get a smooth flat finish. After cleaning this surface, a 2-1/2-inch diameter x 1/32-inch thick disc of porous nickel "A" was then placed on it. These porous plates were manufactured by Pall Corporation and had a mean pore size of 65 microns and 35 microns. The two pieces were pressed together under a pressure of about 5 psi and were fired in a wet hydrogen furnace at 1100 ^{o}C for two hours to create a good metallurgical bond.

5.2.2 Surfaces with an Artificial Cavity and a Permanent Thermocouple

These boiler plates were made of two parts, see Figure (18). One part was made of a nickel "A" disc of 2-9/16-inch diameter x 0.80-inch thick with three holes of 1/16-inch diameter containing removable thermocouples for temperature measurements to obtain the heat flux. The other part was made of a nickel "A" disc of 2-1/4-inch diameter x 0.220-inch thick which was made to fit the first part. This disc contains one cylindrical cavity in the middle. A calibrated Choromel-Alumel thermocouple was put on the other side of the disc with its hot junction facing the cavity hole and exposed to the liquid. This thermocouple was 1/16-inch O.D. inconel sheathed, grounded type with compacted mineral insulation. After chemical treatment, the two parts and the thermocouple were put together with a 0.001-inch thick copper foil and were brazed in a hydrogen furnace to obtain a good metallurgical bond. Afterwards the unit was shaped to its final dimensions, see Figure 18,

and the surface was polished to a mirror finish. To obtain a mirror finish, the following procedure was followed: Rough polishing was done on a Buehler rotary grinder. This grinder contains discs of 240, 320, 400, and 600 grit emergy paper which was attached by adhesive backing to the rotating grinder discs. Water continually flowed over the emergy paper keeping it clean and serving as a lubricant. The test surface was kept in each stage of grinding until all the scratches from the previous stage had disappeared. The final polish was done on a Buehler rotary disc covered by a polishing cloth and using a "B" type solution which is a suspension of fine grade alumina powder in distilled water. At the end of this polishing process, the surface has a mirror-like finish without any scratches. A photograph of this surface taken from the top of the boiler is given in Figure 19. Three surfaces of this type were fabricated, having the following cavity size: 0.010-inch, 0.020-inch, and 0.0465-inch diameter with 0.050-inch depth.

5.2.3 Surfaces with Artificial Cavity and Without a Permanent Thermocouple

These boiler plates were made of a nickel "A" disc of 2-9/16-inch diameter x 0.850-inch thick. Six holes of 1/16-inch diameter were drilled in the plate for temperature measurement from which the heat flux was calculated. Two smaller holes of 0.040-inch diameter were drilled at a distance of 0.050 inch from the surface, for measuring the temperature fluctuations. (See Figure 20.)

In one of these plates one re-entry-type cavity was put at the middle of the surface. This re-entry cavity was fabricated by drilling a hole of 0.0195-inch diameter x 0.030-inch deep in the test surface. The surface was then polished to a mirror finish following the procedure described

in paragraph 5.2.2. A plug, 0.020-inch diameter x 0.020-inch long, which tappered on one end with a 45-degree bevel, was press fitted into the hole in the test surface so that the top of the plug was flush with the top of the surface. This plug had a 0.005-inch diameter hole drilled along its longitudinal axis.

The other plate was first polished to a mirror finish, and then one cylindrical cavity was drilled into the middle of the surface. This cylindrical cavity was 0.0105-inch diameter x 0.150-inch deep.

5.3 Preparation of the System

Before testing a new surface, the previous boiler section had to be removed, and instead the new one had to be installed.

All water and electrical lines were first disconnected from the vacuum chamber. Two hydraulic jacks with a steel support ring were positioned under the vacuum chamber and were raised until they began to support the load. The top and side flanges of the vacuum chamber were then opened, and the vacuum chamber was lowered to the floor by slowly releasing the pressure within the jacks. The entire vacuum chamber unit was then slid to one side of the enclosure. All thermocouples were removed from the test plate and were bent away from the boiler flange. A portable grinder with a 3-inch diameter x 1/4-inch thick abrasive wheel was then used to grind off the weld on the boiler flange. This generally took about thirty minutes. A helium pressure of 3 psi was maintained inside the boiler during this time. When the crack between the two flange faces was visible around the entire circumference of the flange, the weld was broken open by shocking it with a hammer and chisel.

The boiler section containing the sodium was then removed and reacted with n-butyl alcohol in a 55-gallon drum. All burrs on the edges of the top flange and all traces of sodium were removed. This usually took about two minutes during which helium was purged through the system in an effort to prevent oxidation of the sodium inside the apparatus. A new boiler was then clamped in place, taking great care that the thermocouple wells in the test plate were orientated in the same direction as for the previous boiler. The boiler was then welded to the top flange. It took about fifteen minutes to complete this weld, and the system was immediately pumped down to less than 1 mm Hg. and re-pressurized with 5 psi of helium. The boiler flange was then leak tested. When this joint was tight the thermocouples were placedin the test plate, the vacuum chamber with a new metallic "O" ring was raised, and the top and side vacuum flanges were tightened until a vacuum of at least 10^{-5} mm Hg. could be obtained.

Whenever the equipment had been dismantled and re-assembled, leak testing would take place. The entire system was pressurized to 10 psi with helium, and all previously opened joints were checked with a soap solution. The system was considered tight if a pressure of 10 psi was held overnight without any change occurring in the open-end manometer.

The main vacuum system was leak tested after assembly until a vacuum of between 10^{-5} mm Hg and 10^{-6} mm Hg existed. Leaks were checked by spraying all joints with acetone and watching the response of the thermocouple gages for a vacuum between 10^{-2} and 10^{-3} mm Hg and of the ionization gage for a vacuum below 10^{-3} mm Hg.

On some occasions it was found that sodium oxide was deposited on the condenser surface. Whenever this happened the condenser and all the connection lines were removed and were reacted in the same drum containing the n-butyl alcohol. Then all parts were thoroughly washed in hot water, degreased with trichloroethylene, and re-assembled in place.

To re-load the system with a new batch of sodium, the fill tank was disconnected, and its flange was opened. All remaining sodium oxide was removed mechanically. A brick of sodium, 2-1/4-inch diameter x 3-inch long, was put into the fill tank after all surface oxides had been scraped away. Then the cover, with a new viton "O" ring, was bolted in place, and the fill tank was connected to the system. The entire apparatus was immediately evacuated to 1 mm Hg and pressurized to 10 psi with helium. At this stage the system was ready for the new test.

5.4 The Operation Method

The operation started when the sodium system was under a pressure of 5 psi helium and the vacuum chamber under a pressure of 10^{-5} mm Hg or better. Then, the heaters for the fill tank, fill line, and pressure line were turned on. Also, the main heater and the air heater were turned on. All the heaters were kept on for about two hours until the fill tank was at 450 ^{o}F, all lines were near 450 ^{o}F, and the boiler plate was at 400 ^{o}F. When these temperatures were reached, the boiler-condenser part was evacuated to about 1 mm Hg, keeping the fill tank under a pressure of 5 psi. The sodium fill line valve was opened, and the sodium flowed into the boiler. During this transfer operation all the temperatures were recorded, and the change in pressure at the open-end manometer

was observed. The transfer was completed in a few seconds. To clean the lines of any trapped sodium, the fill tank was evacuated while the boiler-condenser part was pressurized keeping the fill line valve closed. Then this valve was opened, and helium flowed from the boiler to the fill tank cleaning the lines. When the blow-back was completed, the fill line valve was closed, and the heaters for the fill tank and a part of the fill line up to the valve were closed. While keeping the rest of the lines including the top of the condenser at a temperature of about 400 ^{o}F, gradually the main power was increased. The system remained under a pressure of 5 psi until the desired working temperatures were obtained; then it was evacuated to the desired pressure.

The sodium level was found by lowering the second probe with the bellows until an electrical contact was made. Then this probe was raised to 1/4 inch above the liquid vapor interface by turning a graduated screw.

Before taking any boiling data, several data points were taken in the natural convection region. This gave a reasonable check for a correct behaviour of all the thermocouples.

When nucleate boiling began, the condenser air blower was turned on, dropping the condenser air inlet temperature to approximately 125 ^{o}F. At the same time the rest of the heaters were still on to keep the auxiliary lines at 400 ^{o}F.

For any given heat flux level the equilibrium condition was reached after about fifteen to twenty minutes. This was observed by watching the temperatures in the liquid and in the solid on the Recording Oscillograph without running the paper. When equilibrium was obtained, the following successions of operations were performed: The barometric

pressure, the Taylor gage, and the open-end manometer were recorded as well as the power input to the main heater. Then all the thermocouples were read twice, as well as the reference temperature, by the Leeds and Northrup type K potentiometer. Afterwards, all the temperatures in the boiler plate together with the temperature of either the liquid or the vapor were recorded on the Recording Oscillograph at a chart speed of either 0.25 inch per second or 1 inch per second. For boiling runs, it was impossible to read the temperature of the two thermocouples close to the surface by the type K potentiometer; therefore, these temperatures were only recorded by the Recording Oscillograph.

After the set of measurements was completed, which took about ten to fifteen minutes, the power to the main heater was changed. Data for both increasing and decreasing heat flux were observed.

The system was shut down by turning off the main heater and pressurizing the system to 5 psi with helium. After a certain time, when the temperature of the liquid was cooled to about 1000 $^{\circ}$F, all the electrical heaters were turned off. The entire system cooled down overnight, and the sodium was left to solidify within the boiler. When the system was cold the vacuum pumps were turned off.

5.5 Reducing of Data

By plotting the translated temperatures from the four thermocouple readings in the boiler plate versus their axial position, the temperature distribution in the boiler plate was obtained. A straight line connecting these temperatures gave the temperature slope from which the heat flux was obtained from

$$q_o = k_w \frac{\Delta T_w}{\Delta X} \qquad (27)$$

The extrapolated wall temperature $T_{w\ ext}$ was obtained by extrapolating the straight line to the boiler surface.

From the Recording Oscillograph the minimum and the maximum temperatures of thermocouple No. 7, which was close to the surface, were reduced. The minimum temperature of this thermocouple was usually on the straight line.

For $\varphi = 1$, Equation (20) becomes

$$\theta_\omega'(0,0) = K\, q_0/k_\omega \tag{28}$$

where K is given in Equation (21).

In order to find the maximum wall temperature, $T_w(0, 0)$, a straight line with a slope of $\theta_w'(0, 0)$ was drawn passing through the maximum temperature obtained by thermocouple 7 and extrapolated to the boiler surface.

Furthermore, the temperature readings of thermocouple No. 7 varied in a periodic way from which the period time φ could be found.

The saturation temperature was found by the temperature measurements of the thermocouple in the vapor and compared with saturation pressure measured by the open-end manometer by the relationship recommended by Bonilla, et al. (17).

$$\log_{10} P = 4.52172 - \frac{5220.42}{T} \tag{29}$$

where P is in atmosphere, and T is in degrees Kelvin. Usually, good agreement was obtained between the two measurements of the saturation temperature within 2 to 3 ^{o}F. In every case the temperature read by the thermocouple was taken to be the temperature of the vapor. The

other three thermocouples in the boiler plate were not taken into account, and they served only for checking radial temperature distribution. For those runs where the Recording Oscillograph was not used, only the heat flux and the extrapolated wall temperature were reduced. A calculated example is given in Appendix G.

6. RESULTS AND DISCUSSION

6.1 Observations

Data for heat transfer from a heating surface of nickel "A" to liquid sodium were taken at heat fluxes ranging from 20,000 to about 300,000 BTU/ft^{2}hr at absolute pressures ranging from 40 to 105 mm Hg. Most of the runs were taken at a pressure of about 60 mm Hg, when the vapor temperature above the liquid was at saturation temperature corresponding to the pressure. The sodium depth in the boiler was usually around 2 inches.

During the experiments of the present work, three different regions of heat transfer were observed.

6.1.1 Natural Convection

Heat transfer by natural convection from the solid surface to the liquid sodium, while evaporation took place at the liquid-vapor interface, was characterized by stable temperatures in the solid and in the liquid with heat transfer coefficients of the order of 800 to 1000 BTU/ft^{2}hr$^\circ$F. This usually took place either at the beginning of each run when the power was gradually increased, or when boiling stopped after decreasing the input power. The data obtained during natural convection were independent of the surface conditions and the pressure at this working range.

6.1.2 Stable Nucleate Boiling

Heat transfer during nucleate stable boiling was characterized by constant temperatures in the boiler plate far away from the solid-liquid interface and constant temperature of the vapor. The liquid temperature,

measured at about 3/4 inch from the solid-liquid interface, was subcooled in the range of 0 to 10 ^{o}F, depending on the heat flux, and its reading was stable. The Chromel-Alumel thermocouples, located in the boiler plate near the surface, measured a periodic fluctuation of temperatures and could only be recorded on the Recording Oscillograph. Once a stable boiling was achieved for a given heat flux, it existed for all the heat fluxes for which the input power was increased. While decreasing the power, stable boiling was observed until reaching a certain heat flux below which boiling stopped and natural convection heat transfer was observed.

6.1.3 Unstable Boiling or Bumping

For each run, before reaching the first heat flux for which stable boiling existed, a transition between natural convection and nucleate boiling was observed. This was characterized by temperature variations in all the boiler plate thermocouples as well as in the liquid and in the vapor. At the same time large pressure variations in the boiler occurred accompanied by a big noise. This noise was detected by the phonograph crystal pickup and was observed on the oscilloscope.

The variations of temperatures were not periodic and could not be read on the type K potentiometer. For any given heat flux, when bumping took place, and after waiting a certain amount of time, the bumping stopped, and the heat was transferred by natural convection only. When the input power was increased, the bumping resumed at that higher heat flux. By further increasing the power, a heat flux was reached for which a sudden transition from natural convection to boiling took place, and after that the boiling was stable. The range of heat fluxes, for

which the bumping phenomena was observed, was between 50,000 to 200,000 BTU/ft^{2}hr, depending on the surface conditions.

The data obtained during bumping could not be accurate since it was very difficult to get the exact temperature measurements. An example for temperature variations during bumping is given in Figure (21).

6.2 Experimental Results

The experimental results of this work are tabulated in Appendix F. Each table, given for each run, contains the surface conditions, the sodium depth, and the important values which were either measured or calculated. Also a short description of the mode of heat transfer is mentioned. A calculated example is given in Appendix G.

The tabulated important parameters are as follows: The saturation temperature T_{sat} measured at the vapor temperature and the corresponding saturation pressure p calculated from equation (29) (in those runs in which the vapor temperature was not measured, the saturation temperature was calculated from the pressure measurements), the liquid temperature T_ℓ, and the extrapolated wall temperature $T_{w\ ext}$. Also are presented the calculated average heat flux q_o, the calculated difference $(T_{w\ ext} - T_{sat})$, the calculated wall superheat $\Theta_w(0,0)$, and the average measured waiting time $\mathcal{T}$.

The best way to analyze the results of this experimental work is to divide them into groups according to the various surfaces.

The first run (No. 1) was made from a porous nickel "A" of 65 microns grade. This run was performed immediately after run No. 30 of Marto (5), where the sodium was left to solidify in the boiler. Table F-1 shows good agreement with Table C-15 of Marto.

Runs No. 3 and 4 were made with porous nickel "A" of 35 microns grade. In these two runs most of the measured points were in the natural convection region, and only a few points were of stable boiling. These stable boiling points were at heat fluxes higher than about 150,000 BTU/ft^{2}hr.

Runs No. 2 and 5 were with twelve re-entry type cavities. This was the same surface as in runs 27, 28 of Marto (5), after the sodium was reacted. In the first of the two runs the surface was chemically cleaned, while in the second run it was also cleaned in an ultrasonic cleaner. In both of these runs bumping took place up to heat fluxes of about 200,000 BTU/ft^{2}hr, where as in runs 27, 28 of Marto, stable boiling was observed from this surface at heat fluxes as low as 100,000 BTU/ft^{2}hr. The explanation to this different behaviour could be found in the following argument. When sodium is reacted in n-butyl alcohol, it frees hydrogen from the reaction. If the hydrogen is trapped in the cavity, it prevents any further reaction with the sodium in the cavity. When this surface is exposed to air, the diffusion of oxygen into the cavity will cause oxidation of the remaining sodium which cannot be removed even with an ultrasonic cleaner. As a result of this, the original re-entry cavity is no longer a re-entry type cavity, but instead, a cylindrical one. This size of cylindrical cavity is the same as was used in run 24 of Marto in which bumping took place at these high heat fluxes.

In all the above-mentioned runs, no measurements were taken of bubble frequency and temperature variation at the surface during stable

boiling. The results of runs 1 to 5, therefore, cannot be used to confirm the theory predicted in Chapter 2.

The second group of runs, 6 to 12, was made with boiler plates of nickel "A" polished to a mirror finish with one cylindrical cavity in the middle and with a permanent thermocouple which was exposed to the liquid. See paragraph 5.2.2.

These runs were recorded on the Recording Oscillograph and contained data points of the three regions of heat transfer mentioned in paragraph 6.1.

From the results of all these runs, it was obvious that the controlling cavity mouth was not the cylindrical cavity which was drilled into the surface, but some smaller size cavity. The arrangement of the permanent thermocouple and the cavity probably formed some re-entry type cavity with a controlling mouth size smaller than the drilled one. From the calculated $\theta_w(0,0)$, for each run, together with the saturation pressure, the average controlling cavity radius was calculated, using Equation (C-13), and was given in each table. Comparing runs 9 and 10 in which the same surface was used, except that run 10 was made after the boiler was removed and the sodium was reacted, show that the controlled cavity radius was smaller in run 10 then in run 9. This confirms once again that any re-entry type cavity may become plugged after the sodium is reacted. The results of runs 6 to 12 were used in establishing the relation between the waiting time, the degree of superheat, and the heat flux.

The third group of runs consists of runs 13 and 14, which have a predescribed cavity size. The boiler plates of runs 13 and 14 were made

of nickel "A" polished to a mirror finish. In run 13 one re-entry type cavity was fabricated in the middle of the surface with a cavity mouth diameter of 0.005 inch, whereas in run 14 one cylindrical cavity of 0.0105-inch diameter x 0.150-inch long was drilled in the middle of the surface. The Chromel-Alumel thermocouples which were near the surface did not touch the cavity in both cases. The results of these runs confirmed the relation (C-13) for the surface superheat during stable boiling and gave more data points for the desired relation between the waiting time, the degree of superheat, and the heat flux.

In order to combine the results of runs 6 to 14 in one single curve, the data points were plotted with $\frac{q_o}{\theta_w(0,0)}$ versus the waiting time τ, in Figure (22). Such plotting eliminates the use of either the cavity radius or the pressure as a parameter, since $\theta_w(0,0)$ combines the two factors. The theoretical curve, Equation (11), is also plotted in Figure (22), which is a general curve for sodium (almost independent of the solid material). For different liquid metals this curve will be shifted according to the liquid properties.

All the experimental data points lie above the theoretical curve; namely, for any value $\frac{q_o}{\theta_w(0,0)}$, the experimental waiting time is longer than the predicted one from Equation (11).

Some recorded temperature fluctuations during stable boiling are given in Figures 23, 24, 25, and 26. At low heat flux and long waiting time, it is very easy to see the periodic behaviour of these fluctuations and to calculate the average waiting time. The calculated temperature variations are plotted versus the time in Figure (27), using

Equations (18) and (19), where the position in the boiler plate is a parameter.

6.3 Empirical Correlation

The model analyzed assumed pure conduction heat transfer to a stagnant liquid.

The difference between the heat transfer q_o and this heat transfer to the liquid determines the rate of rise of the wall surface temperature. Actually the heat transferred to the liquid will be greater than that resulting from the assumption in the model because of convection effects in the liquid. To retain the expression resulting from the conduction model and attempt to account for this convection effect, we alternatively may increase the rate of heat transfer to the liquid or reduce the magnitude of q_o in the equation. As an empirical approximation to account for the convection effect, we tried reducing q_o by an amount equal to 1.4 times the natural convection heat flux corresponding to the maximum wall temperature during the transient existing after boiling has begun.

It is emphasized that this is an empirical correction to attempt to account for the convection effects, but is applied to q_o to reduce the difference between the actual q_o and the heat transferred to the liquid in the simplified conduction model. This leads to the following equation:

$$\sqrt{\tau} = \frac{\theta_w(0,0)\sqrt{k_\ell \rho_\ell c_\ell}}{[q_o - h\,\theta_w(0,0)]}\, I(\beta) \qquad (30)$$

where h is taken here as constant at h = 1200 BTU/ft^{2}hr.

Equation (30) is also plotted in Figure (22). At all waiting times above 0.5 sec., the agreement of the empirical correlation curve with the data points is quite good. At much shorter times the deviation of the data from the curve is greater. This is due to the fact that for short waiting times, the effect of the bubble growth and departure time may become more important and probably cannot be simply neglected as was done in the theoretical model of Chapter 2.

6.4 The Limiting Curve for Stable Boiling

Run No. 14 was made to check the stability criterion, Equation (26). For the cavity size chosen and in the range of heat fluxes used in this experiment, we should expect to obtain regions for which boiling is stable and regions for which boiling stops and natural convection occurs. The limiting points for stable boiling were obtained in the following way: First, stable boiling was achieved at high heat fluxes, and then the power was decreased until boiling stopped. For different pressures different heat fluxes existed for which boiling stopped. It was very difficult to control the exact limiting heat flux since the input power could not be adjusted very sensitively. Figure (28) shows the data points of run 14 where the heat flux q_o is plotted versus the surface superheat $\Theta_w(0,0)$. The limiting points designated by $\oplus$ were stable boiling, and after slightly reducing the power, boiling stopped and natural convection began with increasing boiler plate temperatures. Figure (29) shows a recorded temperature of the thermocouple near the surface when the transition from boiling to natural convection took place while decreasing the input power.

In Figure (28) there are also plotted the predicted limiting curve of this work, Equation (26), and the modified Marto (5) prediction, Equation (22), for the same given cavity length. The figure shows that the predicted Equation (26) is much lower than the experimental points. In the light of paragraph 6.3, the waiting time as well as the relaxation length were found to be greater than that predicted. The empirical correlation (30) together with Equations (13), (23), and (24) will therefore give an empirical correlation for the limiting heat flux

$$q_o > \left[h + \frac{\sqrt{k_\ell \rho_\ell c_{p\ell} \alpha_\omega}}{\ell} \eta(\beta)\, I(\beta)\, J(\beta) \right] \theta_\omega(0,0) \qquad (31)$$

where h is the same constant as in Equation (30), h = 1200 BTU/ft^{2}hr. Equation (31) is also plotted in Figure (28). The agreement of this equation with the experimental results is remarkably good.

Only two cases were found in the literature where cylindrical cavities were used in boiling liquid metals. Marto (5) used ten cylindrical cavities of 0.004-inch diameter x 0.018-inch long. Using this cavity dimension in Equation (31), the limiting heat fluxes for stable boiling of sodium are given in Figure (30). All the data points of run 24 of Marto were below this curve; therefore, stable boiling was not reached.

The other case with a cylindrical cavity was made by Hoffman (18) where potassium was boiled from a surface with a "hot finger" of 0.050-inch diameter x 0.250-inch long, drilled in the boiler surface. Using this cavity length with the properties for potassium in Equation (31), we obtain the limiting heat fluxes, Figure (30).

Hoffman (18) reported that stable boiling was obtained if the "hot finger" temperature was kept more than 65 ^{o}C above the liquid temperature at the measured point. No direct observations of heat fluxes or surface superheat were presented.

6.5 Plots of Heat Fluxes vs. Superheat

Since it is quite common to present any heat transfer data of boiling in a plot of heat flux versus wall superheat, we present here these plots in Figures 31 to 39. It becomes obvious from this work that the term wall superheat in boiling liquid metals is meaningless since any temperature measuring device at the surface will never read a unique temperature. We therefore specify here two terms of wall superheat. The first one is the extrapolated wall temperature minus the saturation temperature ($T_{w\ ext.}-T_{sat}$), and the second one is the maximum wall temperature at each period minus the saturation temperature $\theta_{w}(0,0)$. In Figures 31, 32, and 33 only the first type of superheat was calculated and plotted. In Figures 34 to 39 the two expressions for wall superheat are presented for any heat flux during stable boiling. These two values are connected with a solid line and represent one data point.

The dotted lines in these figures represent bumping data where approximate values were measured. In Figure 33 the three regions of heat transfer are shown schematically.

7. SUMMARY AND CONCLUSIONS

When heat is transferred to liquid sodium in a pool, three different phenomena are observed. At low heat fluxes heat is transferred by natural convection with heat transfer coefficients of the order of 800 to 1,000 BTU/ft^{2}hr$^\circ$F. At higher heat fluxes stable nucleate boiling may exist with much higher heat transfer coefficients. A transition between natural convection and stable nucleate boiling is always observed. This transition phenomenon is called bumping and is characterized by large temperatures and pressure fluctuations due to the fact that no active cavities exist for that given heat flux.

During stable nucleate boiling temperature variations exist in the solid surface and its close vicinity. A simplified theoretical model for the mechanism of heat transfer in pool boiling of liquid alkali metals was presented which predicts the temperature variations in the solid material and the frequency of bubble formation as functions of the wall superheat, the heat flux, and the solid-liquid properties.

From this simplified model a criterion was established for the minimum heat flux for which stable boiling exists. The criterion shows that the minimum heat flux for stable boiling is a function of the liquid-solid properties, liquid pressure, the degree of superheat, and cavity size.

A set of experimental runs was performed on an existing apparatus using various surfaces with artificial cavities. Heat fluxes of 20,000 to 300,000 FTU/ft^{2}hr were obtained at various pressures between 40 to 106 mm Hg.

The experimental results of the period time for bubble formation are in good agreement with an empirical correlation, which is a modification of the theoretical prediction of the simplified model. Also, the experimental results for the criterion of minimum heat fluxes for which stable boiling exists are in good agreement with the predicted one, using the same modificated expression.

Conclusions

1. During stable nucleate pool boiling of sodium, the solid surface temperature fluctuates between the temperature required to initiate an active cavity of a given size and some lower temperature depending on the liquid-solid properties.
2. In liquid metals the frequency of bubble formation from a given cavity is a function of the degree of superheat, the heat flux, and the liquid thermal properties and is almost independent on the solid thermal properties.
3. For uniform distributed cavities of equal size, the degree of superheat and the minimum surface temperature are not functions of the heat flux.
4. Stable nucleate boiling can exist in sodium from cylindrical cavities provided the degree of superheat, the cavity geometry, and the heat flux satisfy the Equation (31).
5. Better stability conditions in boiling sodium can be obtained with solid metals of lower thermal diffusivity.
6. Convection heat transfer has an effect on the period of bubble formation and the stability criterion.

Recommendations

1. Further work should be done at smaller cavity sizes and higher heat fluxes and pressures.
2. An attempt should be made to measure the bubble size and frequency by direct observation of the bubbles.
3. The surface temperature variations during stable nucleate boiling should be measured directly with sensible instruments, similar to what was used by Cooper (9).
4. A simplified model for cavity distribution of various sizes should be adopted from which analytical and experimental work could be performed in order to find the behaviour of any commercial surfaces.

BIBLIOGRAPHY

1. Lyon, R. E., Foust, A. S., and Katz, D. L., "Boiling Heat Transfer with Liquid Metals," Chem. Engr. Prog. Symposium Series No. 17, 51 (1955).

2. Madsen, N. and Bonilla, C. F., "Heat Transfer to Boiling Sodium-Potassium Alloy," Chem. Engr. Prog. Symposium Series No. 30, 56 (1959).

3. Noyes, R. C., "Boiling Studies for Sodium Reactor Safety," Part 1 NAA-SR-7909 (1963).

4. Colver, C. P., "A Study of Saturated Pool Boiling Potassium up to Burnout Heat Fluxes," Ph.D. Thesis, U. of Michigan (1963) (cited in 5).

5. Marto, P. J. and Rohsenow, W. M., "The Effect of Surface Conditions on Nucleate Pool Boiling Heat Transfer to Sodium," Ph.D. Thesis, M.I.T. Report No. 5219-33 (1965).

6. Krakoviak, A. I., "Notes on the Liquid Metal Boiling Phenomenon," ORNL-TM-618 (1963).

7. Moore, F. D. and Mesler, R. B., "The Measurement of Rapid Surface Temperature Fluctuations During Nucleate Boiling of Water," A.I.Ch.E. Jl. (1961).

8. Bonnet, C., Macke, E., and Morin, R., "Visualization of Bubble Formation at Atmospheric Pressure and Related Measurement of the Wall Temperature Variations," EUR 1622.e. (1965).

9. Cooper, M. G. and Lloyd, A. J. P., "Transient Local Heat Flux in Nucleate Boiling," Proceeding of the Third International Heat Transfer Conference, Chicago, Vol. III, pp. 193-203 (1966).

10. Zuber, N. "The Dynamics of Vapor Bubbles in Nonuniform Temperature Fields," Int. J. Heat Mass Transfer, 2 pp. 83-98 (1961).

11. Han, C. Y. and Griffith, P., "The Mechanism of Heat Transfer in Nucleate Pool Boiling - Part I," Int. J. Heat Mass Transfer, 8 pp. 887-904 (1965).

12. Hamburger, L. G., "On the Growth and Rise of Individual Vapor Bubbles in Nucleate Pool Boiling," Int. J. Heat Mass Transfer, 8 pp. 1369-1386 (1965).

13. Deyer, V. I. and Solovyev, A. N., "On the Mechanism of Boiling of Liquid Sodium on a Heating Surface at Free Convection," Translation from Inzhenerno-Fizicheskiy Zhurnal (Russian), Vol. 7 No. 6 (1964).

14. Bankoff, S. G., "Ebullition from Solid Surfaces in the Absence of a Pre-existing Gaseous Phase," Heat Transfer and Fluid Mechanics Institute, Stanford, Cal. (1956).

15. Hsu, S. T. and Schmidt, F. W., "Measured Variations in Local Surface Temperatures in Pool Boiling of Water," ASME-A.I.Ch.E. Heat Transfer Conference, Buffalo, N. Y. (1960).

16. Kroger, D. G., "Heat Transfer During Film Condensation of Potassium Vapor," D.Sc Thesis, M.I.T. Report No. 75239-42 (1966).

17. Bonilla, C. F., Sawhney, D. L., and Makansi, M. M., "Vapor Pressure of Alkali Metals, III Rubidium, Cesium, and Sodium-Potassium Alloy Up To 100 Pounds per Square Inch," Proc. of 1962 High-Temperature Liquid-Metal Heat Transfer Technology Meeting, BNL 756 (1962).

18. Hoffman, E. E., "Metals and Ceramics Div. Annual Progress Report," ORNL-3470, pp. 114-118 (1963).

19. Carslaw, H. S. and Jaeger, J. C., "Conduction of Heat in Solids," Oxford University Press (1950).

20. Bergles, A. E. and Rohsenow, W. M., "The Determination of Forced-Convection Surface-Boiling Heat Transfer," ASME paper 63-HT-22 (1963).

21. Hsu, Y. Y. and Graham, R. W., "An Analytical and Experimental Study of the Thermal Boundary Layer and Ebullition Cycle in Nucleate Boiling," NASA TN-D-594 (1961).

22. Lemmon, A. W., Jr., Deem, H. W., Hall, E. H., and Walling, J. F., "The Thermodynamic and Transport Properties of Potassium," Proceeding of 1963 High-Temperature Liquid-Metal Heat Transfer Technology Meeting, Vol. 1, USAEC Report ORNL-3605 (1964).

23. Achener, P. Y., "The Determination of the Latent Heat of Vaporization and Vapor Pressure of Potassium from 1000 to 1900 °F," Aerojet-General Nucleonics Report AGN-8141 (1965). (Cited in 28)

24. Achener, P. Y., "The Determination of the Latent Heat of Vaporization, Vapor Pressure, Enthalpy, and Density of Liquid Rubidium and Cesium Up To 1800 °F," Proceeding of 1963 High-Temperature Liquid-Metal Heat-Transfer Technology Meeting, Vol. 1, USAEC Report ORNL-3605 (1964).

25. Tepper, F., Murchison, A., Zelenak, J., and Roehlich, F., "Thermophysical Properties of Rubidium and Cesium," Proceeding of 1963 High-Temperature Liquid-Metal Heat Transfer Technology Meeting, Vol. 1, USAEC Report ORNL-3605 (1964).

26. Keenan, J. H. and Keyes, F. G., "Thermodynamic Properties of Steam," John Wiley & Sons, Inc. (1957).

27. Scriven, L. E., "On the Dynamics of Phase Growth," Chem. Engr. Sci., 10 pp. 1-13 (1959).

28. Wichner, R. P. and Hoffman, H. W., "Vapor-Bubble-Growth Rates in Superheated Liquid Metals," USAEC Report ORNL-TM-1413 (1966).

29. Hogan, C. L. and Sawyer, R. B., "The Thermal Conductivity of Metals at High Temperature," Jl. of Applied Physics, 23 p. 177 (1952).

APPENDIX A

SOLUTION TO THE TRANSIENT HEAT CONDUCTION

Following the assumptions given in (2.3.2), the energy equations with their initial and boundary conditions are as follows: (See Figure 2.)

$$\frac{\partial^2 \theta_\omega}{\partial x^2} = \frac{1}{\alpha_\omega} \frac{\partial \theta_\omega}{\partial t} \tag{A-1a}$$

$$\frac{\partial^2 \theta_\ell}{\partial y^2} = \frac{1}{\alpha_\ell} \frac{\partial \theta_\ell}{\partial t} \tag{A-1b}$$

where $\theta = T - T_{sat}$.

At $t = 0$

$$0 \leq x \leq L \qquad \theta_\omega(x,0) = a + bx + c x^2 \tag{A-2a}$$

where

$$a = \theta_\omega(0,0)$$

$$b = \theta_\omega'(0,0)$$

$$c = \frac{\theta_\omega''(0)}{2} \quad \text{(not function of position)}$$

Therefore,

$$\theta_\omega(x,0) = \theta_\omega(0,0) + \theta_\omega'(0,0)\, x + \theta_\omega''(0) \frac{x^2}{2} \tag{A-2b}$$

$$0 \leq y \qquad \theta_\ell(y,0) = 0 \tag{A-2c}$$

at $t > 0$

$$x = L \qquad k_\omega \frac{\partial \theta_\omega(L,t)}{\partial x} = q_o \quad \text{(constant)} \tag{A-3a}$$

$$y \to \infty \qquad \theta_\ell(\infty, t) = 0 \tag{A-3b}$$

At $t > 0$, $x = 0$, $y = 0$

$$\theta_\ell(0,t) = \theta_\omega(0,t) \tag{A-4a}$$

$$-k_\ell \frac{\partial \theta_\ell(0,t)}{\partial y} = k_\omega \frac{\partial \theta_\omega(0,t)}{\partial x} \tag{A-4b}$$

The Laplace Transformations of Equations (A-1a and A-1b) after using the initial conditions (A-2b and A-2c) are:

$$\frac{d^2\bar{\theta}_\omega}{dx^2} - \frac{s}{\alpha_\omega}\bar{\theta}_\omega + \frac{\theta_\omega(x,0)}{\alpha_\omega} = 0 \tag{A-5a}$$

$$\frac{d^2\bar{\theta}_\ell}{dy^2} - \frac{s}{\alpha_\ell}\bar{\theta}_\ell = 0 \tag{A-5b}$$

where s is a complex variable, and

$\bar{\theta}$ is the Laplace Transformation of θ.

The transformed boundary conditions become:

At $x = L$ $$k_\omega \frac{d\bar{\theta}_\omega(L,s)}{dx} = \frac{q_o}{s} \tag{A-6a}$$

$$y \to \infty \qquad \bar{\theta}_\ell(\infty, s) = 0 \tag{A-6b}$$

At $x = 0$, $y = 0$

$$\bar{\theta}_\ell(0,s) = \bar{\theta}_\omega(0,s) \tag{A-7a}$$

$$-k_\ell \frac{d\bar{\theta}_\ell(0,s)}{dy} = k_\omega \frac{d\bar{\theta}_\omega(0,s)}{dx} \tag{A-7b}$$

The solutions to Equations (A-5a and A-5b) are:

$$\bar{\theta}_\omega(x,s) = C_1 e^{-\sqrt{s/\alpha_\omega}\,x} + C_2 e^{\sqrt{s/\alpha_\omega}\,x} + \frac{\theta_\omega(x,0)}{s} + \frac{\alpha_\omega}{s^2}\,\theta_\omega''(0) \qquad \text{(A-8a)}$$

$$\bar{\theta}_\ell(y,s) = C_3 e^{-\sqrt{s/\alpha_\ell}\,y} + C_4 e^{\sqrt{s/\alpha_\ell}\,y} \qquad \text{(A-8b)}$$

From Equation (A-6a)

$$k_\omega \frac{d\bar{\theta}_\omega(L,s)}{dx} = k_\omega \sqrt{s/\alpha_\omega}\left(-C_1 e^{-\sqrt{s/\alpha_\omega}\,L} + C_2 e^{\sqrt{s/\alpha_\omega}\,L}\right) + k_\omega \frac{\theta_\omega'(L,0)}{s} = \frac{q_o}{s}$$

but $\theta_\omega'(L,0) = \frac{q_o}{k_\omega}$;

therefore,

$$C_1 = C_2 e^{2L\sqrt{s/\alpha_\omega}} \qquad \text{(A-9a)}$$

and from Equation (A-6b) $\qquad C_4 = 0 \qquad \text{(A-9b)}$

Using the conditions (A-9) in Equations (A-8), we get

$$\bar{\theta}_\omega(x,s) = C_2\left[e^{\sqrt{s/\alpha_\omega}\,x} + e^{-\sqrt{s/\alpha_\omega}\,(x-2L)}\right] + \frac{\theta_\omega(x,0)}{s} + \frac{\alpha_\omega}{s^2}\theta_\omega''(0) \qquad \text{(A-10a)}$$

$$\bar{\theta}_\ell(y,s) = C_3 e^{-\sqrt{s/\alpha_\ell}\,y} \qquad \text{(A-10b)}$$

Applying Equation (A-7a) gives

$$C_3 = C_2\left(1 + e^{\sqrt{s/\alpha_\omega}\,2L}\right) + \frac{\theta_\omega(0,0)}{s} + \frac{\alpha_\omega}{s^2}\,\theta_\omega''(0) \qquad \text{(A-11a)}$$

and Equation (A-7b) gives

$$k_\ell\sqrt{s/\alpha_\ell}\,C_3 = C_2 k_\omega \sqrt{s/\alpha_\omega}\left(1 - e^{2L\sqrt{s/\alpha_\omega}}\right) + \frac{k_\omega\,\theta_\omega'(0,0)}{s} \qquad \text{(A-11b)}$$

Defining the following values

$$\left.\begin{aligned} \beta &= \frac{k_\omega \sqrt{\alpha_\ell}}{k_\ell \sqrt{\alpha_\omega}} & \varepsilon &= \frac{\beta - 1}{\beta + 1} \\ \gamma &= \sqrt{\alpha_\omega / \alpha_\ell} & q &= \sqrt{s/\alpha_\omega} \end{aligned}\right\} \qquad \text{(A-12)}$$

Now, solving the two Equations (A-11) and using the above definitions (A-12), we can find the two unknowns c_2 and c_3.

$$C_2 = \frac{e^{-2Lq}\left[\frac{\beta\theta_\omega'(0,0)}{sq} - \frac{\theta_\omega(0,0)}{s} - \frac{\alpha_\omega \theta_\omega''(0)}{s^2}\right]}{(1+\beta)\left[1 - \varepsilon\, e^{-2Lq}\right]} \qquad \text{(A-13a)}$$

$$C_3 = \frac{\theta_\omega(0,0)}{s} + \frac{\alpha_\omega \theta_\omega''(0)}{s^2} + \frac{\left[\frac{\beta\theta_\omega'(0,0)}{sq} - \frac{\theta_\omega(0,0)}{s} - \frac{\alpha_\omega\theta_\omega''(0)}{s^2}\right]\left[1 + e^{-2Lq}\right]}{(1+\beta)\left[1 - \varepsilon\, e^{-2Lq}\right]} \qquad \text{(A-13b)}$$

The term $\frac{1}{1 - \varepsilon\, e^{-2Lq}}$ can be expanded into a series, since $|\varepsilon| < 1$ and $2Lq > 0$. After expansion this term becomes:

$$\frac{1}{1 - \varepsilon e^{-2Lq}} = \sum_{n=0}^{\infty} \varepsilon^n e^{-2nLq} \qquad . \qquad \text{(A-14)}$$

Putting Equations (A-13) and (A-14) into Equations (A-10), we finally find the solutions for $\bar{\theta}_\omega(x,s)$ and $\bar{\theta}_\ell(y,s)$.

$$\bar{\theta}_\omega(x,s) = \frac{1}{1+\beta}\left[\frac{\beta\theta_\omega'(0,0)}{sq} - \frac{\theta_\omega(0,0)}{s} - \frac{\alpha_\omega\theta_\omega''(0)}{s^2}\right]\left[\sum_{n=0}^{\infty} \varepsilon^n \left(e^{-q[(n+1)2L - x]} + e^{-q(2nL+x)}\right)\right] +$$

$$+ \frac{\theta_\omega(x,0)}{s} + \frac{\alpha_\omega\theta_\omega''(0)}{s^2} \qquad \text{(A-15a)}$$

$$\bar{\theta}_\ell(y,s) = \frac{1}{1+\beta}\left[\frac{\beta\theta_\omega'(0,0)}{sq} - \frac{\theta_\omega(0,0)}{s} - \frac{\alpha_\omega\theta_\omega''(0)}{s^2}\right]\left[\sum_{n=0}^{\infty} \varepsilon^n \left(e^{-q[(n+1)2L + \gamma y]} + e^{-q(2nL + \gamma y)}\right)\right] +$$

$$+ \left[\frac{\theta_\omega(0,0)}{s} + \frac{\alpha_\omega\theta_\omega''(0)}{s^2}\right] e^{-q\gamma y} \qquad \text{(A-15b)}$$

The inverted equations of the above Laplace Transformations involved the following terms:

$$erfc.\left[\frac{(n+1)2L-X}{2\sqrt{\alpha_\omega t}}\right] \quad ; \quad erfc.\left[\frac{2nL+X}{2\sqrt{\alpha_\omega t}}\right] \quad ;$$

$$exp\left\{-\left[\frac{(n+1)2L-X}{2\sqrt{\alpha_\omega t}}\right]^2\right\} \quad ; \quad exp\left\{-\left[\frac{2nL+X}{2\sqrt{\alpha_\omega t}}\right]^2\right\} \quad ;$$

As will be shown later these terms approach zero for any value of $n > 0$ since $\frac{L}{\sqrt{\alpha_\omega t}} > 1.55$ for all times of a full cycle. We shall therefore use terms with n = 0 only.

After using the inversion of Laplace Transformations from (19), we find the temperature history in the solid and in the liquid.

$$\theta_\omega(X,t) = \theta_\omega(X,0) + \alpha_\omega t\,\theta_\omega''(0) - \frac{\theta_\omega(0,0)}{1+\beta}\left[erfc\left(\frac{X}{2\sqrt{\alpha_\omega t}}\right) + erfc\left(\frac{2L-X}{2\sqrt{\alpha_\omega t}}\right)\right] +$$

$$+\frac{\beta}{1+\beta}\theta_\omega'(0,0)\left[2\sqrt{\frac{\alpha_\omega t}{\pi}}\left(e^{-\frac{X^2}{4\alpha_\omega t}} + e^{-\frac{(2L-X)^2}{4\alpha_\omega t}}\right) - X\,erfc\left(\frac{X}{2\sqrt{\alpha_\omega t}}\right) - (2L-X)\,erfc\left(\frac{2L-X}{2\sqrt{\alpha_\omega t}}\right)\right] +$$

$$+\frac{\alpha_\omega\theta_\omega''(0)}{1+\beta}\left[(2L-X)\sqrt{\frac{t}{\pi\alpha_\omega}}\,e^{-\frac{(2L-X)^2}{4\alpha_\omega t}} - \left(t+\frac{(2L-X)^2}{2\alpha_\omega}\right)erfc\left(\frac{2L-X}{2\sqrt{\alpha_\omega t}}\right)\right] +$$

$$+\frac{\alpha_\omega\theta_\omega''(0)}{1+\beta}\left[X\sqrt{\frac{t}{\pi\alpha_\omega}}\,e^{-\frac{X^2}{4\alpha_\omega t}} - \left(t+\frac{X^2}{2\alpha_\omega}\right)erfc\left(\frac{X}{2\sqrt{\alpha_\omega t}}\right)\right] \qquad \text{(A-16a)}$$

$$\theta_\ell(y,t) = \frac{\beta}{1+\beta}\theta_\omega(0,0)\left[erfc.\left(\frac{y}{2\sqrt{\alpha_\ell t}}\right) - \frac{1}{\beta}\,erfc\left(\frac{2L+\gamma y}{2\sqrt{\alpha_\omega t}}\right)\right] +$$

$$+\frac{\beta}{1+\beta}\theta_\omega'(0,0)\left\{2\sqrt{\frac{\alpha_\omega t}{\pi}}\left[e^{-\frac{y^2}{4\alpha_\ell t}} + e^{-\frac{(2L+\gamma y)^2}{4\alpha_\omega t}}\right] - \gamma y\,erfc\left(\frac{y}{2\sqrt{\alpha_\ell t}}\right) - (2L+\gamma y)\,erfc\left(\frac{2L+\gamma y}{2\sqrt{\alpha_\omega t}}\right)\right\} +$$

$$+\frac{1}{1+\beta}\alpha_\omega\theta_\omega''(0)\left\{(2L+\gamma y)\sqrt{\frac{t}{\pi\alpha_\omega}}\,e^{-\frac{(2L+\gamma y)^2}{4\alpha_\omega t}} - \left[t+\frac{(2L+\gamma y)^2}{2\alpha_\omega}\right]erfc\left(\frac{2L+\gamma y}{2\sqrt{\alpha_\omega t}}\right)\right\} +$$

$$+\frac{\beta}{1+\beta}\alpha_\omega\theta_\omega''(0)\left[\left(t+\frac{y^2}{2\alpha_\ell}\right)erfc\left(\frac{y}{2\sqrt{\alpha_\ell t}}\right) - y\sqrt{\frac{t}{\pi\alpha_\ell}}\,e^{-\frac{y^2}{4\alpha_\ell t}}\right] \qquad \text{(A-16b)}$$

These two equations satisfy the two differential equations and the initial and boundary conditions; therefore, they are a complete solution to the problem.

Since y > 0 and as mentioned before $\frac{L}{\sqrt{\alpha_\omega t}} > 1.55$, we can neglect all terms containing L in Equation (A-16b)

$$\theta_\ell(y,t) = \frac{\beta}{1+\beta}\left\{\theta_\omega(0,0)\,\mathrm{erfc}\left(\frac{y}{2\sqrt{\alpha_\ell t}}\right) + \theta_\omega'(0,0)\left[2\sqrt{\frac{\alpha_\omega t}{\pi}}\,e^{-\frac{y^2}{4\alpha_\omega t}} - \gamma y\,\mathrm{erfc}\left(\frac{y}{2\sqrt{\alpha_\ell t}}\right)\right] + \right.$$

$$\left. + \alpha_\omega \theta_\omega''(0)\left[\left(t+\frac{y^2}{2\alpha_\ell}\right)\mathrm{erfc}\left(\frac{y}{2\sqrt{\alpha_\ell t}}\right) - y\sqrt{\frac{t}{\pi\alpha_\ell}}\,e^{-\frac{y^2}{4\alpha_\ell t}}\right]\right\} \qquad \text{(A-16c)}$$

Furthermore, for values of x near the surface where x = 0, we can neglect all terms containing L also in the solution (A-16a)

$$\theta_\omega(x,t) = \theta_\omega(x,0) + \alpha_\omega t\,\theta_\omega''(0) - \frac{\theta_\omega(0,0)}{1+\beta}\,\mathrm{erfc}\left(\frac{x}{2\sqrt{\alpha_\omega t}}\right) +$$

$$+ \frac{\beta}{1+\beta}\,\theta_\omega'(0,0)\left[2\sqrt{\frac{\alpha_\omega t}{\pi}}\,e^{-\frac{x^2}{4\alpha_\omega t}} - x\,\mathrm{erfc}\left(\frac{x}{2\sqrt{\alpha_\omega t}}\right)\right] +$$

$$+ \frac{\alpha_\omega \theta_\omega''(0)}{1+\beta}\left[x\sqrt{\frac{t}{\pi\alpha_\omega}}\,e^{-\frac{x^2}{4\alpha_\omega t}} - \left(t+\frac{x^2}{2\alpha_\omega}\right)\mathrm{erfc}\left(\frac{x}{2\sqrt{\alpha_\omega t}}\right)\right] \qquad \text{(A-16d)}$$

The solutions (A-16c and A-16d) are functions of position, time, and initial temperature profile in the solid. This initial temperature profile will be found later in Appendix B by applying the conditions of a periodic process.

APPENDIX B

THE CONDITIONS FOR A PERIODIC PROCESS

In order to satisfy a periodic process, we have to fulfill the following three requirements:

I. The surface temperature varies with a period time $\mathcal{T}$ or

$$\theta_\omega(0,\mathcal{T}) = \theta_\omega(0,0) \tag{B-1}$$

II. The temperature slope at the surface varies with the same period time

$$\frac{\partial \theta_\omega(0,\mathcal{T})}{\partial X} = \theta'_\omega(0,0) \tag{B-2}$$

III. The average heat flux at the surface during the period time is equal to the constant heat flux far away from the surface at $x \geq L$, or

$$q_0 = \frac{k_\omega}{\mathcal{T}} \int_0^{\mathcal{T}} \frac{\partial \theta_\omega(0,t)}{\partial X}\, dt \tag{B-3}$$

Applying x = 0 to Equation (10-a) will give us the surface temperature as a function of time

$$\theta_\omega(0,t) = \frac{\beta}{1+\beta}\left[\theta_\omega(0,0) + 2\sqrt{\frac{\alpha_\omega t}{\pi}}\,\theta'_\omega(0,0) + \alpha_\omega t\,\theta''_\omega(0)\right] \tag{B-4}$$

Also taking the derivitive of Equation (10-a) with respect to x and applying x = 0, we shall get the temperature slope at the surface as a function of time.

$$\frac{\partial \theta_\omega(0,t)}{\partial X} = \frac{1}{1+\beta}\left[\theta'_\omega(0,0) + \frac{\theta_\omega(0,0)}{\sqrt{\pi \alpha_\omega t}} + 2\sqrt{\frac{\alpha_\omega t}{\pi}}\,\theta''_\omega(0)\right] \tag{B-5}$$

Now, we put the requirement (B-1) into (B-4) and the requirement (B-2) into (B-5) to get

$$\theta_\omega(0,0) = 2\beta\sqrt{\frac{\alpha_\omega \mathcal{T}}{\pi}}\,\theta_\omega'(0,0) + \alpha_\omega \mathcal{T} \beta\, \theta_\omega''(0) \tag{B-6a}$$

$$\beta\,\theta_\omega'(0,0) = \frac{\theta_\omega(0,0)}{\sqrt{\pi \alpha_\omega \mathcal{T}}} + 2\sqrt{\frac{\alpha_\omega \mathcal{T}}{\pi}}\,\theta_\omega''(0) \tag{B-6b}$$

We can express the two unknowns in Equations (6) as a function of the period time $\mathcal{T}$ and the superheat $\theta_\omega(0,0)$

$$\theta_\omega'(0,0) = \frac{\theta_\omega(0,0)}{\sqrt{\pi \alpha_\omega \mathcal{T}}}\,\frac{\pi(2+\beta)}{\beta(\pi\beta+4)} \tag{B-7}$$

$$\theta_\omega''(0) = \frac{\theta_\omega(0,0)}{\alpha_\omega \mathcal{T}}\left(\frac{\pi-2}{\pi\beta+4}\right) \tag{B-8}$$

Using (B-7) and (B-8) in (B-5) and applying the third condition (B-3)

$$q_o = \frac{k_\omega\,\theta_\omega(0,0)}{\mathcal{T}\sqrt{\pi \alpha_\omega \mathcal{T}}} \int_0^{\mathcal{T}} \left[\frac{\pi(2+\beta)}{\beta(\pi\beta+4)} + \sqrt{\frac{\mathcal{T}}{t}} + \frac{2(\pi-2)}{\pi\beta+4}\sqrt{\frac{t}{\mathcal{T}}}\right] dt \tag{B-9}$$

After performing the integration and rearranging the terms, we finally come to the relation between the heat flux, the degree of superheat, and the waiting time $\mathcal{T}$.

$$q_o = \frac{k_\omega\,\theta_\omega(0,0)}{\beta\sqrt{\alpha_\omega \mathcal{T}}}\, I(\beta) \tag{B-10}$$

where

$$I(\beta) = \frac{6\pi + 6\pi\beta^2 + 7\pi\beta + 16\beta}{3\sqrt{\pi}\,(1+\beta)(\pi\beta+4)} \tag{B-11}$$

Using the definition of $\beta = \dfrac{k_\omega\sqrt{\alpha_\ell}}{k_\ell\sqrt{\alpha_\omega}}$, we rearrange Equation (B-10)

$$\sqrt{\mathcal{T}} = \frac{\theta_\omega(0,0)\sqrt{k_\ell\,\rho_\ell\,c_\ell}}{q_o}\, I(\beta) \tag{B-12}$$

APPENDIX C

LIQUID SUPERHEAT DURING STABLE BOILING

Today it is quite commonly accepted that boiling takes place from discrete points on the solid surface. These points are cavities containing vapor or gas phase in equilibrium with the surrounding liquid.

If we assume that the boiling was maintained for quite some time, then the effect of gas can be neglected, and only the vapor in the cavity should be considered. Furthermore, we shall assume that far away from the solid surface the liquid is at the saturation temperature corresponding to the liquid pressure.

At the point just before the bubble starts to grow from the cavity, Bergles and Rohsenow (20), following Hsu and Graham (21), consider an hemispherical vapor bubble of radius r in a mechanical and thermodynamic equilibrium with the liquid. The mechanical equilibrium requires that

$$P_{vr} - P_{sat.} = \frac{2\sigma}{r} \qquad \text{(C-1)}$$

where P_{vr} is the vapor pressure in a curvature interface, σ is the surface tension, and r is the cavity radius. The thermodynamic equilibrium requires that

$$T_v = T_\ell \qquad \text{(C-2)}$$

where T_v is the vapor temperature in the cavity, and T_ℓ is the liquid temperature around the bubble. Since $P_{vr} > P_{sat}$ for the bubble to grow, the liquid is superheated in respect to its pressure.

In order to find the amount of superheat in the liquid, Bergles and Rohsenow (20) applied the Clapeyron equation together with the perfect gas approximation to obtain

$$T_v - T_{sat.} = \frac{T_v T_{sat.} R_v}{h_{fg}} \ln\left(1 + \frac{2\sigma}{r P_{sat.}}\right) \tag{C-3}$$

where R_v is the vapor constant and h_{fg} is the heat of vaporization.

A similar expression can be obtained by using the pressure-temperature relation along the saturation line for a flat interface. This relation is most commonly given in the following form:

$$\log_{10} P = A - \frac{B}{T} \tag{C-4}$$

In fact most of the data on liquid metals are presented in the form of Equation (C-4). (17), (22), (24).

Writing Equation (C-4) for the two pressures, P_{sat} and P_v, and subtracting one from the other, we get

$$\log_{10}\left(P_v/P_{sat.}\right) = B\left(\frac{1}{T_{sat.}} - \frac{1}{T_v}\right) \tag{C-5}$$

This relation exists on a flat interface, and, therefore, P_v is slightly higher than P_{vr} for a curvature interface. If we assume that $P_v \approx P_{vr}$, then, after applying Equation (C-1), we get

$$T_v - T_{sat.} = \frac{T_v T_{sat.}}{B} \log_{10}\left(1 + \frac{2\sigma}{r P_{sat.}}\right) \tag{C-6}$$

In comparison between Equation (C-6) and (C-3), we find that they are equivalent if

$$B = \frac{h_{fg}}{R_v \ln 10} \tag{C-7}$$

While in Equation (C-3) the value $\frac{h_{fg}}{R_v}$ has to be evaluated for each pressure, B in Equation (C-6) is very nearly a constant for a wide range of pressures. This makes Equation (C-6) more useful.

Solving T_v in Equation (C-5), we get

$$T_v = \frac{T_{sat.}}{1 - \frac{T_{sat.}}{B} \log_{10}\left(1 + \frac{2\sigma}{r P_{sat.}}\right)} \qquad \text{(C-8)}$$

Since for all practical values of $\frac{2\sigma}{r P_{sat.}}$, the term

$\frac{T_{sat.}}{B} \log_{10}\left(1 + \frac{2\sigma}{r P_{sat.}}\right) \ll 1$ we can expand (C-8) into a Taylor series and solve for $(T_v - T_{sat})$

$$T_v - T_{sat.} = \frac{T_{sat.}^2}{B} \log_{10}\left(1 + \frac{2\sigma}{r P_{sat.}}\right)\left[1 + \frac{T_{sat.}}{B} \log_{10}\left(1 + \frac{2\sigma}{r P_{sat.}}\right)\right] \qquad \text{(C-9)}$$

Equation (C-9) is applicable to any fluid once the value B for that particular fluid is known. Some values of B for different fluids are given below:

Sodium	Potassium	Rubidium	Cesium	Water
9396.75 (17)	7797.6 (22)	6994.68 (24)	6880.18 (24)	3732.83 (*)
	7707.31(23)	7062.45 (25)	6631.74 (25)	
		6983.03 (17)	6665.30 (17)	

All values of B are in (^{o}R).

(*) The value was calculated from the Steam Tables (26) in the range of pressures between 30 psi to 960 psi.

For all practical purposes, Equation (C-9) can be simplified to

$$T_v - T_{sat.} = \frac{T_{sat.}^2}{B} \log_{10}\left(1 + \frac{2\sigma}{r P_{sat.}}\right) \qquad \text{(C-10)}$$

since the second term on the right-hand side is always small to the order of 2 percent.

Equation (C-10) provides means to calculate the liquid temperature in equilibrium with the ready-to-grow bubble if the saturation pressure or temperature as well as the cavity radius are known. The surface tension σ should be calculated at the vapor temperature rather than at the saturation temperature, but since the variations of σ with temperature are small for moderate superheat, it is a good approximation to evaluate σ at the saturation conditions.

As was assumed by Bergles and Rohsenow (20), the bubble will grow if the liquid temperature at a distance y = r from the wall is equal or greater than the vapor temperature in the hemispherical bubble.

Since r is much smaller than the thickness of the thermal layer, a linear temperature profile in the liquid was approximated.

$$T_w - T_\ell = q_o \frac{r}{k_\ell} \quad , \tag{C-11}$$

or at the moment when the bubble is ready to grow,

$$\theta_w(0,0) = T_w(0,0) - T_{sat.} = (T_v - T_{sat.}) + q_o \frac{r}{k_\ell} \tag{C-12}$$

For liquid metals having high thermal conductivity, the second term in Equation (C-12) can be safely neglected, which makes the wall superheat during stable boiling to be

$$\theta_w(0,0) = \frac{T_{sat.}^2}{B} \log_{10}\left(1 + \frac{2\sigma}{r P_{sat.}}\right) \tag{C-13}$$

Equation (C-13) is plotted for sodium with B = 9396.75 ($^\circ$R) in Figure (40) where the saturation pressure is a parameter.

APPENDIX D

BUBBLE GROWTH AND DEPARTURE IN LIQUID METALS

The main purpose of this Appendix is to get an idea about the time of bubble growth and departure in liquid metals and to compare it to the required time to build the thermal layer (or the waiting time). The material which follows is not an attempt to develop a new theory of bubble growth, but rather is an attempt to obtain an approximation for the relative times for bubble growth and waiting period.

For one component system there are three possible mechanisms which might control the rate of bubble growth:

I. Heat Conduction

II. Rate of Evaporation

III. Mass Inertia of the Displaced Liquid

We shall adopt here for each of the above mechanisms a known theory in the literature and try to apply the same average values which are applicable for sodium. Although the three mechanisms are interrelated, we shall analyze them separately.

D.1 Growth Controlled by Heat Conduction

For the case of a single bubble growing in an unlimited superheated liquid, Scriven (27) presents a complete solution as a function of one parameter β^*. This parameter can be found from the liquid properties and the degree of superheat. When $\rho_v/\rho_\ell \ll 1$, the function of β^* is given below

$$\phi(\beta^*) = \frac{(T_\ell - T_{sat})\,\rho_\ell\, c_\ell}{\rho_v\, h_{fg}} \qquad \text{(D-1)}$$

In the case of sodium boiling at low pressures around 60 mm Hg from a cavity of radius $r = 2.5 \times 10^{-3}$ inch, the superheat is 58 °F. We find that $\phi(\beta^*) = 247$. Using Table I in (27), we find $\beta^* = 240$.

The rate of growth and the bubble radius are given (27)

$$\dot{R} = \beta^* \sqrt{\frac{\alpha_\ell}{t}} \tag{D-2}$$

$$R = 2\beta^* \sqrt{\alpha_\ell t} \tag{D-3}$$

If we assume a maximum bubble radius at departure to be 1 inch, then

$$t_d \leq 4.5 \times 10^{-5} \text{ sec.},$$

and the rate of growth

$$\dot{R}_d = 920 \text{ ft/sec.}$$

If the bubble size is smaller than 1 inch, then the growth time is smaller.

D.2 Growth Controlled by Evaporation

For the same conditions of pressure and temperatures as in D.1, we can find the rate of growth by using kinetic theory (16)

$$\dot{R} = \frac{2\sigma^*}{2-\sigma^*} \left(\frac{Mg}{2\pi R_v T_\ell}\right)^{1/2} \frac{h_{fg}(T_\ell - T_{sat})}{T_\ell} \tag{D-4}$$

where σ^* is an accommodation coefficient found experimentally for liquid metals by Kroger (16) and for the pressure mentioned above $\sigma^* = 0.11$.

Equation (D-4) will give a constant rate of growth of R = 29 ft/sec. By assuming that $R_d \leq 1$ inch, we find the growth time to be

$$t_d \leq 2.9 \times 10^{-3} \text{ sec.}$$

D.3 Growth Controlled by Mass Inertia of Displaced Liquid

Wichner and Hoffman (28) have solved the Rayleigh equation for a bubble growing in a superheated liquid metal when the inertia is the only controlling factor. Their results involve a dimensionless parameter Y given below:

$$Y = \frac{2g^2 \rho_\ell^{3/2} (\rho_\ell - \rho_v) r^3}{g\mu \left(\frac{2\sigma}{r}\right)^{3/2}} \qquad \text{(D-5)}$$

For a cavity size of $r = 2.5 \times 10^{-3}$ inch and at the pressure given in D.1, $Y = 1.74 \times 10^{-6}$.

A dimensionless time is also presented in (28)

$$\tau^* = \frac{\sqrt{\frac{2\sigma}{\rho_\ell r}}}{r} t \qquad \text{(D-6)}$$

For a bubble radius at departure of $R_d \leq 1$ inch, we find from Figure 1 of (28) that

$$\tau_d^* = 220 \quad \text{or} \quad t_d = 5.9 \times 10^{-3} \text{ sec.},$$

and the rate of growth is $\dot{R}_d = 23$ ft/sec.

From Equation (11) using the properties in D.1 and heat flux of 10^5 BTU/ft.hr, the waiting time τ is calculated to be $\tau \approx 0.7$ sec.

We can see from the three mechanisms analyzed above that the bubble growth time is about two orders of magnitude smaller than the waiting time calculated from Equation (11).

This suggests that, indeed, the waiting time to build the thermal layer is dominant in liquid metals.

APPENDIX E

THE CRITICAL PENETRATING DISTANCE

Following the considerations and assumptions given in paragraph 3.3, two conditions must be satisfied in order to find the critical penetrating distance x_{cr}. These conditions are as follows:

$$\frac{\partial \theta_\omega(x_{cr}, t_{cr})}{\partial t} = 0 \tag{E-1}$$

and

$$\theta_\omega(x_{cr}, t_{cr}) = \theta_\omega(0,0) \tag{E-2}$$

Rewriting Equation (10-a) after using Equation (B-7) and (B-8), we get

$$\theta_\omega(x,t) = \theta_\omega(x,0) - \frac{\theta_\omega(0,0)}{1+\beta}\, erfc\left(\frac{x}{2\sqrt{\alpha_\omega t}}\right) +$$

$$+ \frac{(\pi-2)\,\theta_\omega(0,0)}{(1+\beta)(\pi\beta+4)\pi}\left[t\left(1+\beta-erfc\left(\frac{x}{2\sqrt{\alpha_\omega t}}\right)\right) - \frac{x^2}{2\alpha_\omega}\, erfc\left(\frac{x}{2\sqrt{\alpha_\omega t}}\right) + x\sqrt{\frac{t}{\pi\alpha_\omega}}\, e^{-\frac{x^2}{4\alpha_\omega t}}\right] +$$

$$+ \frac{\pi(2+\beta)\,\theta_\omega(0,0)}{(1+\beta)(\pi\beta+4)\sqrt{\pi\alpha_\omega\pi}}\left[2\sqrt{\frac{\alpha_\omega t}{\pi}}\, e^{-\frac{x^2}{4\alpha_\omega t}} - x\, erfc\left(\frac{x}{2\sqrt{\alpha_\omega t}}\right)\right] \tag{E-3}$$

The time derivitive of Equation (E-3) becomes

$$\frac{\partial \theta_\omega(x,t)}{\partial t} = \frac{\theta_\omega(0,0)}{1+\beta}\left\{\frac{2+\beta}{(\pi\beta+4)\sqrt{\pi t}}\, e^{-\frac{x^2}{4\alpha_\omega t}} - \frac{x}{2\sqrt{\pi\alpha_\omega}\, t^{3/2}}\, e^{-\frac{x^2}{4\alpha_\omega t}} + \right.$$

$$\left. + \frac{\pi-2}{(\pi\beta+4)\pi}\left[1+\beta - erfc\left(\frac{x}{2\sqrt{\alpha_\omega t}}\right)\right]\right\} \tag{E-4}$$

Defining

$$Z_o = \frac{X_{cr}}{2\sqrt{\alpha_\omega t_{cr}}} \quad , \tag{E-5}$$

applying condition (E-1) to Equation (E-4), and using the definition (E-5), we get

$$Z_o = \frac{\sqrt{\pi}(2+\beta)}{\pi\beta+4}\sqrt{\frac{t_{cr}}{\tau}}\left[1 + \frac{(\pi-2)}{2+\beta}\sqrt{\frac{t_{cr}}{\tau}}\, e^{Z_o^2}\left(1+\beta-\operatorname{erfc} Z_o\right)\right] \tag{E-6}$$

As will be shown later $Z_o < 1$ and also $\sqrt{\frac{t_{cr}}{\tau}} < 1$, we can simplify Equation (E-6) by neglecting the second term on the right-hand side. Therefore,

$$Z_o = \frac{\sqrt{\pi}\,(2+\beta)}{\pi\beta+4}\sqrt{\frac{t_{cr}}{\tau}} \tag{E-7}$$

To satisfy condition (E-2) we use Equation (18) with the definition (E-5) to obtain

$$\theta_\omega(0,0) = \frac{\theta_\omega(0,0)}{1+\beta}\left\{1+\beta-\operatorname{erfc} Z_o + \frac{2(2+\beta)}{\pi\beta+4}\sqrt{\frac{t_{cr}}{\tau}}\left[\sqrt{\pi}\,Z_o\left(1+\beta-\operatorname{erfc} Z_o\right) + e^{-Z_o^2}\right] + \right.$$

$$\left. + \frac{(\pi-2)}{\pi\beta+4}\,\frac{t_{cr}}{\tau}\left[\left(1+2Z_o^2\right)\left(1+\beta-\operatorname{erfc} Z_o\right) + \frac{2Z_o}{\sqrt{\pi}}\, e^{-Z_o^2}\right]\right\} \tag{E-8}$$

Re-arrange Equation (E-8)

$$\operatorname{erfc} Z_o = \frac{2(2+\beta)}{\pi\beta+4}\sqrt{\frac{t_{cr}}{\tau}}\left[\frac{1+\beta}{\beta}\sqrt{\pi}\,Z_o + e^{-Z_o^2}\left(1 - \sqrt{\pi}\,Z_o\, e^{Z_o^2}\operatorname{erfc} Z_o\right)\right] +$$

$$+\left(\frac{\pi-2}{\pi\beta+4}\right)\frac{t_{cr}}{\tau}\left[\left(1+2Z_o^2\right)(1+\beta) - \operatorname{erfc} Z_o + \frac{2Z_o}{\sqrt{\pi}}\, e^{-Z_o^2}\left(1 - \sqrt{\pi}\,Z_o\, e^{Z_o^2}\operatorname{erfc} Z_o\right)\right] \tag{E-9}$$

We shall use the following approximation, Figure 41,

$$\left(1+\sqrt{\pi}\, Z_o\right) e^{Z_o^2} \operatorname{erfc} Z_o = 1 \tag{E-10}$$

The approximation (E-10) simplifies the following term

$$e^{-Z_o^2}\left(1-\sqrt{\pi}\, Z_o e^{Z_o^2} \operatorname{erfc} Z_o\right) = \operatorname{erfc} Z_o \tag{E-11}$$

Now, we re-write Equation (E-9) with the approximation (E-11) together with the Equation (E-7) and get the final equation for Z_o

$$\left(1-\frac{2Z_o}{\sqrt{\pi}}\right)\operatorname{erfc} Z_o\left[1+\frac{(\pi-2)(\pi\beta+4)}{\pi(2+\beta)^2} Z_o^2\right] = \frac{2(1+\beta)Z_o^2}{\beta}\left[1+\frac{(\pi-2)(\pi\beta+4)\beta}{2\pi(2+\beta)^2}\left(1+2Z_o^2\right)\right] \tag{E-12}$$

The best way to solve Equation (E-12) is by a graphical method. The left-hand side of Equation (E-12) would not vary much with β, but the right-hand side is a strong function of β. By using various values of β and solving Equation (E-12), we find Z_o as a function of β. See Table (1).

Using the definition (E-5) in Equation (E-7) and solving X_{cr}, we get

$$X_{cr} = \frac{2(\pi\beta+4)}{\sqrt{\pi}(2+\beta)} \sqrt{\alpha_\omega \mathcal{T}}\, Z_o^2 \tag{E-13}$$

Define, now, the ratio between the critical distance and the relaxation length

$$\eta = \frac{X_{cr}}{L} \tag{E-14}$$

Combining Equations (E-13) and (13) with the definition (E-14), we get

$$\eta = \frac{2(\pi\beta+4)\, Z_o^2}{\sqrt{\pi}(2+\beta)\, J(\beta)} \tag{E-15}$$

η is a function of β only and is given in Table (1) and plotted in Figure (5).

Re-arranging Equation (E-7) we find the ratio of the critical time to the waiting time.

$$\sqrt{\frac{t_{cr}}{\tau}} = \frac{\eta\beta+4}{\sqrt{\eta}(2+\beta)} Z_o \qquad \text{(E-16)}$$

This ratio is a function of β only and is given in Table (1). The magnitude of this term is of the order of 0.5 and, therefore, justifies the approximation of Equation (E-6) to (E-7).

APPENDIX F

TABULATION OF EXPERIMENTAL RESULTS

In the following tables several symbols were used to designate the modes of heat transfer which were observed while taking the data.

N.C. - Natural Convection

N.C. (S.C.) - Natural Convection, the Liquid is Sub-Cooled

B.B. - Before Bumping

A.B. - After Bumping

Bumping - Bumping

S.B. - Stable Boiling

Run No. 1

Boiler plate made of nickel "A," coated with porous nickel "A," 65 micron grade, 1/32-inch thick. After had been solidified from Marto's (5) run 30.

Sodium depth: 2.5 in.

P (mm Hg)	T_{sat} (^{o}F)	T_{ℓ} (^{o}F)	$T_{w\ ext.}$ (^{o}F)	$T_{w\ ext.}-T_{sat}$ (^{o}F)	q_o (BTU/ft^{2}hr)	Remarks
58.0	1206	1027	1050	23	29,000	N.C. (S.C.)
56.5	1203	1198	1230	32	45,000	N.C. (S.C.)
59.0	1209	1212	1273	64	71,000	Bumping
61.5	1214	1210	1236	22	92,000	S.B.
58.0	1206	1205	1240	34	127,000	S.B.
55.0	1199	1198	1242	43	161,000	S.B.
54.5	1198	1200	1248	50	197,000	S.B.
56.5	1203	1203	1234	31	111,000	S.B.
58.5	1207	1206	1229	22	77,000	S.B.
59.0	1209	1209	1228	19	44,000	S.B.
62.0	1215	1170	1220	50	30,000	N.C. (S.C.)

Run No. 2

Boiler plate made of nickel "A" with twelve re-entry type cavities of ∅ 0.004 in. After was cleaned from Marto's (5) run No. 28.

Sodium depth: 1-1/2 in.

P (mm Hg)	T_{sat} (^{o}F)	T_{ℓ} (^{o}F)	$T_{w\ ext.}$ (^{o}F)	$T_{w\ ext.}-T_{sat}$ (^{o}F)	q_o (BTU/ft^{2}hr)	Remarks
64.0	1219	1162	1183	21	23,000	N.C. (S.C.)
58.5	1208	1202	1235	27	43,000	Bumping
59.5	1210	1195	1238	28	99,000	Bumping
59.5	1210	1195	1226	16	87,000	Bumping
57.5	1205	1206	1261	56	109,000	Bumping
57.5	1205	1206	1236	31	122,000	Bumping
60.5	1212	1199	1232	20	173,000	Bumping
59.5	1210	1201	1229	19	203,000	Bumping

Run No. 3

Boiler plate made of nickel "A," coated with porous nickel "A," 35 microns grade, 1/32-inch thick.

Sodium depth: 2 in.

P (mm Hg)	T_{sat} (^{o}F)	T_{ℓ} (^{o}F)	$T_{w\ ext.}$ (^{o}F)	$T_{w\ ext.}-T_{sat}$ (^{o}F)	q_o (BTU/ft^{2}hr)	Remarks
58.5	1208	1193	1206	13	25,000	N.C. (S.C.)
58.5	1208	1201	1220	19	26,000	N.C. (S.C.)
60.0	1211	1226	1252	41	39,000	N.C.
57.0	1204	1221	1261	57	54,000	B.B.
57.0	1204	1200	1228	24	61,000	A.B.

Run No. 4

Same as in run 3. System cooled down and sodium solidified; then reheated, and tests were repeated.

P (mm Hg)	T_{sat} (^{o}F)	T_{ℓ} (^{o}F)	$T_{w\ ext.}$ (^{o}F)	$T_{w\ ext.}-T_{sat}$ (^{o}F)	q_{o} (BTU/ft^{2}hr)	Remarks
55.5	1201	1194	1243	49	44,000	N.C. (S.C.)
56.0	1202	1197	1286	89	73,000	N.C. (S.C.)
57.0	1204	1199	1296	92	98,000	B.B.
57.0	1204	1201	1235	31	100,000	A.B.
58.0	1206	1201	1325	119	106,000	N.C.
58.5	1207	1202	1271	64	54,000	N.C.
58.5	1207	1202	1235	28	33,000	N.C.
50.0	1187	1191	1255	68	55,000	N.C.
56.0	1202	1200	1293	91	87,000	N.C.
60.5	1212	1206	1240	28	141,000	S.B.
61.0	1213	1210	1240	27	195,000	S.B.
60.5	1212	1204	1239	27	233,000	S.B.

Run No. 5

Same boiler as in run 2 after the sodium was removed by reacting in n-butyl alcohol and the surface was cleaned by an ultrasonic cleaner.

Sodium depth: 1-1/2 in.

P (mm Hg)	T_{sat} (^{o}F)	T_{ℓ} (^{o}F)	$T_{w\ ext.}$ (^{o}F)	$T_{w\ ext.}-T_{sat}$ (^{o}F)	q_o (BTU/ft^{2}hr)	Remarks
60.0	1211	1193	1215	22	29,000	N.C. (S.C.)
61.5	1214	1234	1264	50	49,000	B.B.
61.5	1214	1207	1231	17	61,000	A.B.
63.0	1217	1217	1240	23	90,000	A.B.
63.5	1218	1217	1243	25	130,000	A.B.
50.0	1188	1195	1218	30	100,000	Bumping
58.5	1207	1210	1263	56	84,000	Bumping
59.0	1209	1214	1228	19	140,000	Bumping
59.0	1209	1239	1288	79	71,000	B.B.
59.0	1209	1209	1231	22	90,000	A.B.
61.0	1213	--	1235	22	187,000	S.B.
60.0	1211	1230	1265	54	47,000	N.C.

Run No. 6

Boiler plate made of two pieces of nickel "A," copper brazed with a permanent T.C. One cylindrical cavity of ∅ 0.010 in. x 0.050 in.*

Sodium depth: 2 in.

P (mm Hg)	T_{sat} (^{o}F)	T_{ℓ} (^{o}F)	$T_{w\ ext.}$ (^{o}F)	$T_{w\ ext.} - T_{sat}$ (^{o}F)	q_o ($\frac{BTU}{ft^2 hr}$)	$\theta_w(0,0)$ (^{o}F)	τ (sec)	Remarks
60.5	1212	1166	1189	23	22,000	--	--	N.C. (S.C.)
63.5	1218	1210	1253	35	33,000	--	--	N.C.
57.5	1205	1212	1258	53	45,000	--	--	N.C.
60.0	1211	1228	1286	75	64,000	--	--	N.C.
53.5	1196	1225	1287	91	69,000	--	--	B.B.
53.5	1196	1202	1247	51	92,000	--	--	A.B.
66.0	1223	1212	1273	50	136,000	--	--	A.B.
60.5	1212	1200	1292	80	163,000	106	8.0	S.B.
54.5	1198	1188	1294	96	225,000	110	1.0	S.B.
58.5	1207	1200	1310	103	200,000	117	2.0	S.B.
59.5	1210	1203	1290	80	158,000	101	4.5	S.B.
63.5	1218	1209	1290	72	104,000	108	7.0	S.B.
54.5	1198	1196	1263	65	65,000	--	--	N.C.
56.0	1202	1191	1289	87	168,000	114	4.5	S.B.
60.5	1212	1200	1303	91	190,000	107	3.2	S.B.
60.5	1212	1202	1312	100	300,000	109	0.7	S.B.

*Calculated effective cavity radius $r = 1.15 \times 10^{-3}$ in.

Run No. 7

Same as run 6. System cooled and sodium solidified; then reheated and tests repeated.*

P (mm Hg)	T_{sat} (^{o}F)	T_{ℓ} (^{o}F)	$T_{w\ ext.}$ (^{o}F)	$T_{w\ ext.} - T_{sat}$ (^{o}F)	q_o ($\frac{BTU}{ft^2 hr}$)	$\theta_w(0,0)$ (^{o}F)	$\mathcal{T}$ (sec)	Remarks
59.5	1210	1204	1230	24	18,000	--	--	N.C.
60.0	1211	1210	1244	33	22,000	--	--	N.C.
60.0	1211	1218	1260	49	35,000	--	--	N.C.
60.5	1212	1223	1282	70	52,000	--	--	N.C.
60.5	1212	1228	1325	113	80,000	--	--	N.C.
62.5	1216	1206	1287	71	164,000	100	3.5	S.B.
64.5	1220	1214	1285	65	210,000	90	1.9	S.B.
71.0	1233	1227	1303	70	250,000	93	1.0	S.B.
79.5	1248	1238	1330	82	260,000	95	0.6	S.B.
65.0	1221	1211	1285	64	128,000	85	4.6	S.B.
65.0	1221	1214	1301	80	70,000	--	--	N.C.
68.0	1227	1222	1305	77	180,000	95	2.2	S.B.

*Calculated effective cavity radius $r = 1.15 \times 10^{-3}$ in.

Run No. 8

Boiler plate made of two pieces of nickel "A," copper brazed with a permanent T. C. One cylindrical cavity of ϕ 0.0465 in. x 0.050 in.*

Sodium depth: 2 in.

P (mm Hg)	T_{sat} (^{o}F)	T_{ℓ} (^{o}F)	$T_{w\ ext.}$ (^{o}F)	$T_{w\ ext.} - T_{sat}$ (^{o}F)	q_o ($\frac{BTU}{ft^2 hr}$)	$\theta_w(0,0)$ (^{o}F)	$\mathcal{T}$ (sec)	Remarks
60.5	1212	1182	1200	18	15,000	--	--	N.C. (S.C.)
63.0	1217	1224	1240	23	20,000	--	--	N.C.
59.0	1209	1232	1255	46	28,000	--	--	N.C.
67.0	1225	1235	1265	40	30,000	--	--	N.C.
60.5	1212	1218	1260	48	46,000	--	--	N.C.
64.5	1220	1220	1250	30	92,000	40	1.3	S.B.
72.0	1235	1226	1266	31	140,000	39	1.1	S.B.
74.5	1239	1229	1275	36	202,000	40	0.4	S.B.
45.5	1176	1176	1210	34	80,000	50	7.0	S.B.
56.0	1202	1202	1233	31	89,000	49	4.7	S.B.
68.5	1228	1227	1260	32	110,000	40	1.5	S.B.
88.0	1262	1257	1300	38	240,000	42	0.3	S.B.
60.5	1212	1212	1250	38	30,000	--	--	N.C.

---

*Calculated effective cavity radius $r = 3.3 \times 10^{-3}$ in.

Run No. 9

Same as run 8. System cooled and sodium solidified; then reheated and tests repeated.*

P (mm Hg)	T_{sat} (^{o}F)	T_{ℓ} (^{o}F)	$T_{w\ ext.}$ (^{o}F)	$T_{w\ ext.} - T_{sat}$ (^{o}F)	q_o ($\frac{BTU}{ft^2 hr}$)	$\theta_w(0,0)$ (^{o}F)	τ (sec)	Remarks
62.5	1216	1227	1252	36	24,000	--	--	N.C.
60.5	1212	1232	1267	55	30,000	--	--	N.C.
60.5	1212	1242	1290	78	50,000	--	--	N.C.
60.5	1212	1257	1312	100	71,000	--	--	N.C.
61.0	1213	1213	1255	42	125,000	52	1.6	S.B.
64.5	1220	1218	1267	47	150,000	53	0.8	S.B.
95.5	1273	1270	1320	47	224,000	51	0.4	S.B.
74.0	1238	1236	1282	44	109,000	50	1.0	S.B.
59.0	1209	1209	1245	36	80,000	55	7.0	S.B.
55.0	1200	1200	1238	38	60,000	60	11.0	S.B.
61.5	1214	1214	1270	56	35,000	--	--	N.C.
66.5	1224	1224	1259	35	75,000	58	9.0	S.B.
79.0	1247	1246	1287	40	100,000	53	2.0	S.B.
91.0	1266	1264	1310	44	168,000	50	0.7	S.B.
83.0	1254	1250	1292	38	88,000	51	5.4	S.B.
69.5	1230	1230	1287	57	44,000	--	--	N.C.
76.0	1242	1242	1282	40	80,000	52	9.0	S.B.

*Calculated effective cavity radius $r = 2.3 \times 10^{-3}$ in.

Run No. 10

Same surface as in runs 8 and 9 after the sodium was reacted, and the surface re-polished.*

Sodium depth: 2-1/4 in.

P (mm Hg)	T_{sat} (^{o}F)	T_{ℓ} (^{o}F)	$T_{w\ ext.}$ (^{o}F)	$T_{w\ ext.} - T_{sat}$ (^{o}F)	q_o ($\frac{BTU}{ft^2 hr}$)	$\theta_w(0,0)$ (^{o}F)	$\mathcal{T}$ (sec)	Remarks
62.5	1216	1145	1168	23	17,000	--	--	N.C. (S.C.)
63.0	1217	1228	1247	30	28,000	--	--	N.C.
60.0	1211	1237	1265	54	40,000	--	--	N.C.
63.0	1217	1230	1286	69	52,000	--	--	N.C.
67.0	1225	1236	1302	77	77,000	--	--	N.C.
69.0	1229	1229	1304	75	90,000	--	--	Bumping
77.5	1244	1241	1286	42	108,000	69	9.0	S.B.
88.0	1262	1261	1310	48	145,000	70	5.0	S.B.
73.5	1237	1246	1316	79	77,000	--	--	N.C.
62.5	1216	1216	1283	67	62,000	--	--	N.C.
62.5	1216	1214	1266	50	140,000	83	6.0	S.B.
79.0	1247	1240	1315	68	215,000	78	2.0	S.B.

---

*Calculated effective cavity radius $r = 1.5 \times 10^{-3}$ in.

Run No. 11

Same as run 10. System cooled and sodlum solidified; then reheated and tests repeated.*

P (mm Hg)	T_{sat} (^{o}F)	T_{ℓ} (^{o}F)	$T_{w\ ext.}$ (^{o}F)	$T_{w\ ext.} - T_{sat}$ (^{o}F)	q_o ($\frac{BTU}{ft^2 hr}$)	$\theta_w(0,0)$ (^{o}F)	$\mathcal{T}$ (sec)	Remarks
52.0	1192	1165	1185	20	22,000	--	--	N.C. (S.C.)
52.0	1192	1178	1206	28	35,000	--	--	N.C. (S.C.)
52.0	1192	1192	1230	38	42,000	--	--	N.C.
56.0	1202	1222	1260	58	54,000	--	--	N.C.
58.5	1207	1233	1277	70	67,000	--	--	N.C.
60.5	1212	1238	1297	85	82,000	--	--	N.C.
62.0	1215	1215	1315	100	100,000	--	--	Bumping
60.0	1211	1210	1267	56	128,000	91	10.0	S.B.
68.5	1228	1227	1283	55	158,000	76	2.6	S.B.
72.0	1235	1233	1290	55	148,000	72	2.3	S.B.
59.0	1208	1207	1262	54	150,000	74	4.0	S.B.
60.5	1212	1212	1280	68	135,000	80	8.0	S.B.

*Calculated effective cavity radius $r - 1.5 \times 10^{-3}$ in.

Run No. 12

Boiler plate made of two nickel "A," copper brazed with a permanent T. C. One cylindrical cavity of ϕ 0.020 in. x 0.050 in.*

Sodium depth: 2-1/2 in.

P (mm Hg)	T_{sat} (^{o}F)	T_{ℓ} (^{o}F)	$T_{w\ ext.}$ (^{o}F)	$T_{w\ ext.} - T_{sat}$ (^{o}F)	q_o ($\frac{BTU}{ft^2 hr}$)	$\theta_w(0,0)$ (^{o}F)	$\mathcal{T}$ (sec)	Remarks
56.0	1202	1209	1236	34	23,000	--	--	N.C.
59.0	1209	1224	1252	43	35,000	--	--	N.C.
60.5	1212	1214	1252	40	55,000	--	--	Bumping
60.5	1212	1213	1252	40	77,000	65	8.0	S.B.
62.0	1215	1215	1262	47	93,000	65	3.0	S.B.
65.5	1222	1221	1272	50	126,000	62	2.0	S.B.
70.5	1232	1229	1280	48	152,000	57	1.0	S.B.
78.0	1245	1241	1294	49	213,000	58	0.3	S.B.
61.5	1214	1212	1262	48	128,000	58	1.5	S.B.
59.5	1210	1207	1254	44	100,000	57	1.8	S.B.
54.5	1199	1198	1244	45	90,000	61	5.6	S.B.
49.5	1186	1186	1233	47	40,000	--	--	N.C.
49.5	1186	1185	1233	47	72,000	66	9.0	S.B.
66.0	1223	1221	1275	52	195,000	59	0.7	S.B.
70.5	1232	1230	1290	58	280,000	65	0.3	S.B.

---

*Calculated effective cavity radius $r = 2.2 \times 10^{-3}$ in.

Run No. 13

Boiler plate made of nickel "A," with one re-entry type cavity of ∅ 0.005 in.

Sodium depth: 2 in.

P (mm Hg)	T_{sat} (^{o}F)	T_{ℓ} (^{o}F)	$T_{w\ ext.}$ (^{o}F)	$T_{w\ ext.} - T_{sat}$ (^{o}F)	q_o ($\frac{BTU}{ft^2 hr}$)	$\theta_w(0,0)$ (^{o}F)	$\mathcal{T}$ (sec)	Remarks
34.0	1140	1141	1160	20	14,000	--	--	N.C.
36.5	1149	1156	1182	33	26,000	--	--	N.C.
36.5	1149	1166	1199	50	40,000	--	--	N.C.
37.0	1150	1169	1207	57	50,000	--	--	N.C.
39.0	1156	1188	1242	86	73,000	--	--	N.C.
41.5	1164	1217	1267	103	111,000	--	--	B.B.
42.0	1166	1158	1205	39	190,000	94	5.0	S.B.
64.5	1220	1213	1255	35	126,000	69	8.0	S.B.
64.5	1220	1212	1255	35	160,000	60	1.3	S.B.
65.5	1222	1213	1255	33	233,000	51	0.5	S.B.
64.0	1219	1210	1253	34	113,000	61	4.0	S.B.
64.0	1219	1211	1259	40	136,000	66	6.0	S.B.
105.5	1287	1278	1310	23	137,000	38	1.1	S.B.
105.5	1287	1277	1311	24	99,000	44	2.5	S.B.
106.5	1288	1279	1308	20	212,000	35	0.3	S.B.
104.0	1285	1277	1310	25	90,000	47	8.0	S.B.
39.5	1159	1150	1198	39	180,000	83	10.0	S.B.

Run No. 14

Boiler plate made of nickel "A." One cylindrical cavity of ∅ 0.0105 in x 0.150 in.

Sodium level: 2-1/4 in.

P (mm Hg)	T_{sat} (°F)	T_ℓ (°F)	$T_{w\ ext.}$ (°F)	$T_{w\ ext.} - T_{sat}$ (°F)	q_o ($\frac{BTU}{ft^2 hr}$)	$\theta_w(0,0)$ (°F)	τ (sec)	Remarks
37.0	1151	1154	1177	26	20,000	--	--	N.C.
37.5	1152	1158	1190	38	24,000	--	--	N.C.
41.0	1163	1175	1212	49	36,000	--	--	N.C.
37.5	1152	1170	1210	58	46,000	--	--	N.C.
37.5	1152	1180	1230	78	65,000	--	--	N.C.
40.5	1161	1207	1293	132	90,000	--	--	N.C.
50.0	1188	1180	1213	25	159,000	38	0.3	S.B.
46.0	1177	1169	1206	29	126,000	39	0.6	S.B.
39.0	1157	1152	1192	35	90,000	49	4.5	S.B.
36.0	1147	1139	1200	61	60,000	--	--	N.C. (S.C.)
38.0	1153	1145	1225	80	97,000	--	--	N.C. (S.C.)
39.5	1158	1149	1198	40	106,000	57	6.2	S.B.
42.0	1166	1157	1198	32	138,000	51	2.4	S.B.
58.0	1206	1200	1229	23	190,000	33	0.3	S.B.
56.0	1202	1198	1227	25	123,000	35	1.0	S.B.
96.0	1274	1331	1415	141	125,000	--	--	N.C.
96.0	1274	1267	1290	16	133,000	23	0.2	S.B.
96.0	1274	1267	1290	16	88,000	24	0.3	S.B.
90.5	1265	1258	1282	17	58,000	24	0.7	S.B.
50.0	1187	1180	1215	28	115,000	38	1.1	S.B.
54.0	1197	1189	1222	25	147,000	33	0.2	S.B.
67.0	1225	1220	1249	24	110,000	33	0.5	S.B.
67.0	1225	1221	1248	23	86,000	35	1.5	S.B.
67.0	1225	--	1318	93	80,000	--	--	N.C.

APPENDIX G

CALCULATED EXAMPLE

The method of reducing the data is described in paragraph 5.5, but it will be more clear by arbitrarily selecting one data point and calculating it numerically. We have selected here the data point 12 of run 14. The reduced temperatures and the measured pressure are given in Table G.1

Table G.1

T.C. No.	Distance from Boiler Surface (in.)	Temperature (^{o}F)	Remarks
1	0.750	1399	
2	0.550	1345	
3	0.350	1292	
4	0.150	1242	
5	0.550	1348	
6	0.150	1237	
7 max.	0.050	1224	
7 min.		1208	
8 ave.	0.050	1220	
9	0.75	1149	In the liquid
11	Above liquid surface	1158	In the vapor

The measured pressure by the open-end manometer P = 39 mm Hg.

The temperatures presented in Table G.1 were measured by the type K potentiometer, except those of T.C 7 which were recorded on the Recording Oscillograph.

Thermocouples 5, 6, and 8 were used only for indication of radial effects and were not used in any further calculations.

In order to find the heat flux, the temperatures measured by T.C 1, 2, 3, and 4 were plotted versus their positions in the boiler plate. (See Figure (42).) Usually a reasonable straight line was found to connect these points from which the heat flux was obtained from

$$q_o = k_\omega \frac{\Delta T_\omega}{\Delta X} \qquad \text{(G-1)}$$

where the thermal conductivity of nickel is given by Hogan and Sawyer (29).

$$k_w = 20.3 + 0.00965\ T \qquad \text{(G-2)}$$

k_w is in (BTU/ft.hr ^oF) and T in (^oF).

Using the average wall temperature for the four thermocouples, which is about 1300 ^oF, the thermal conductivity is found to be k_w = 33 BTU/ft.hr ^oF, and the heat flux

$$q_o = 106{,}000\ \text{BTU/ft}^2\text{hr}\ .$$

The saturation temperature was taken as the measured vapor temperature which was in this case T_{sat} = 1158 ^oF. From the saturation temperature, the saturation pressure is found by using Equation (29)

$$\log_{10} P = 4.52172 - \frac{5220.42}{T_{sat}} \qquad \text{(G-3)}$$

which in this case is found to be

$$p = 39.5\ \text{mm Hg.}$$

By extrapolating to the surface the straight line connecting the four thermocouples, we found the extrapolated wall temperature

$$T_{w\ ext} = 1198\ ^{o}F \text{ and}$$

$$T_{w\ ext} - T_{sat} = 40\ ^{o}F$$

The measured liquid temperature was $T_{\ell} = 1149\ ^{o}F$.

For the liquid-solid combination used in this work, namely, sodium in contact with nickel, the value of β which was defined by Equation (A-12) was found to be

$$\beta = 1.92 \qquad \text{(G-4)}$$

From Equation (28) we get the temperature gradient $\theta_w'(0,0)$ when the bubble is ready to grow by using the value of K = 0.67 given in Table 1 for $\beta = 1.92$. By passing a line with the slope of $\theta_w'(0,0)$ through the maximum temperature measured by thermocouple 7 and extrapolating it to the surface, we get $T_w(0,0)$. (See Figure (42).)

$$T_w(0,0) = 1215\ ^{o}F$$

or $$\theta_w(0,0) = 57\ ^{o}F \qquad \text{(G-5)}$$

Using Equation (C-13) for the given cavity size and pressure used in this case, we find that the predicted surface superheat is 49 ^{o}F which is in fair agreement with (G-5).

The period time τ is found from the recorded temperature variations of thermocouple 7. The recorded temperatures of this point are given in Figure (26b) from which τ is found to be $\tau = 6.2$ sec.

Using Equation (30) the calculated time is $\tau = 5.0$ sec.

APPENDIX H

Table I

$$\beta = \frac{k_\omega \sqrt{\alpha_\ell}}{k_\ell \sqrt{\alpha_\omega}}$$ Equation (A-12)

$$I = \frac{6\pi + 6\pi\beta^2 + 7\pi\beta + 16\beta}{3\sqrt{\pi}\,(1+\beta)(\pi\beta+4)}$$ Equation (12)

$$J = \frac{3\pi\beta - 2\pi + 16}{3\sqrt{\pi}\,(1+\beta)(\pi-2)}$$ Equation (14)

$$K = \frac{3\pi(1+\beta)(2+\beta)}{6\pi + 6\pi\beta^2 + 7\pi\beta + 16\beta}$$ Equation (21)

$Z_o(\beta)$ Equation (E-12)

$$\sqrt{\frac{t_{cr.}}{\sigma}} = \frac{(\pi\beta+4)\,Z_o}{\sqrt{\pi}\,(2+\beta)}$$ Equation (E-16)

$$\eta = \frac{2(\pi\beta+4)\,Z_o^2}{\sqrt{\pi}\,(2+\beta)\,J}$$ Equation (E-15)

β	0.5	1.0	1.92	10
I	0.959	1.0	1.035	1.102
J	1.59	1.58	1.57	1.56
K	0.83	0.75	0.67	0.52
Z_o	0.27	0.31	0.33	0.34
$\sqrt{t_{cr}/\sigma}$	0.339	0.415	0.475	0.567
η	0.115	0.1635	0.201	0.247

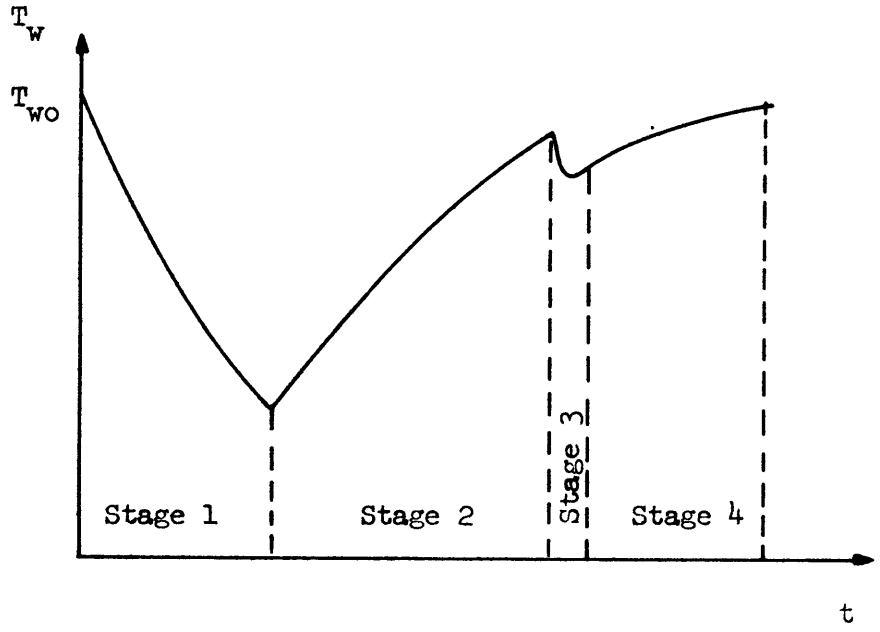

Stage 1: Evaporation from a microlayer, surface temperature decreases.

Stage 2: The microlayer was evaporated, low rate of heat transfer to the vapor. Surface temperature increases.

Stage 3: The bubble left the surface. Heat is transferred to the liquid with decreasing surface temperature.

Stage 4: Normal thermal boundary layer is re-formed.

FIG. 1: WALL SURFACE TEMPERATURE VARIATIONS DURING BUBBLE FORMATION AND DEPARTURE OF LIQUID TOLUENE FROM GLASS (COPIED FROM COOPER (9))

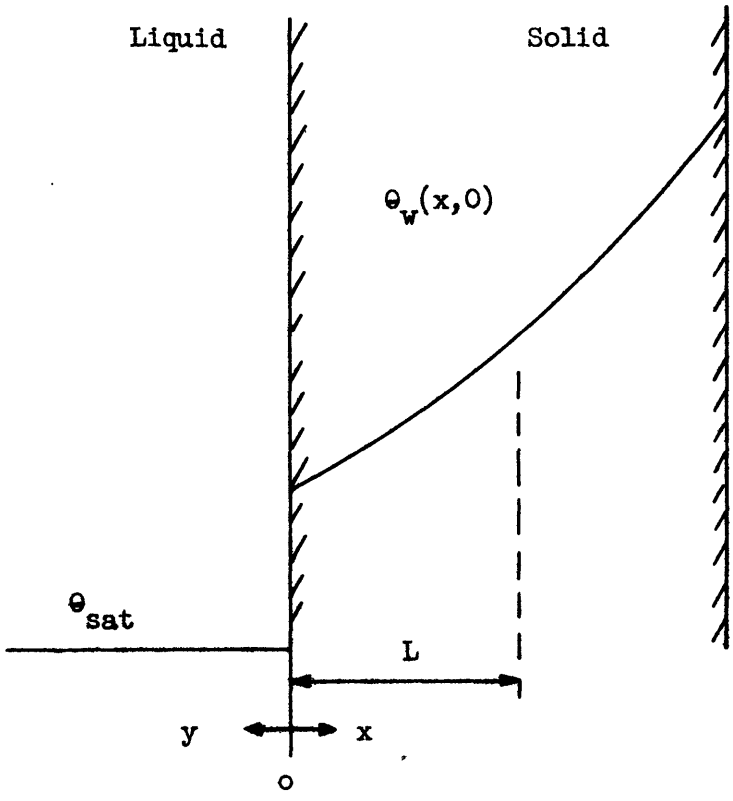

FIG. 2: INITIAL TEMPERATURE DISTRIBUTION IN THE SOLID AND IN THE LIQUID

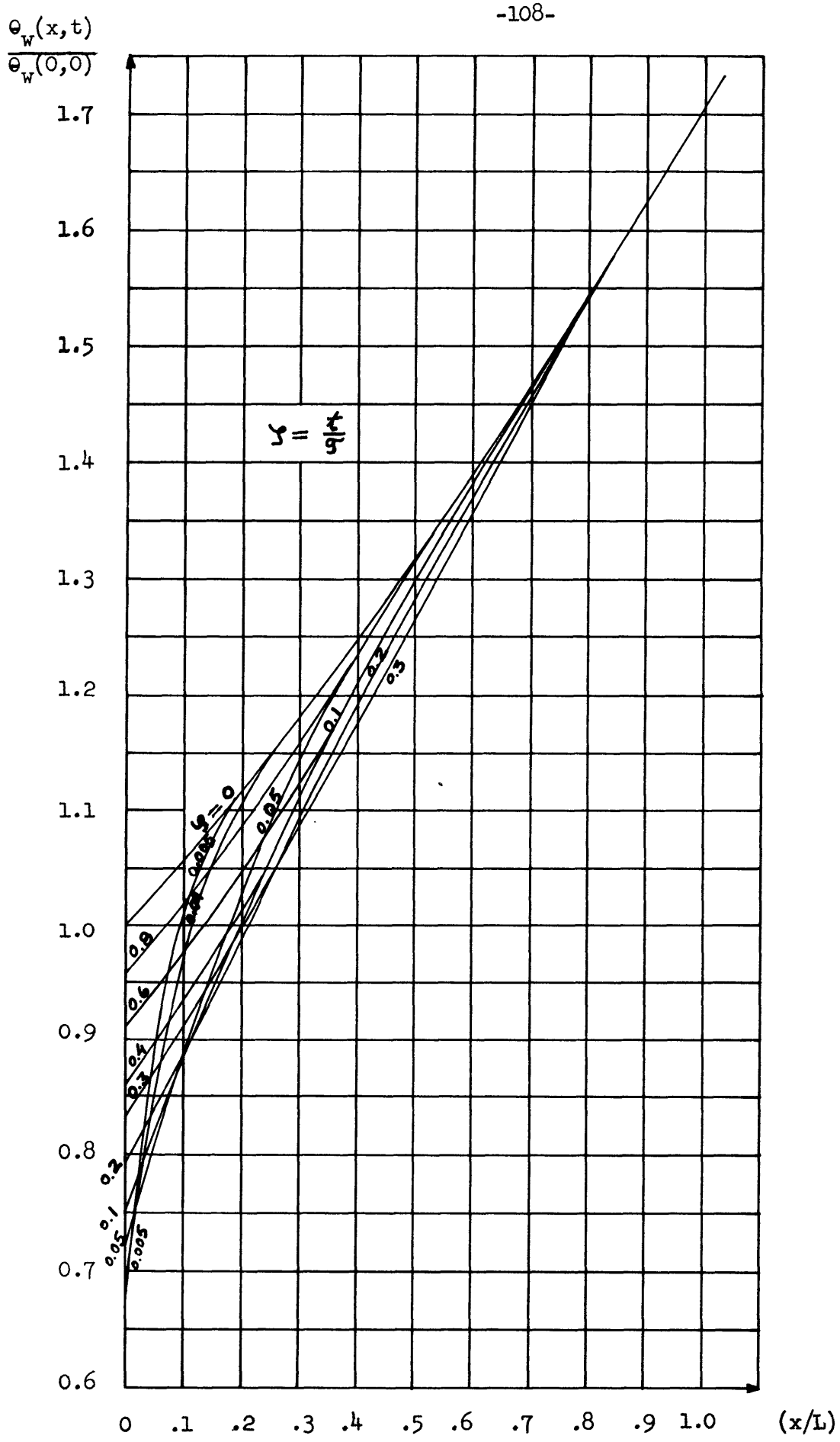

FIG. 3: TEMPERATURE VARIATIONS IN THE SOLID. EQUATION (18)
($P = 1.92$)

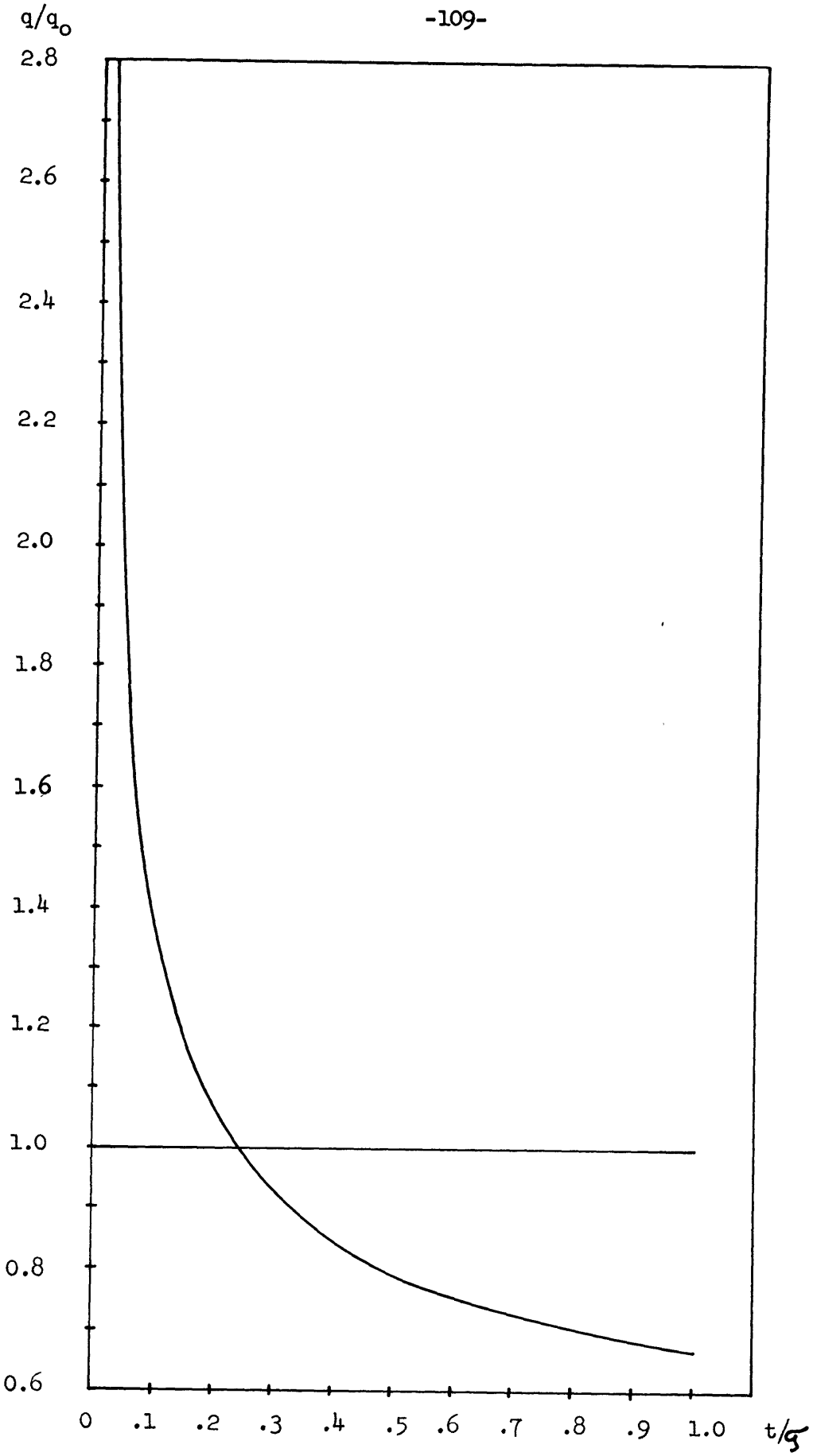

FIG. 4: VARIATIONS OF HEAT FLUX AT THE SURFACE. EQUATION 20 (FOR $\beta = 1.92$)

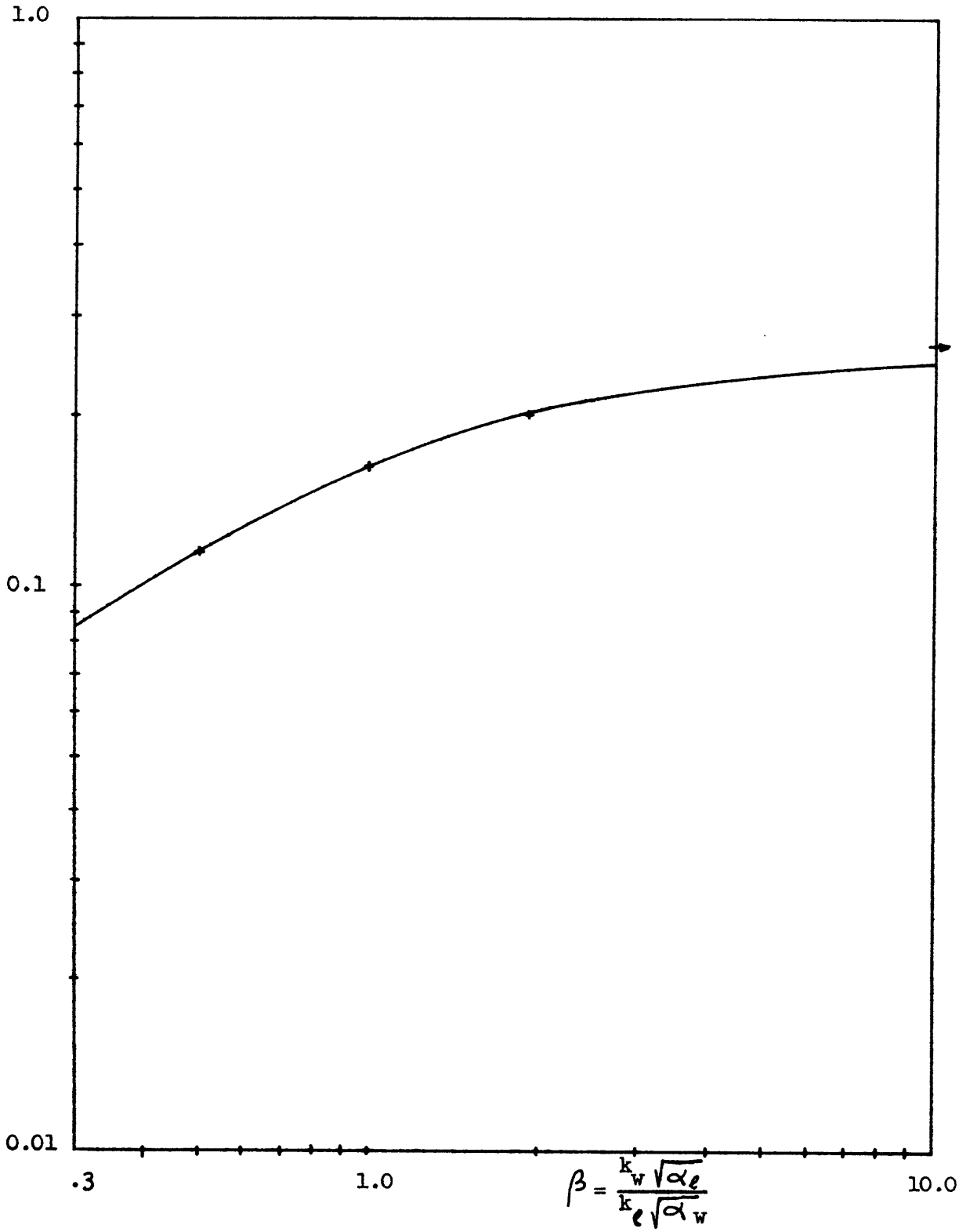

FIG. 5: THE RATIO OF THE INITIAL CAVITY LENGTH TO THE RELAXATION LENGTH. (EQUATION (E-15)

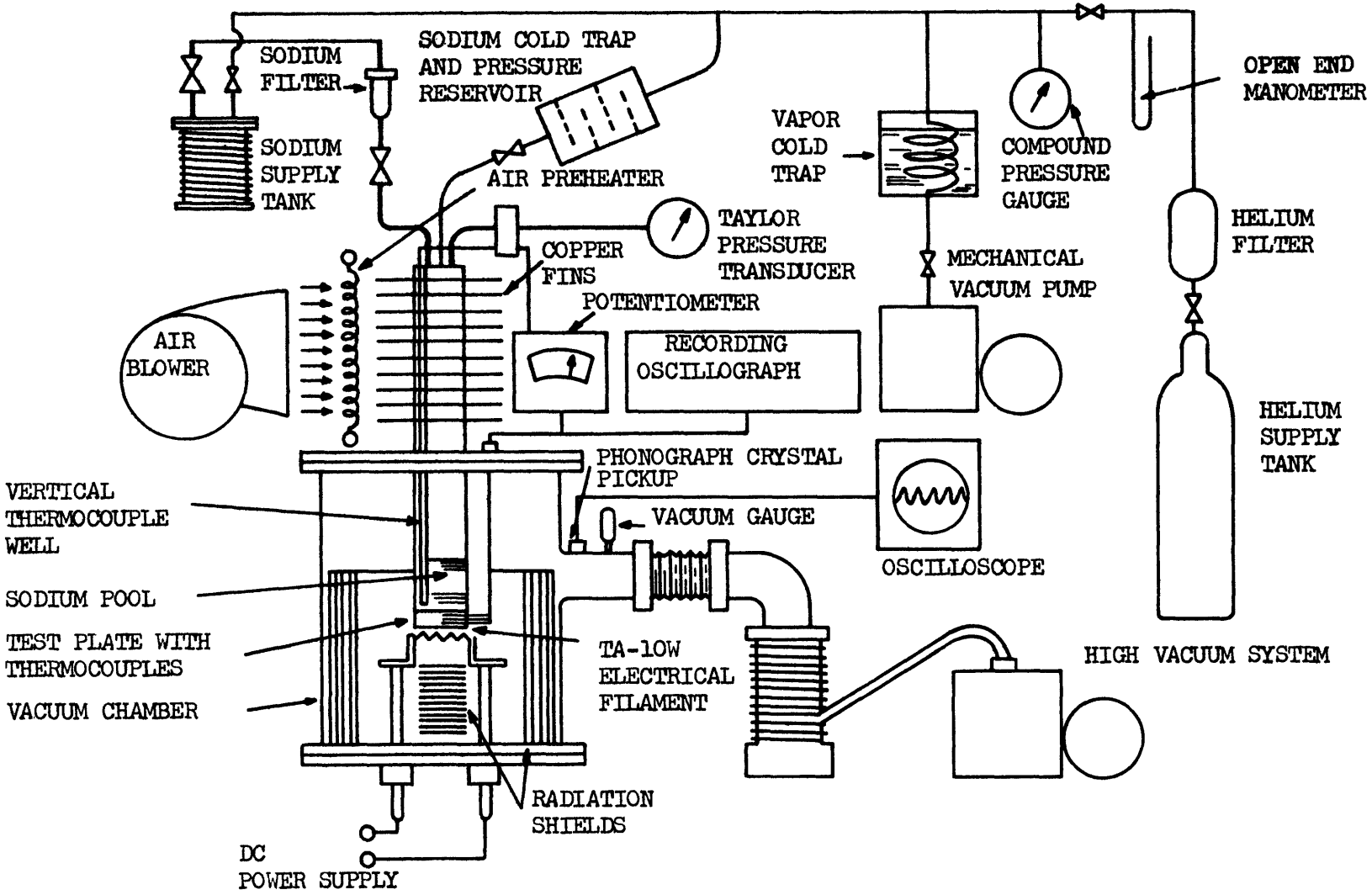

FIG. 6 SCHEMATIC DIAGRAM OF APPARATUS

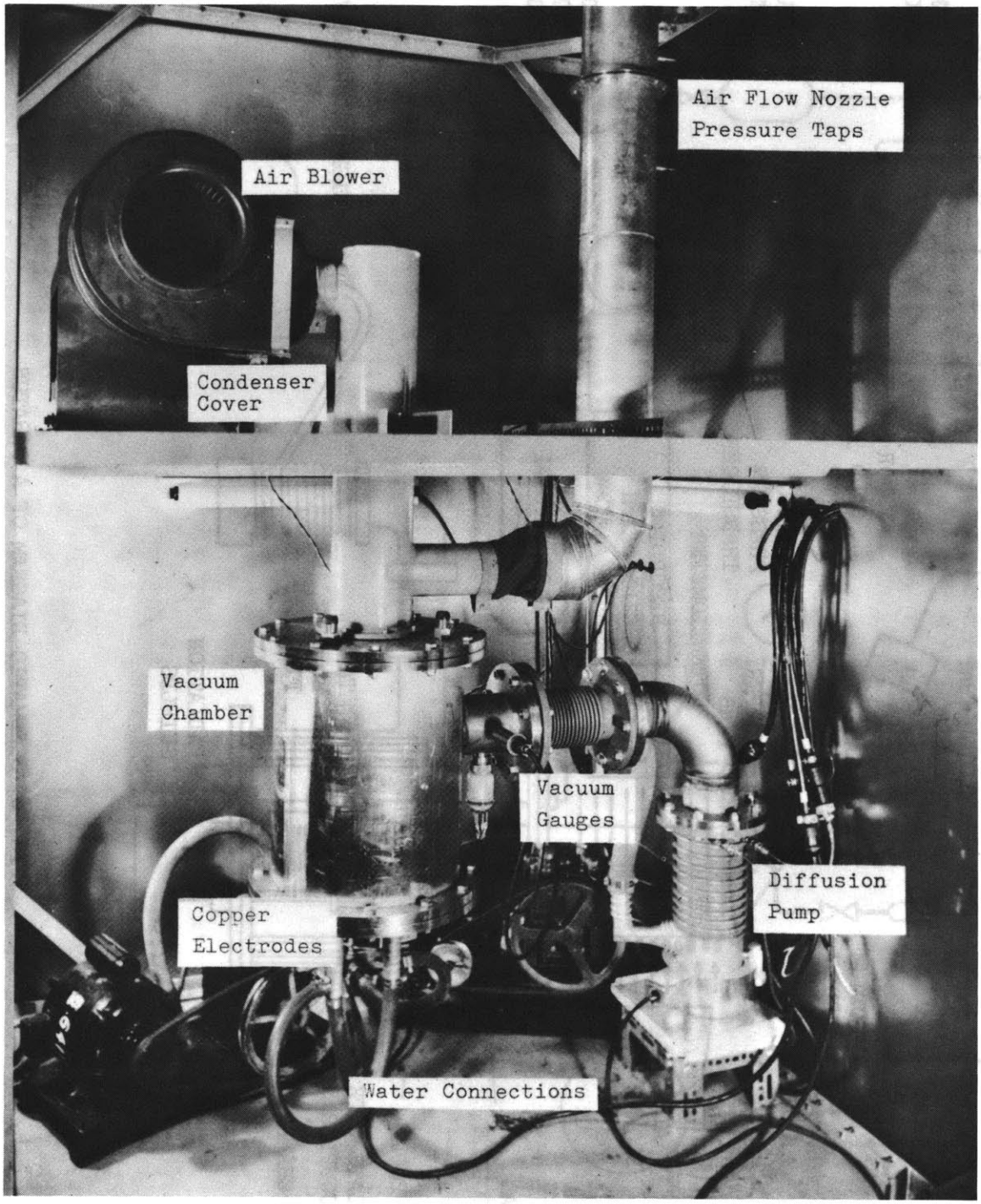

FIG. 7. PARTIAL ASSEMBLY OF EQUIPMENT

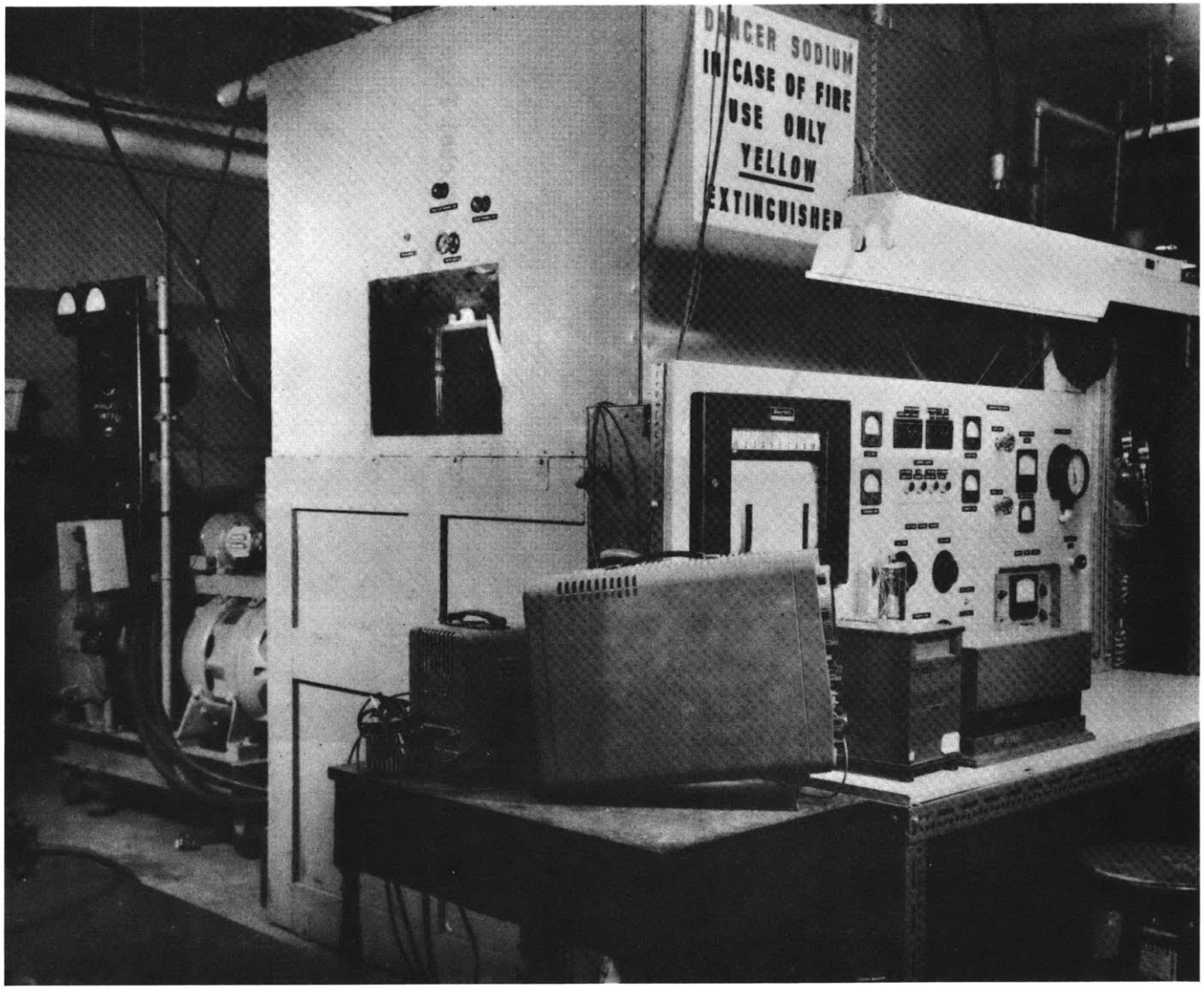

FIG. 8. GENERAL VIEW OF HEAT TRANSFER FACILITY

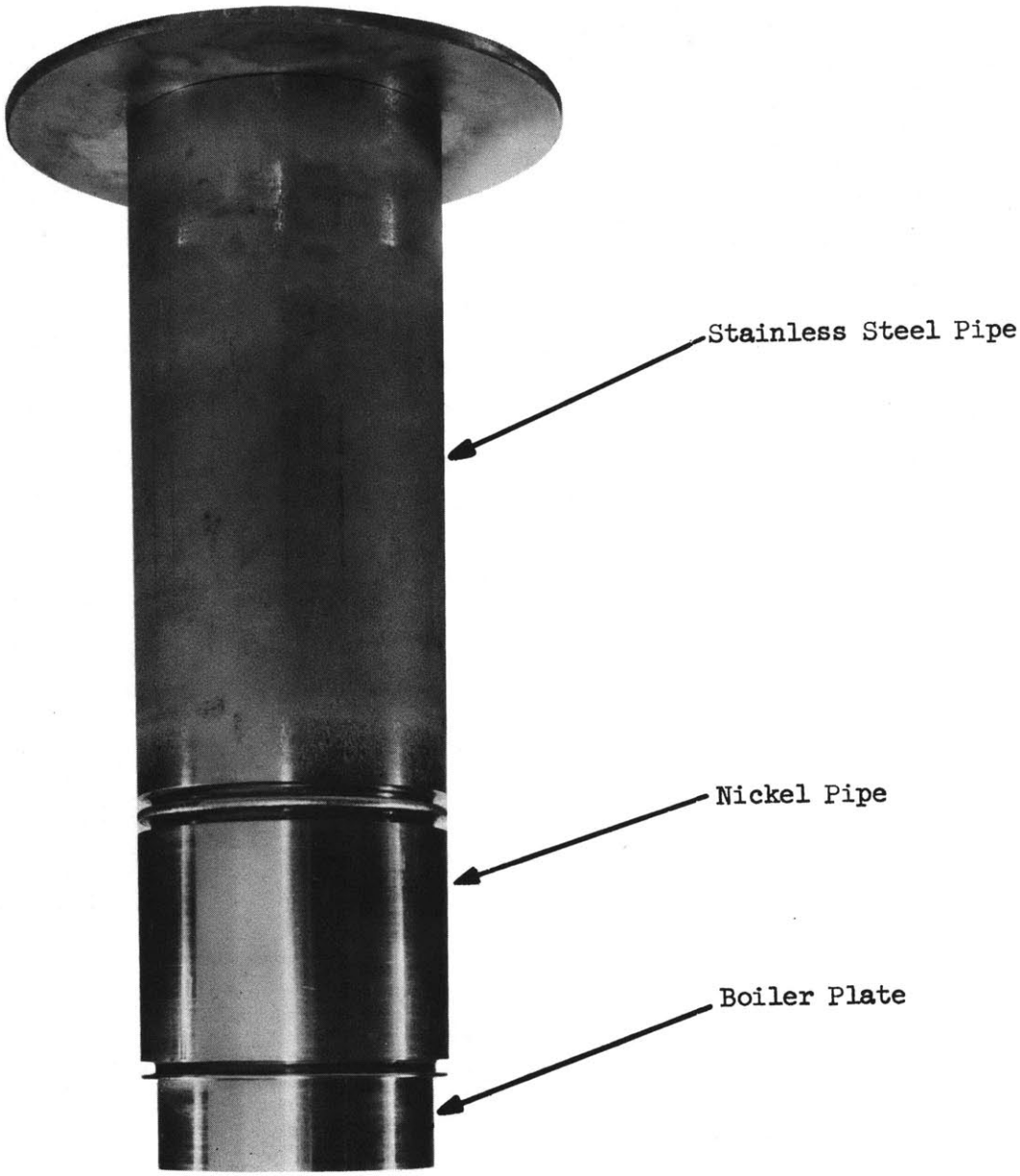

FIG. 9 BOILER PARTS

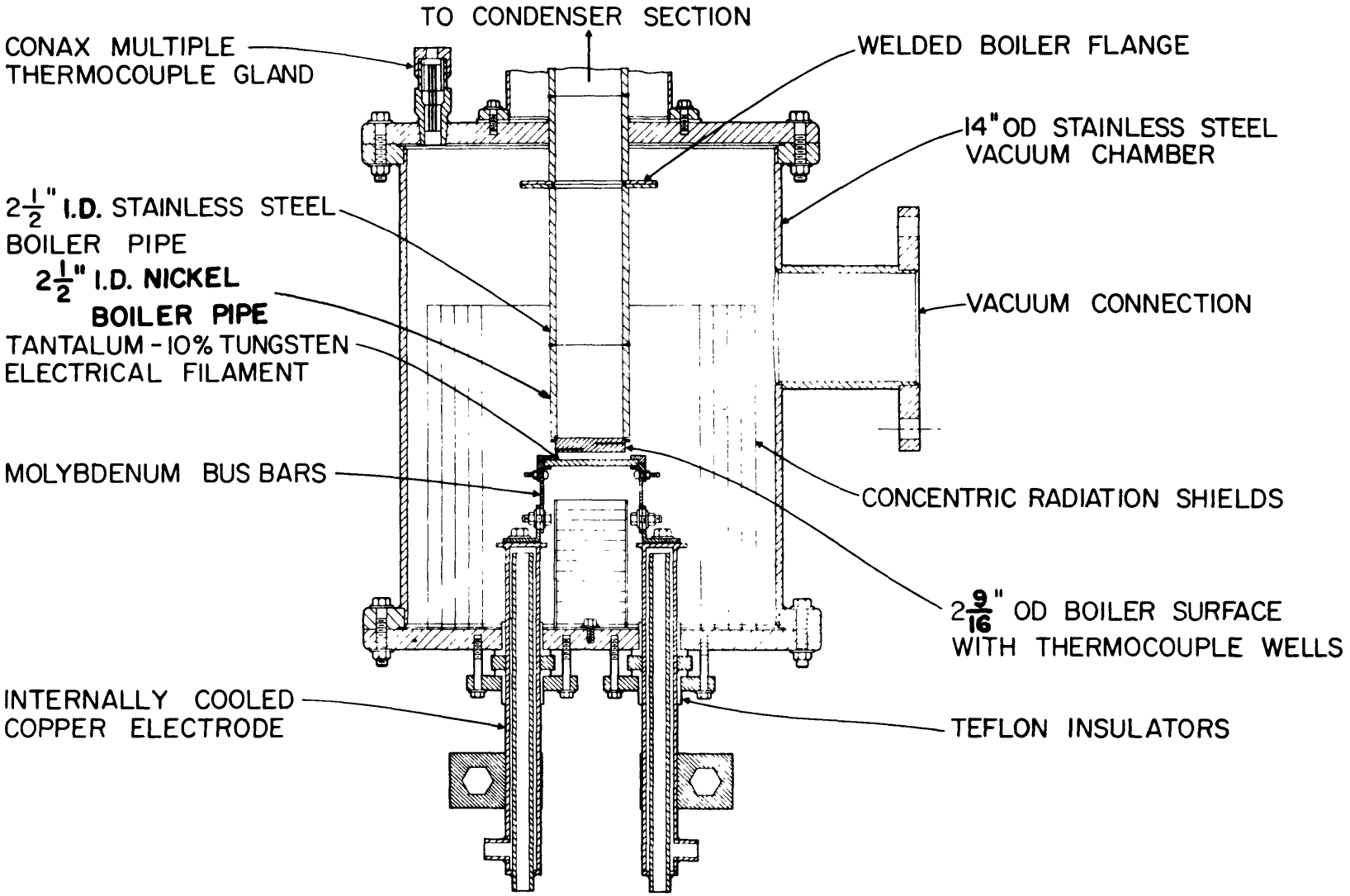

FIG. 10 HEATER & BOILER SECTIONAL DRAWING

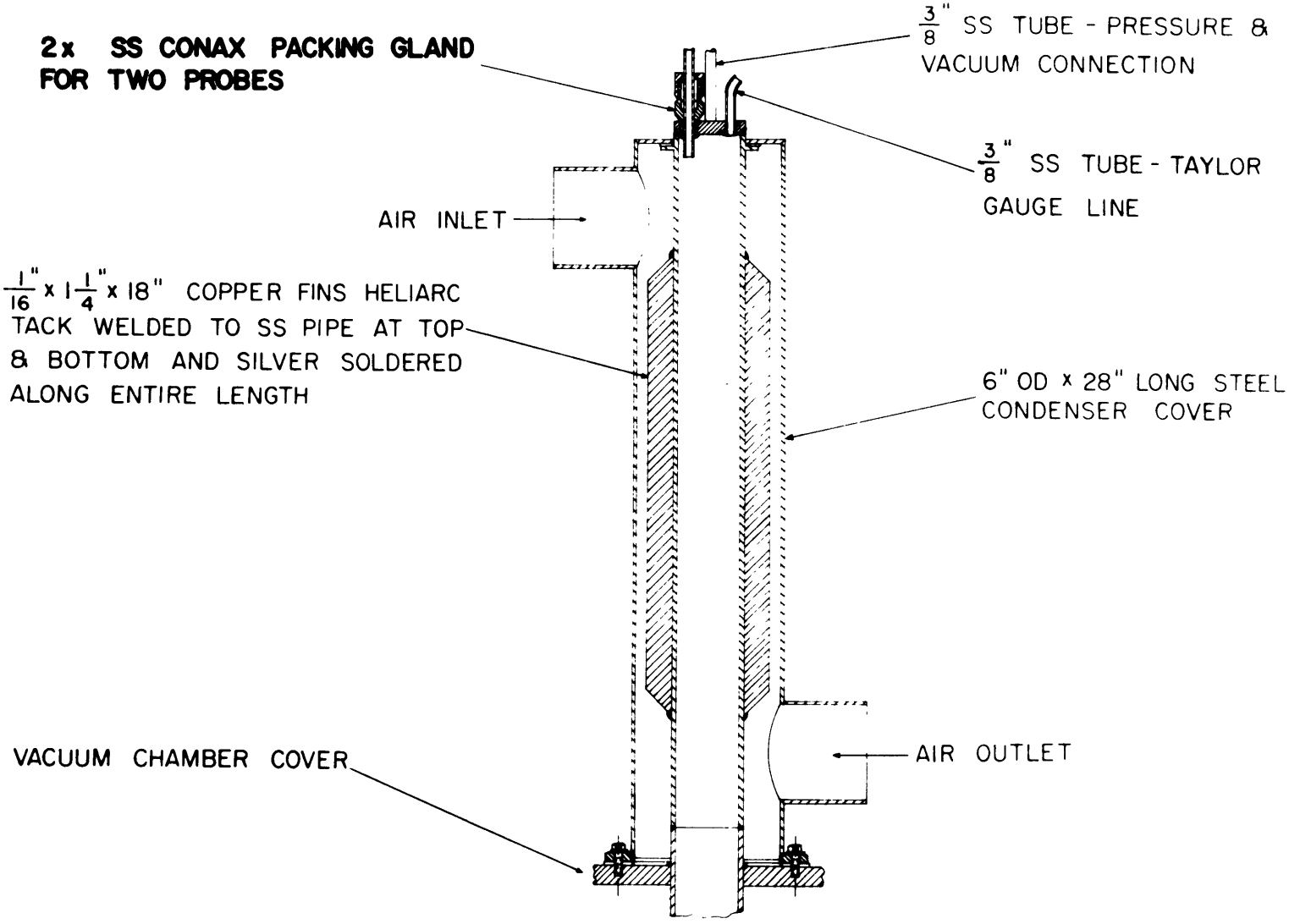

FIG 11 CONDENSER SECTIONAL DRAWING

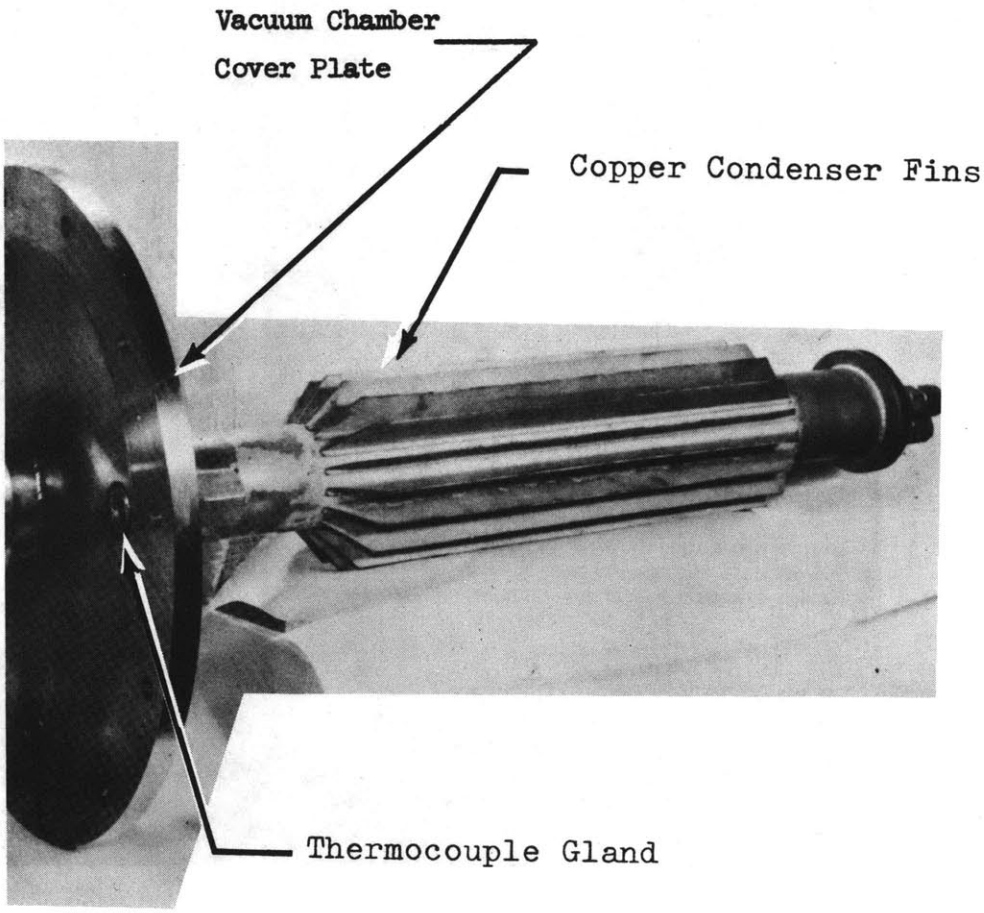

FIG. 12 VIEW OF CONDENSER

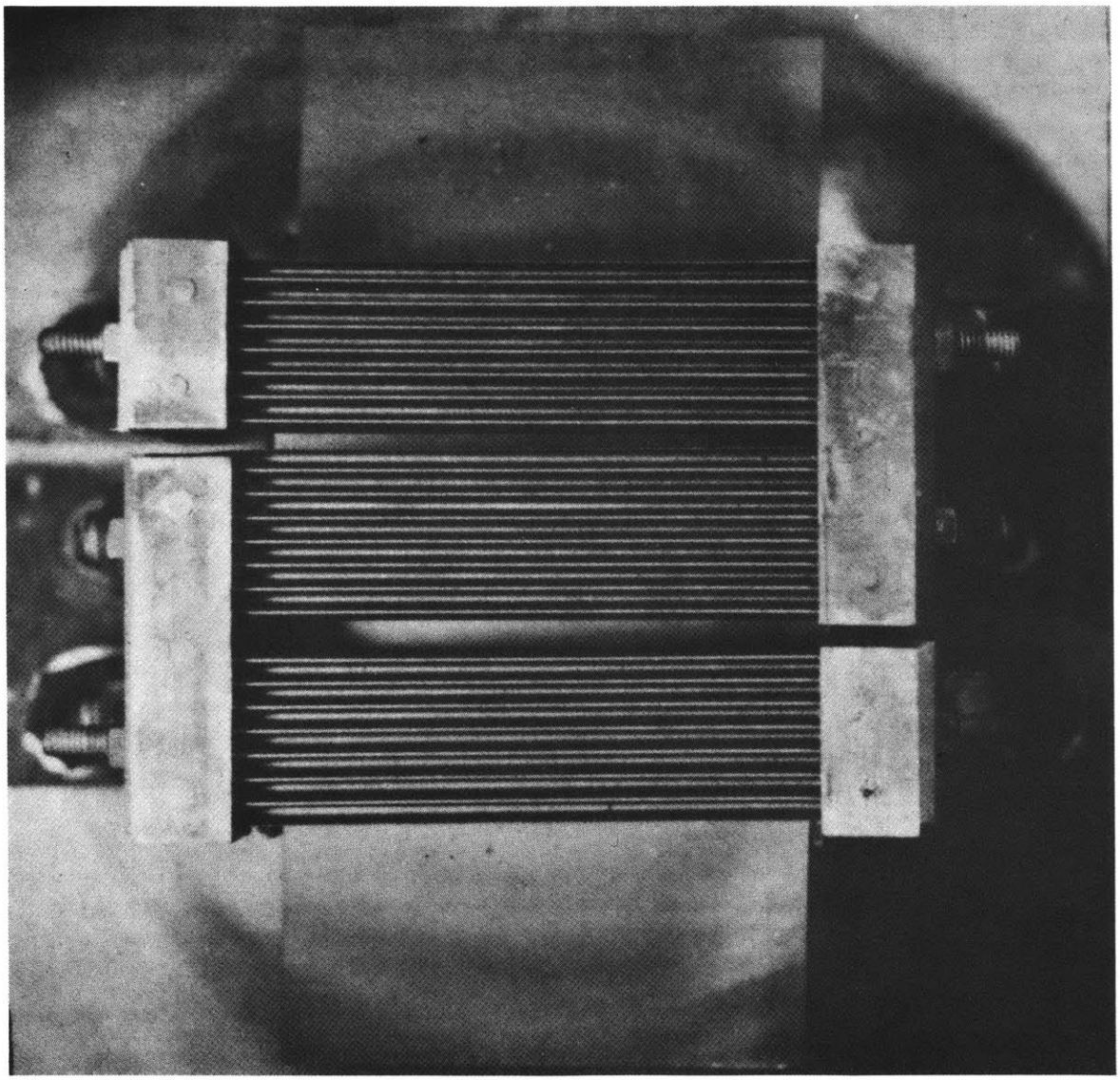

FIG. 13. OVERHEAD VIEW OF MAIN HEATER

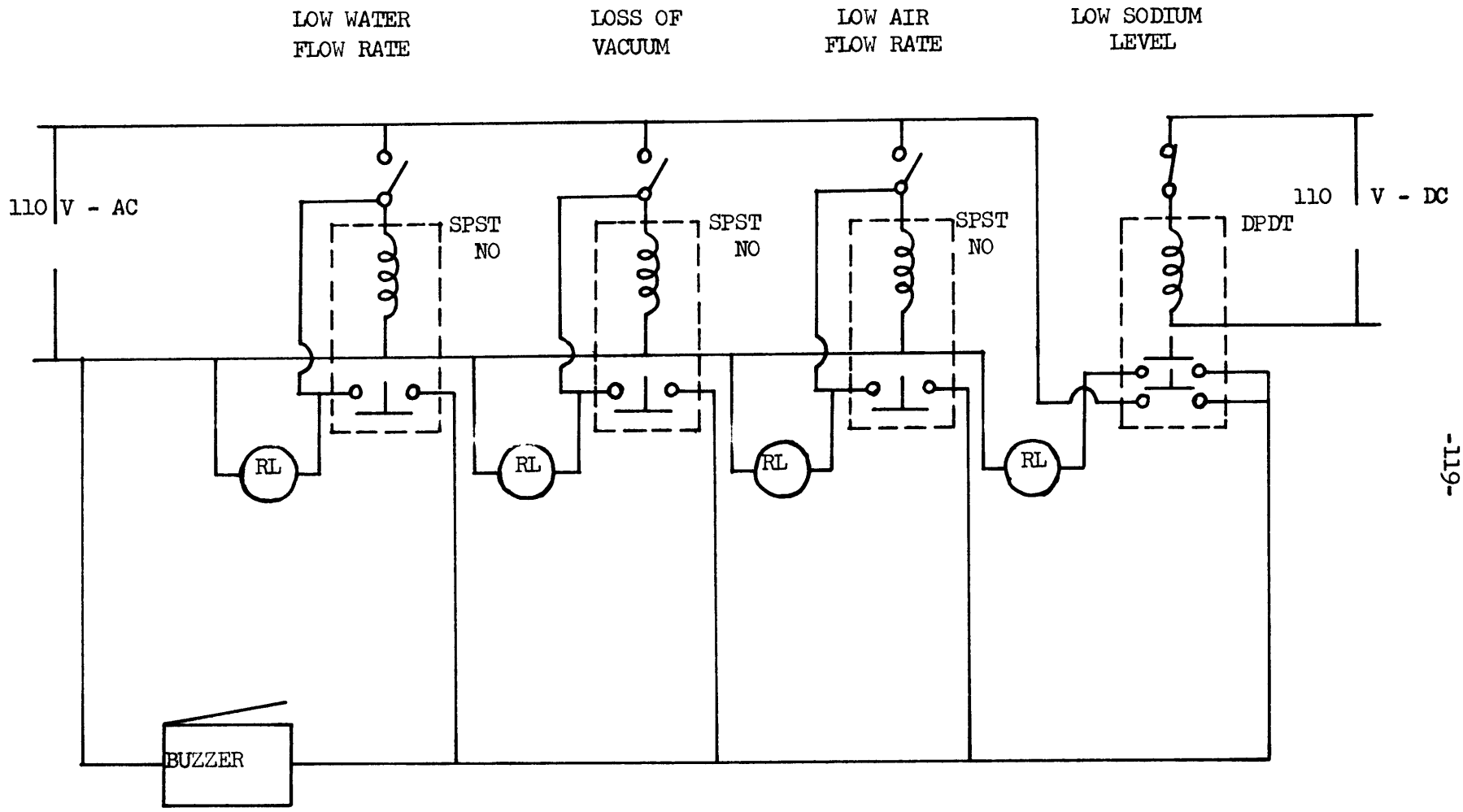

FIG. 14: ELECTRICAL WIRING DIAGRAM FOR CONTROL SYSTEM

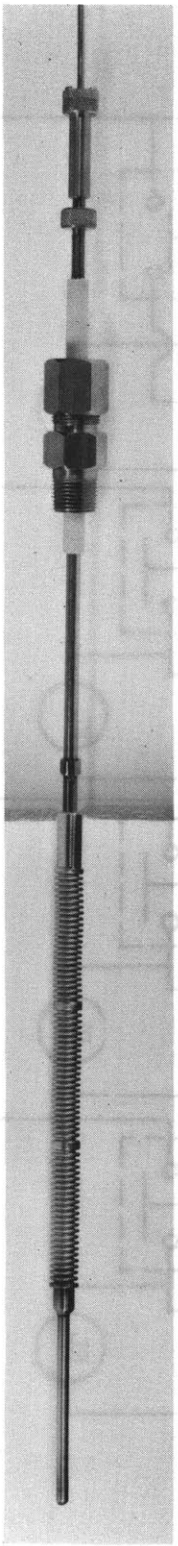

FIG. 15 ADJUSTABLE VERTICAL PROBE

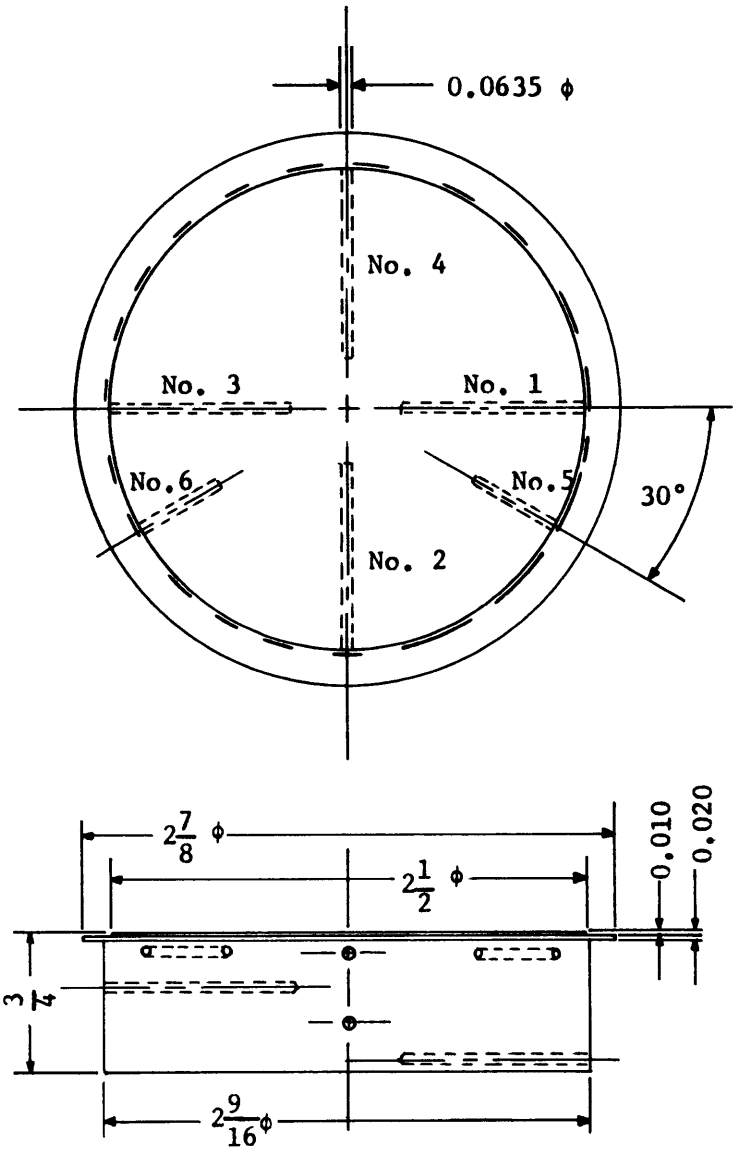

T.C. No.	Immersion Length	℄ DISTANCE To Boiler Surface
1	1.0 in.	0.660 in.
2	1.0 in.	0.470 in.
3	1.0 in.	0.280 in.
4	1.0 in.	0.090 in.
5	0.5 in.	0.090 in.
6	0.5 in.	0.090 in.

FIG. 16: BOILER PLATE OF MARTO (5)

FIG. 17. SAMPLE OF DOUBLY RE-ENTRANT CAVITY
0.004 IN. MOUTH DIA. X 0.025 IN. DEEP
(75X) MARTO

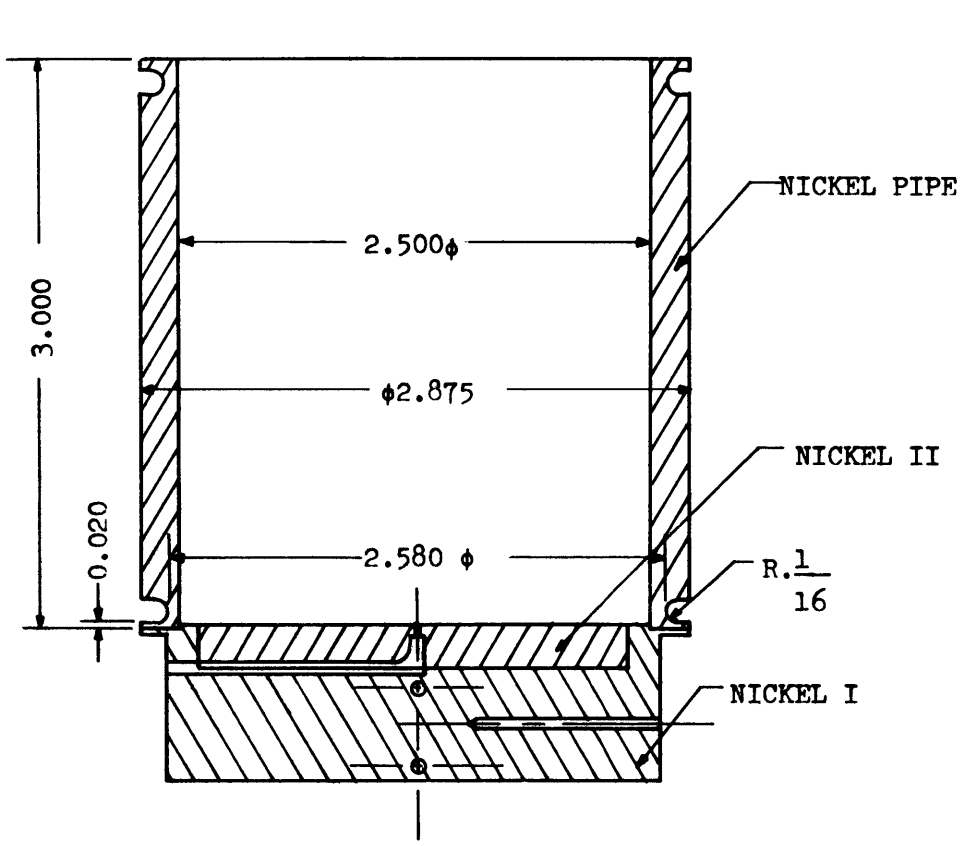

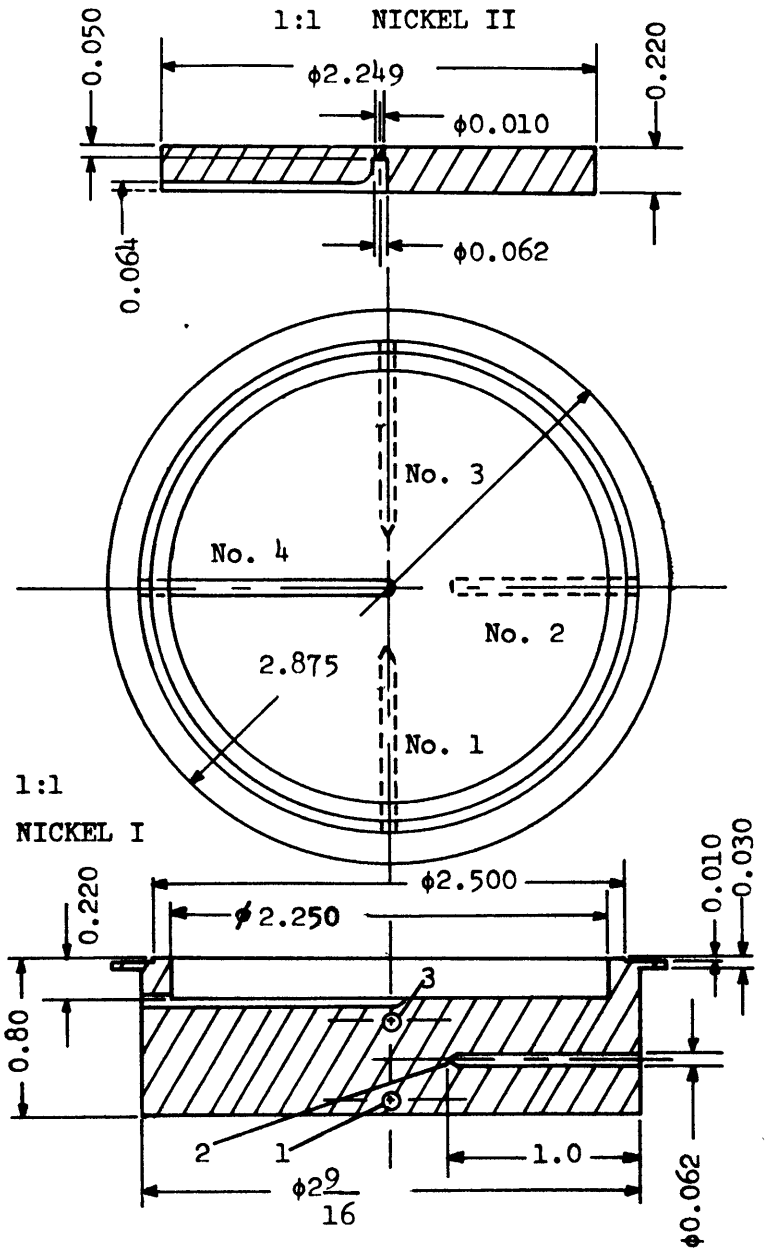

T.C. No.	Immersion Length	℄ Distance From Boiler Surface
1	1.0 in.	0.710 in.
2	1.0 in.	0.510 in.
3	1.0 in.	0.310 in.
4	Under Cavity	0.050 in.

FIG. 18: BOILER PLATE WITH PERMANENT T. C.

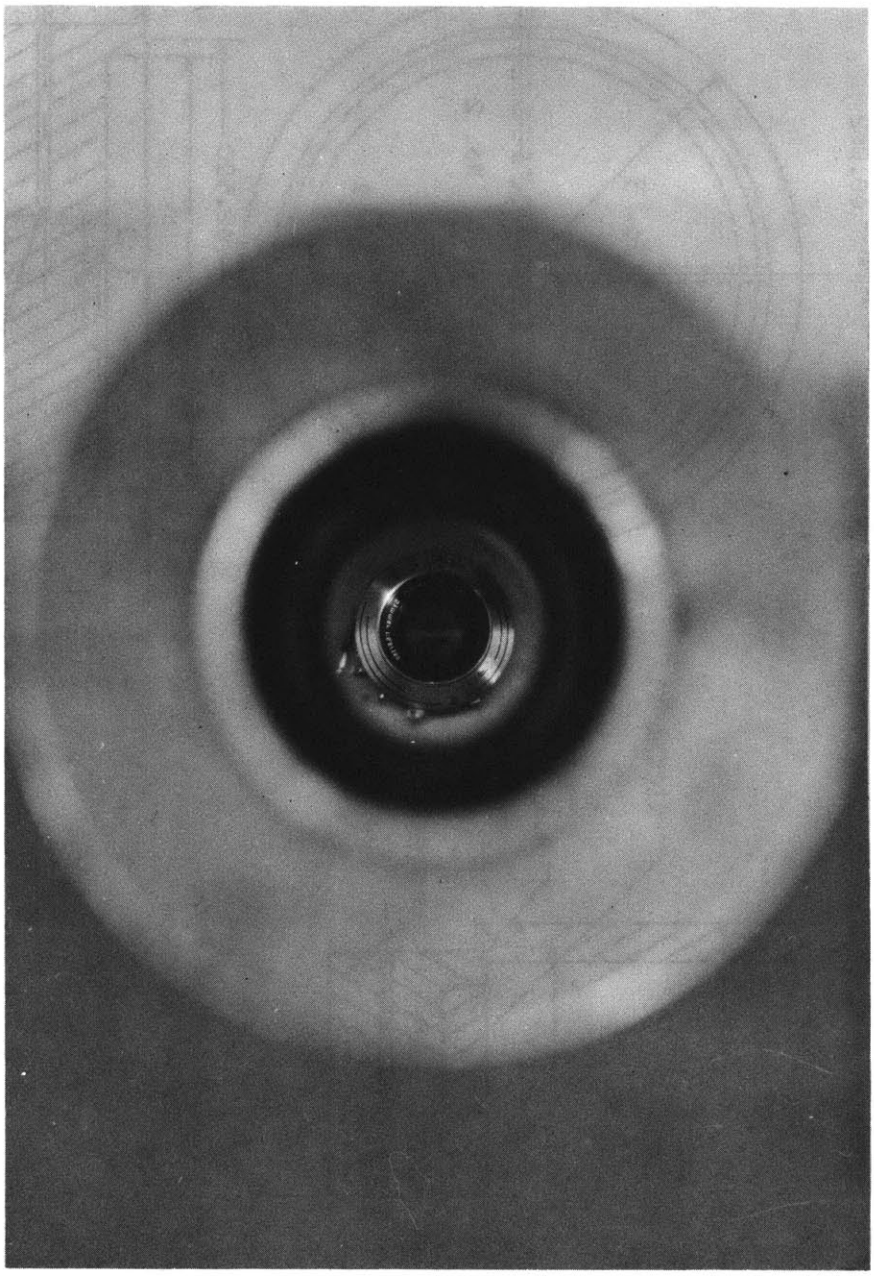

FIG. 19 SURFACE WITH MIRROR FINISH
(Looking from the Top of the Boiler)

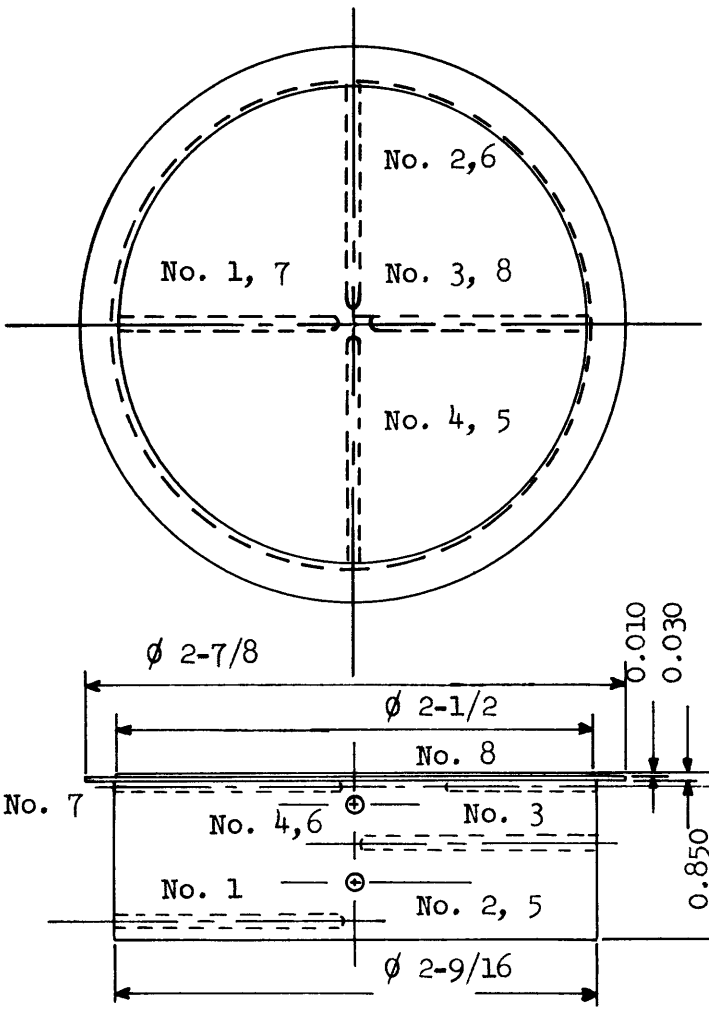

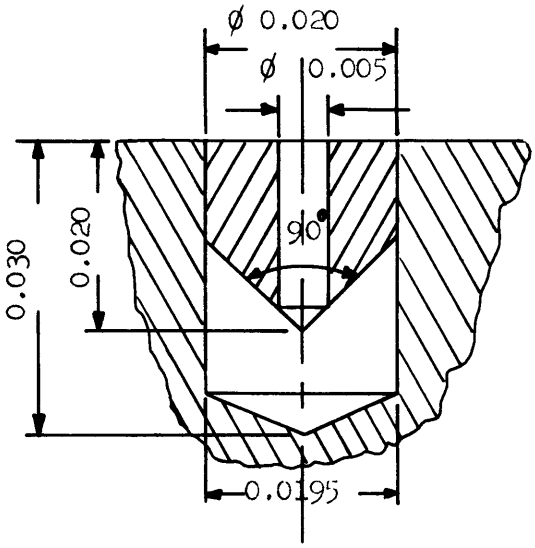

Run: 13: Re-Entry Cavity
Scale 50:1

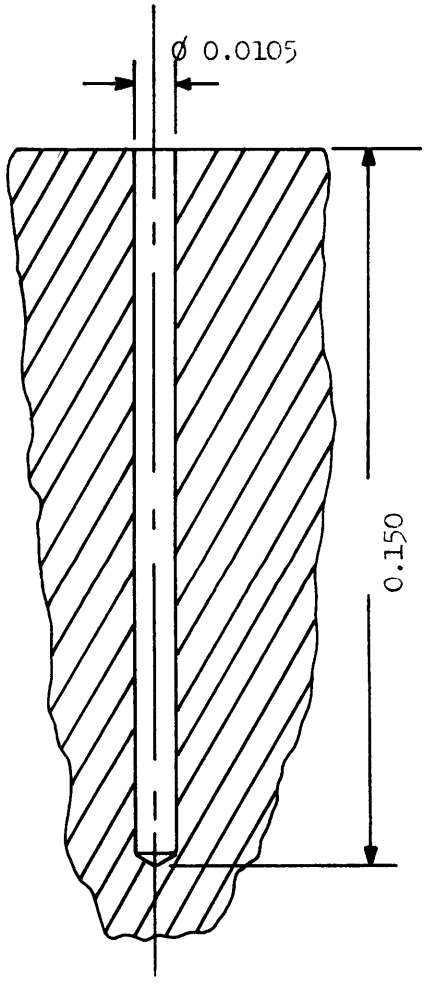

Run 14: Cylindrical
Cavity. Scale 25:1

T.C. No.	Diameter (in.)	Immersion Length(in.)	℄ Distance From Surface (in.)
1	0.0625	1.275	0.750
2	0.0625	1.275	0.550
3	0.0625	1.275	0.350
4	0.0625	1.275	0.150
5	0.0625	0.650	0.550
6	0.0625	0.650	0.150
7	0.040	1.100	0.050
8	0.040	0.800	0.050

FIG. 20: BOILER PLATE WITH ARTIFICIAL CAVITIES

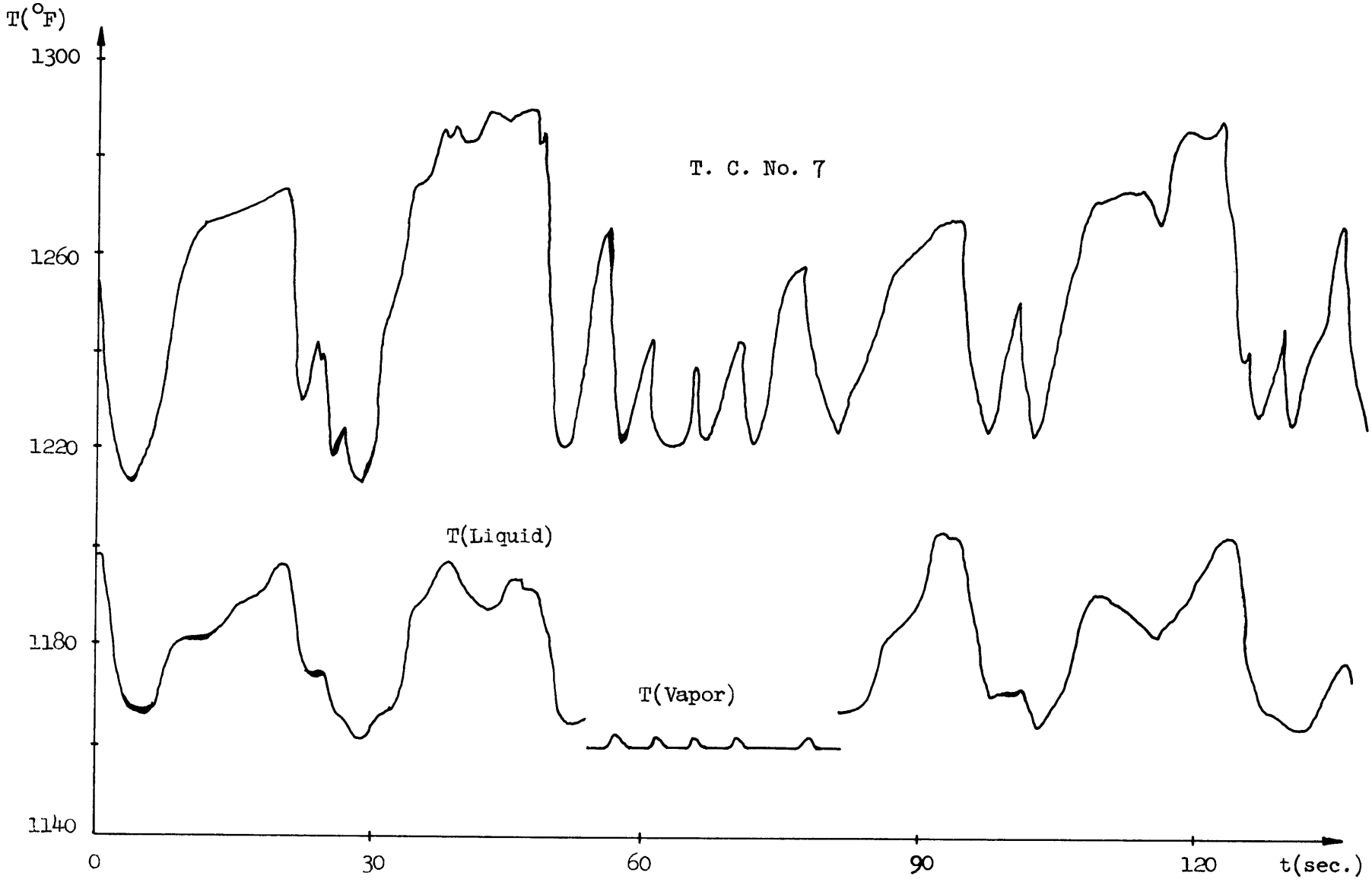

FIG. 21 TEMPERATURE VARIATIONS DURING BUMPING

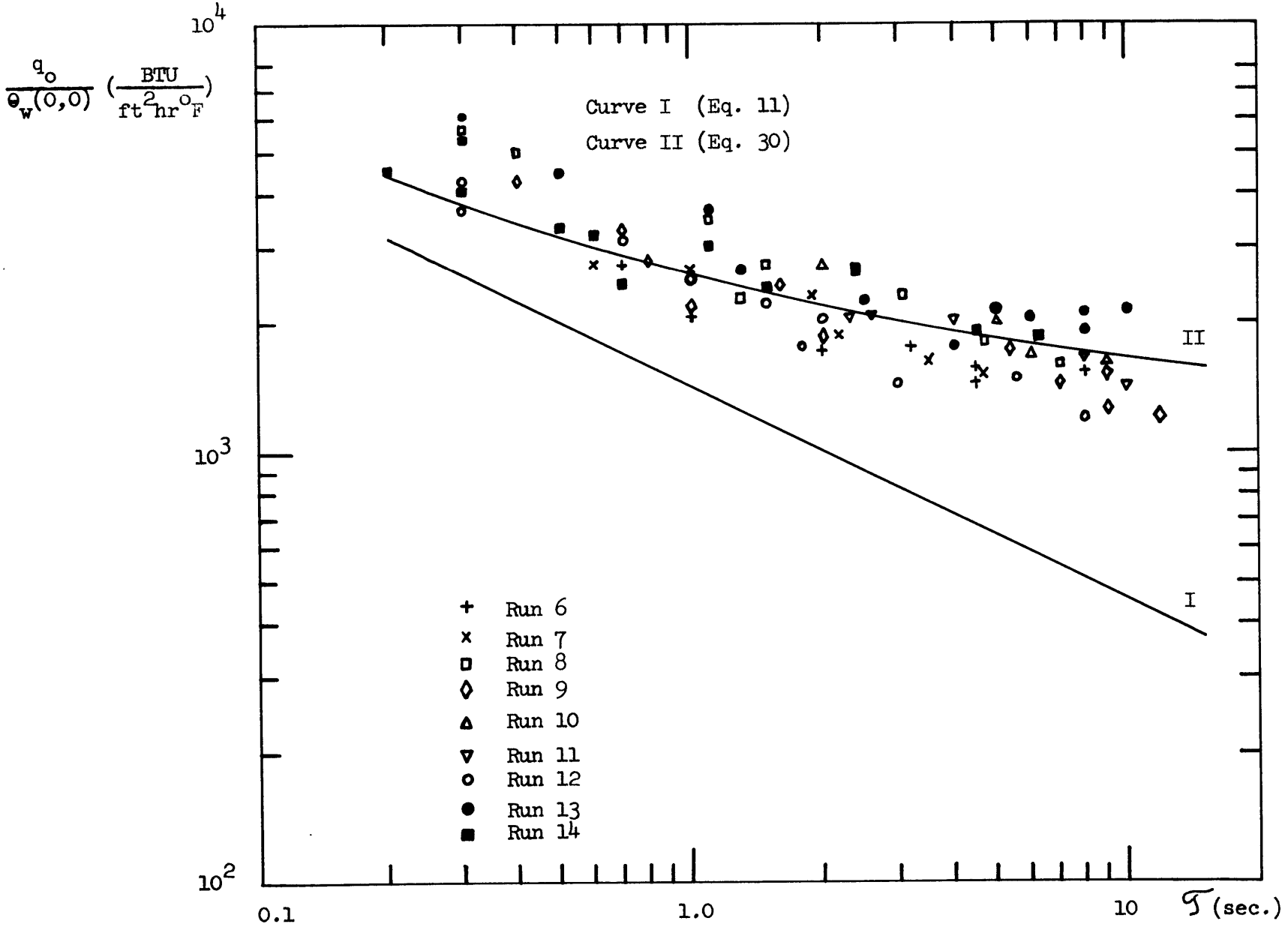

FIG. 22: $\frac{q_o}{\theta_w(0,0)}$ vs. τ

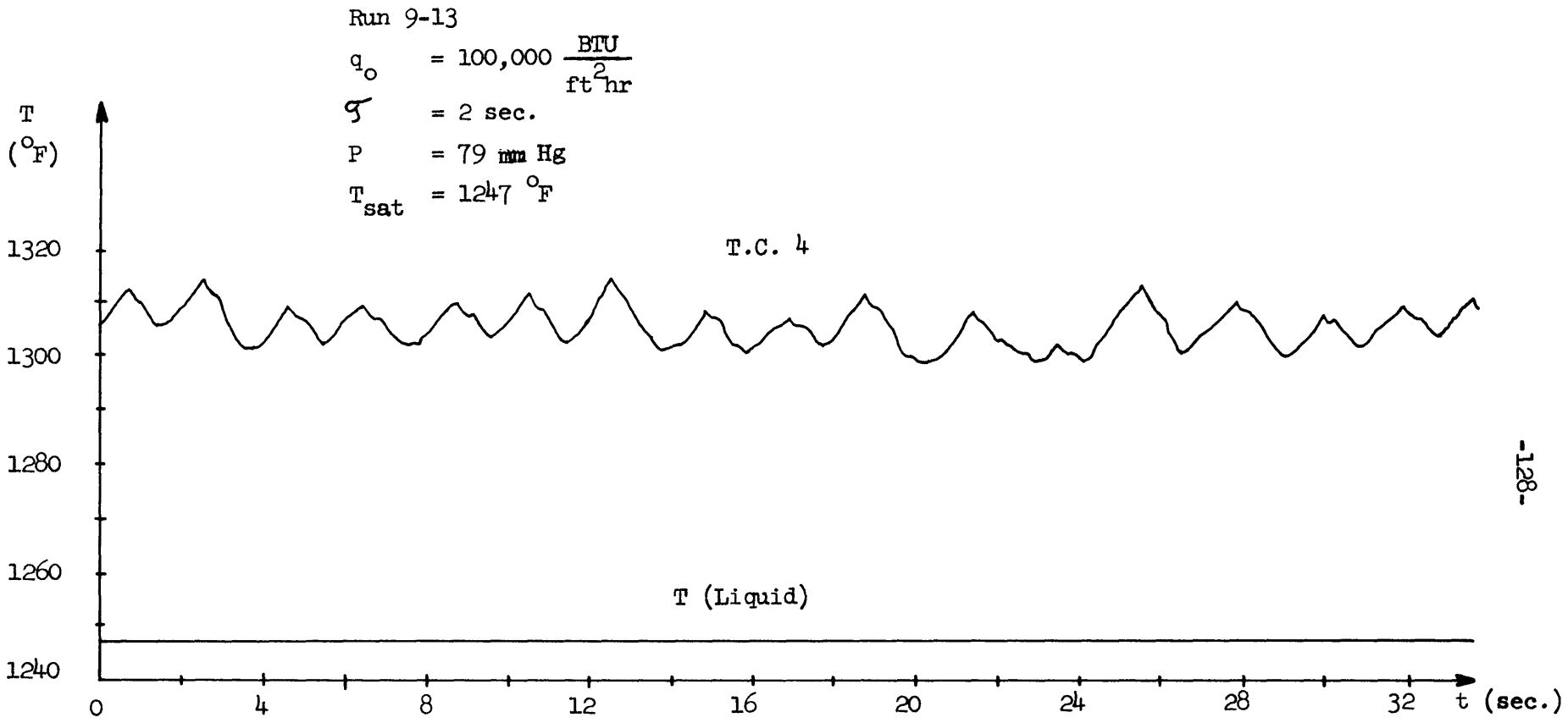

FIG. 23a: TRACES OF TEMPERATURE VARIATION DURING STABLE BOILING

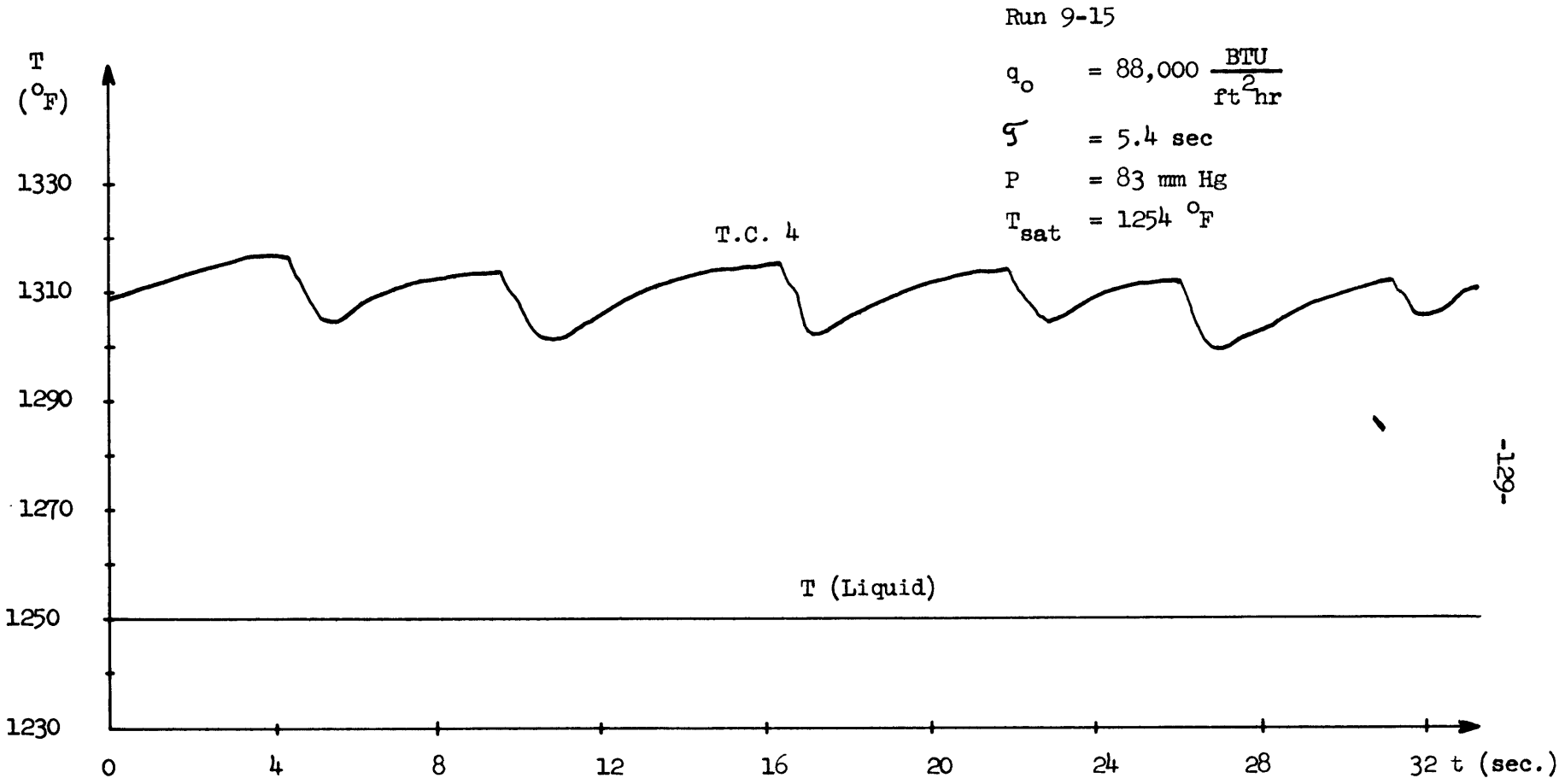

FIG. 23b: TRACES OF TEMPERATURE VARIATION DURING STABLE BOILING

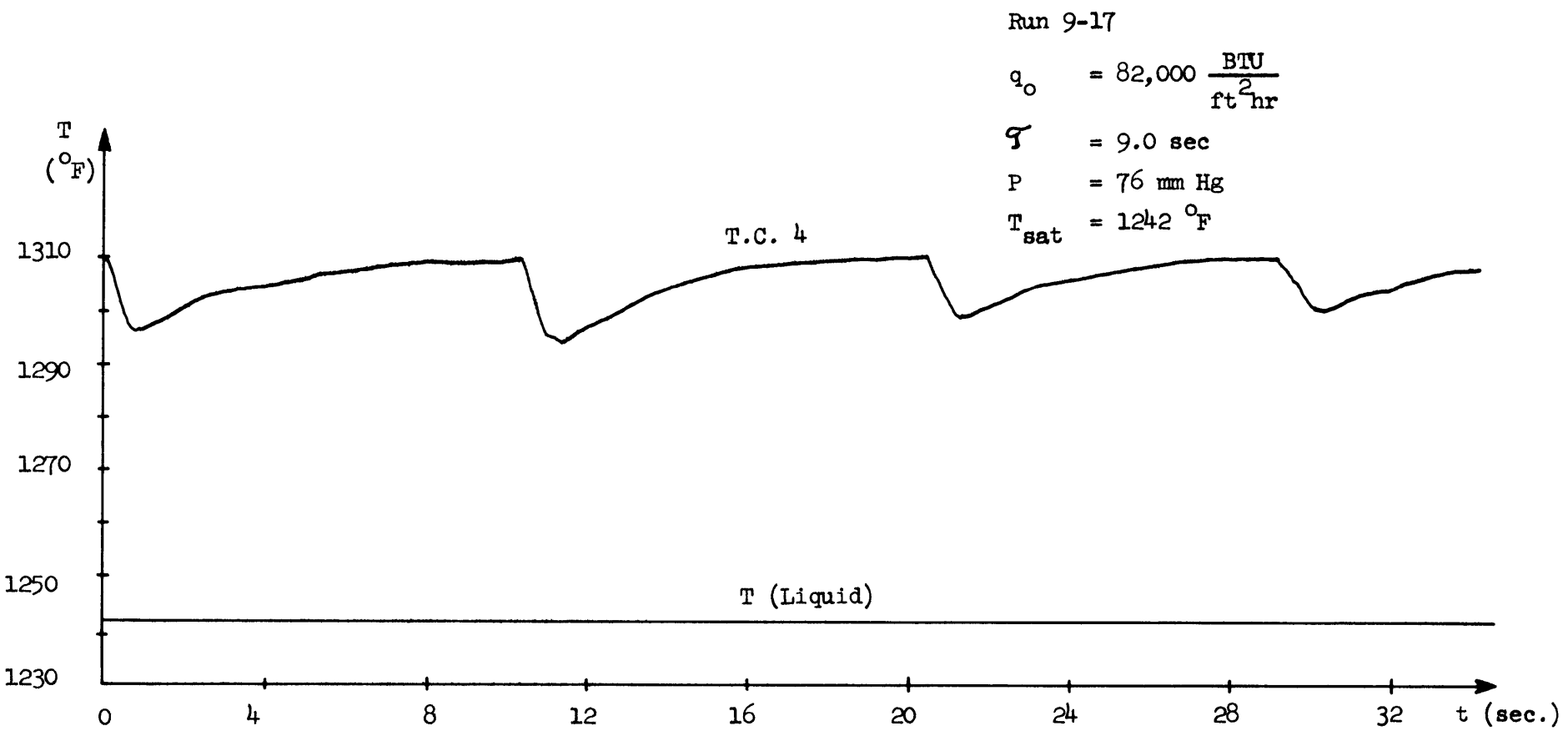

FIG. 23c: TRACES OF TEMPERATURE VARIATION DURING STABLE BOILING

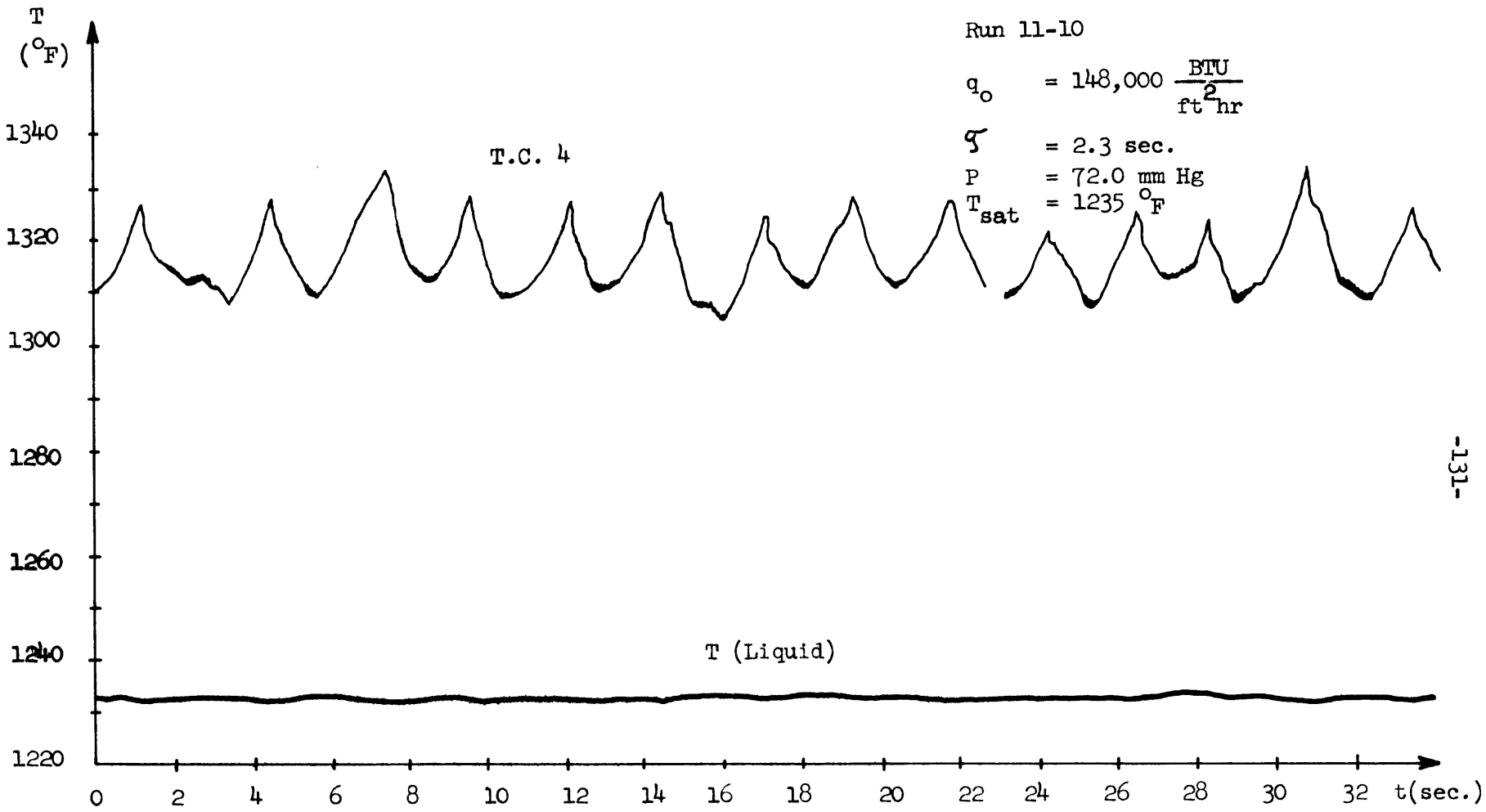

FIG. 24a: TRACES OF TEMPERATURE VARIATION DURING STABLE BOILING

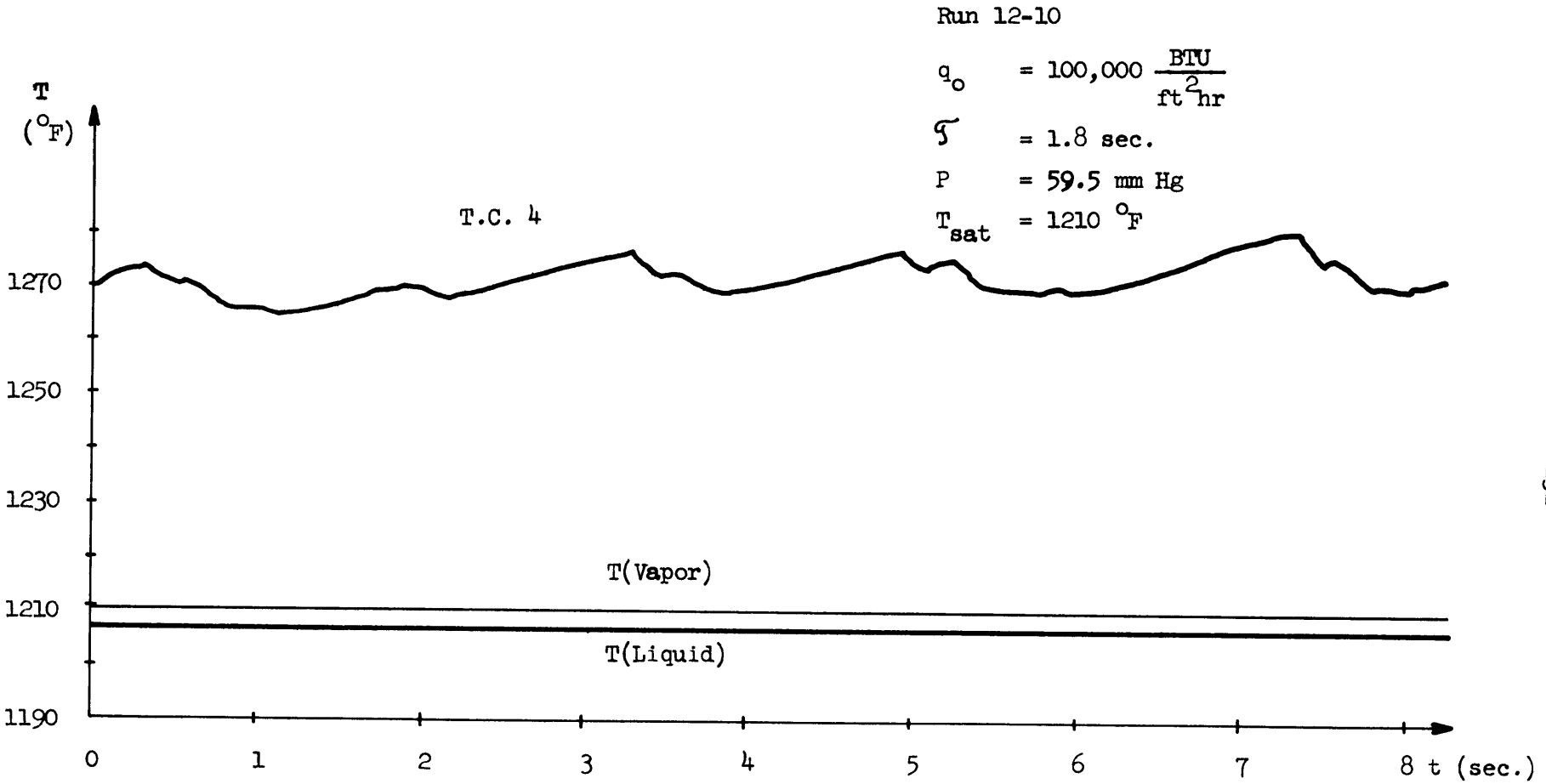

FIG. 24b: TRACES OF TEMPERATURE VARIATION DURING STABLE BOILING

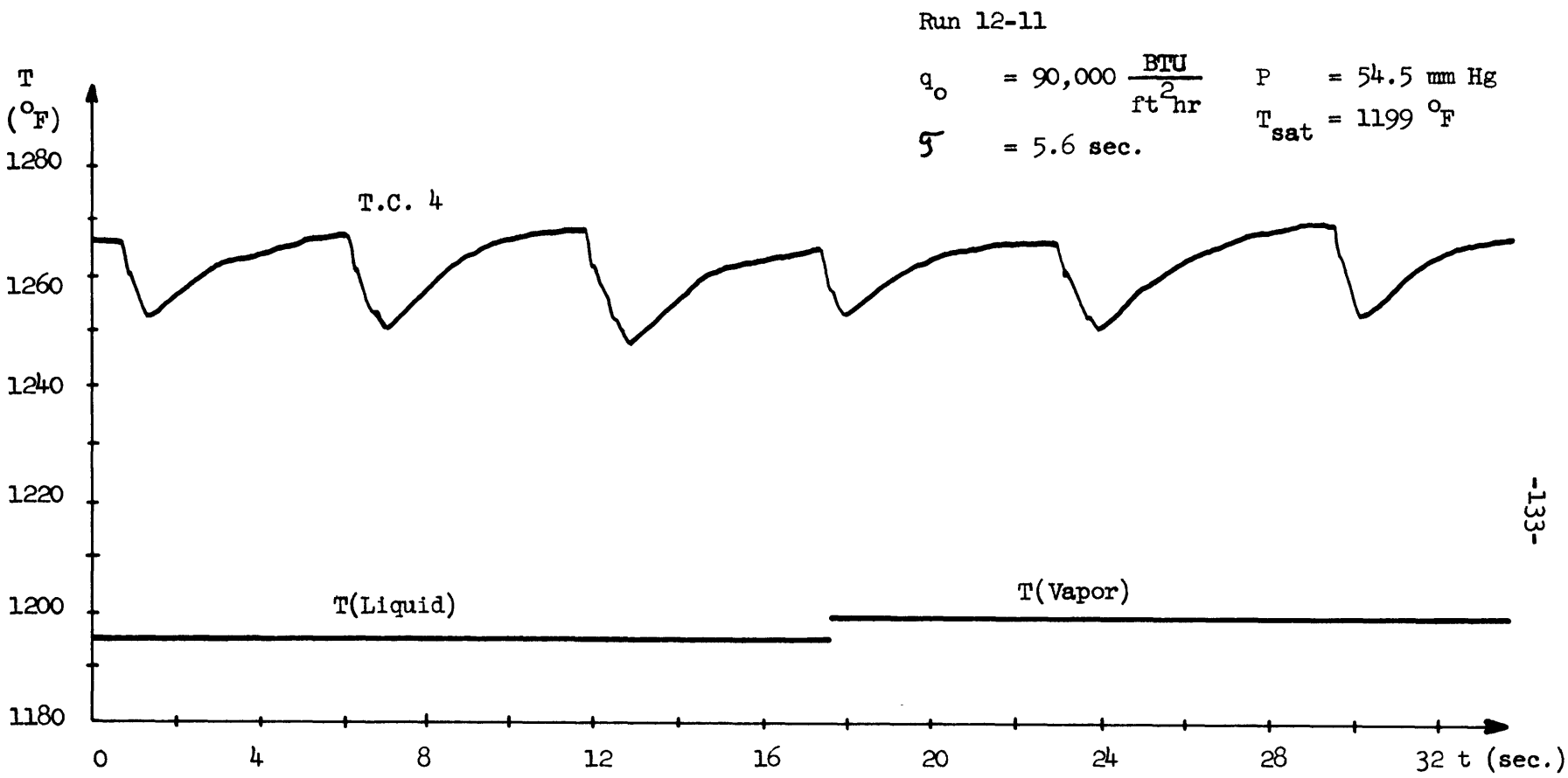

FIG. 24c: TRACES OF TEMPERATURE VARIATION DURING STABLE BOILING

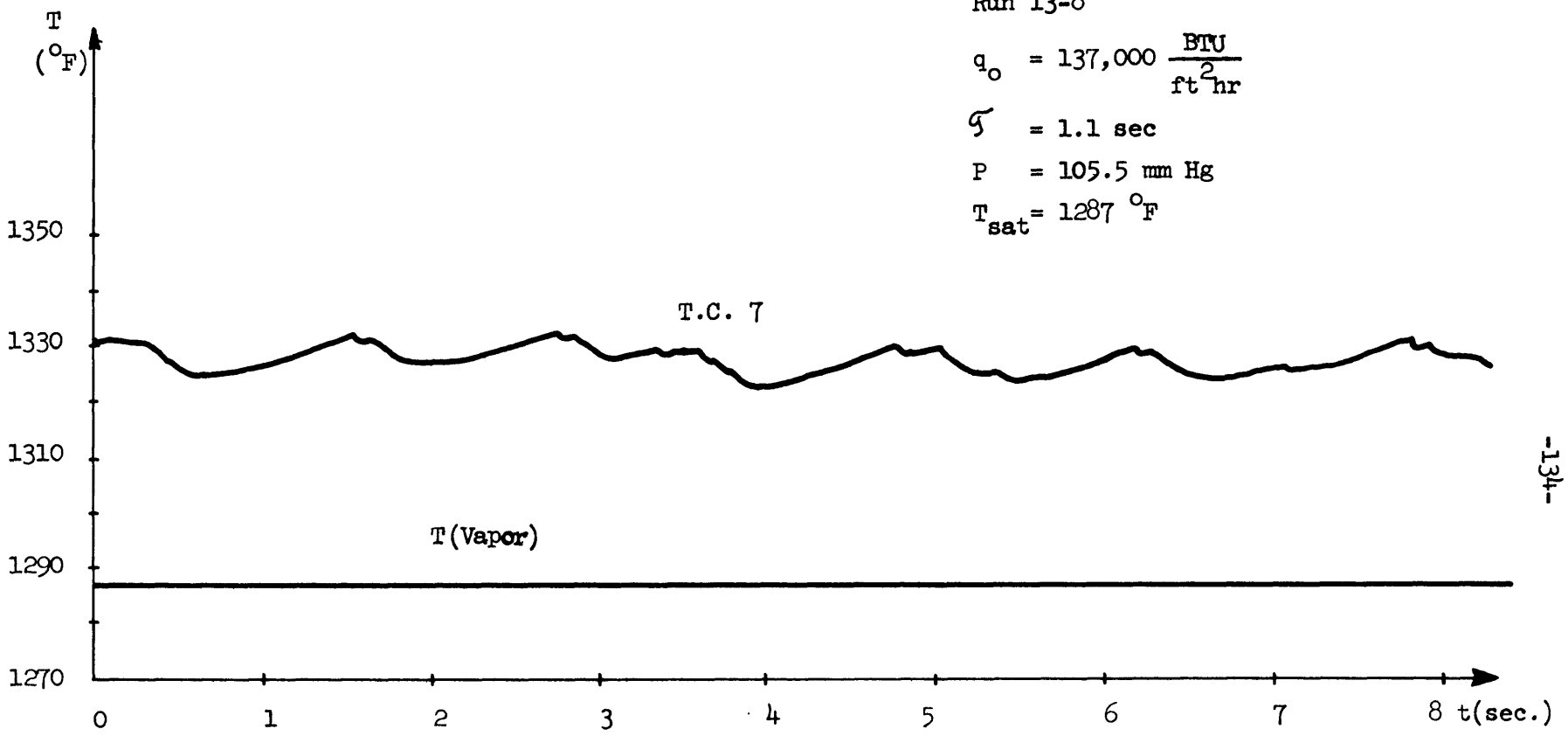

FIG. 25a: TRACES OF TEMPERATURE VARIATION DURING STABLE BOILING

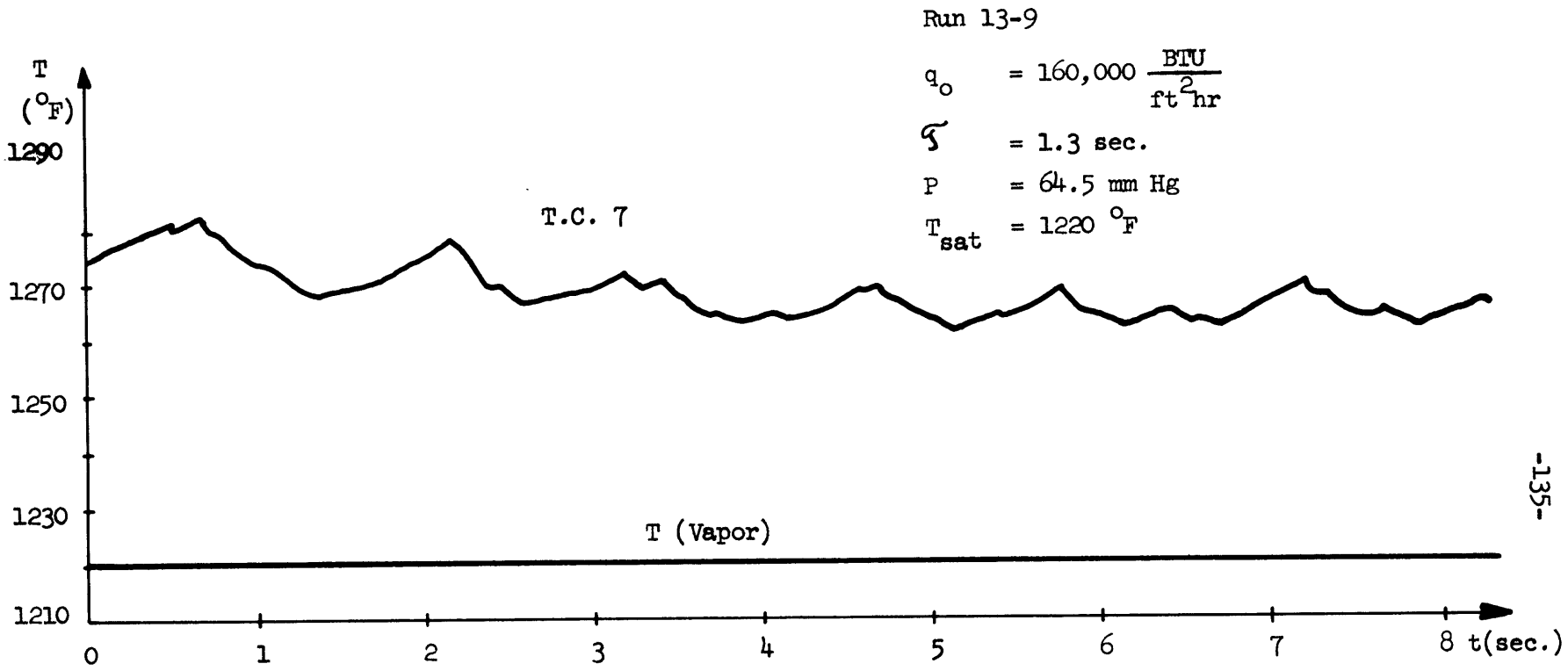

FIG. 25b: TRACES OF TEMPERATURE VARIATION DURING STABLE BOILING

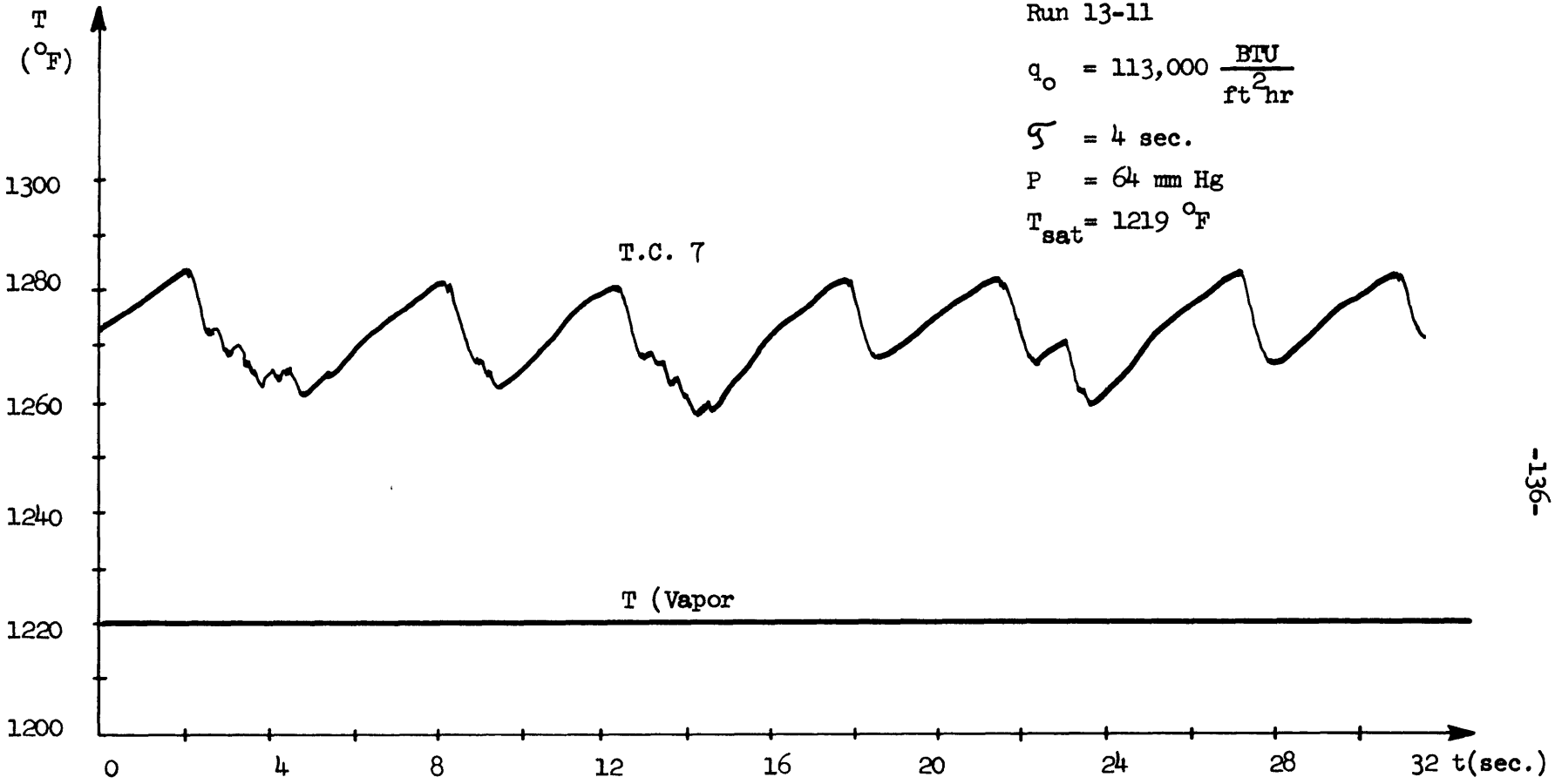

FIG. 25c: TRACES OF TEMPERATURE VARIATION DURING STABLE BOILING

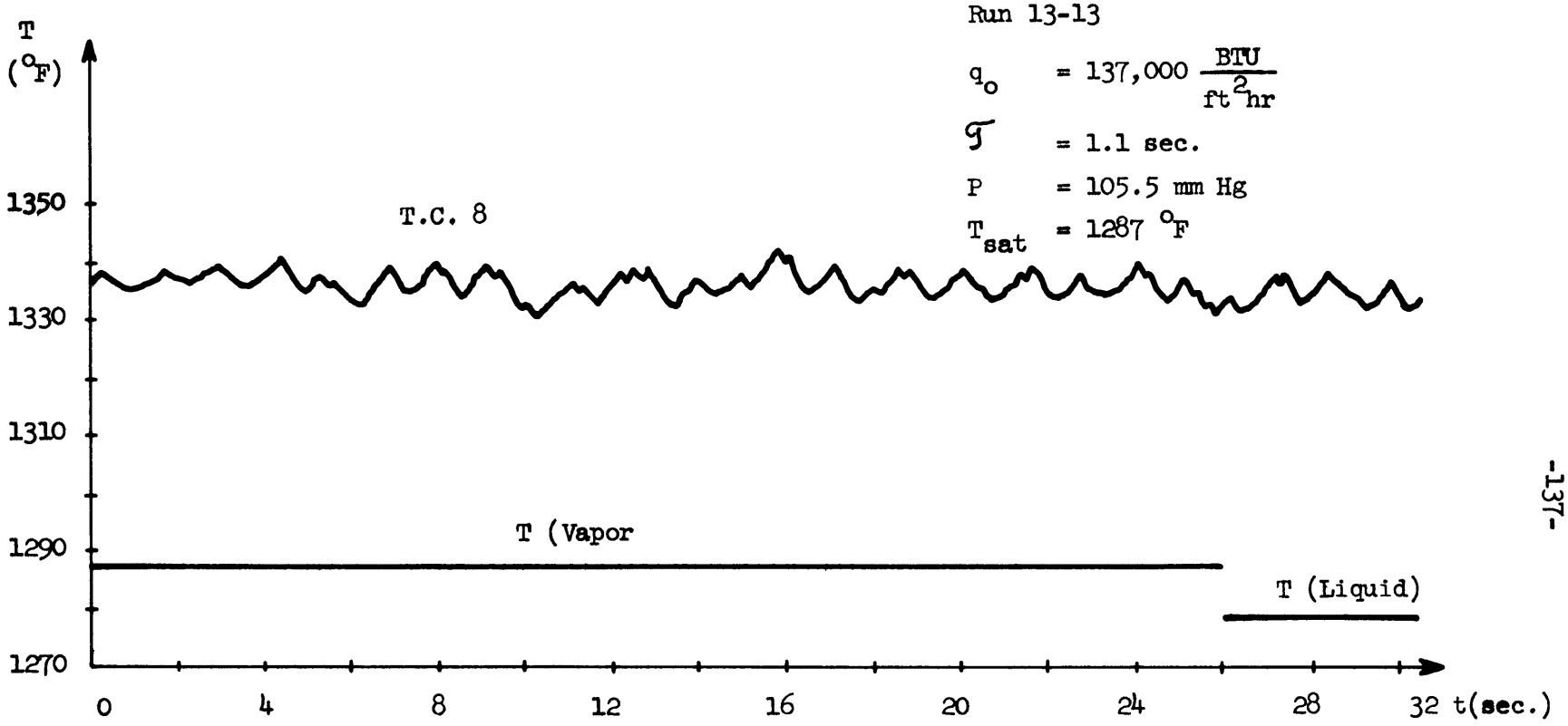

FIG. 25d: TRACES OF TEMPERATURE VARIATION DURING STABLE BOILING

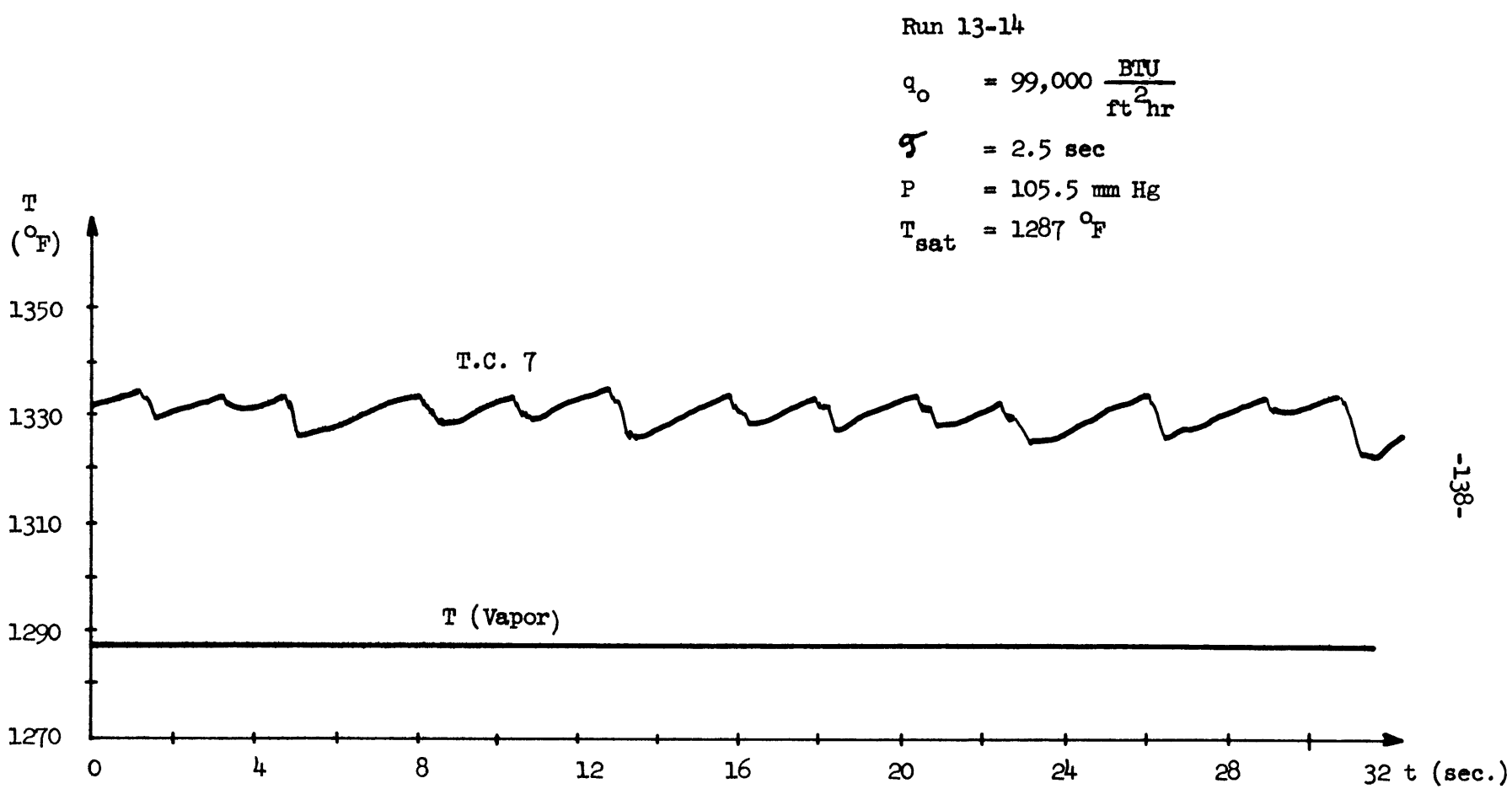

FIG. 25e: TRACES OF TEMPERATURE VARIATION DURING STABLE BOILING

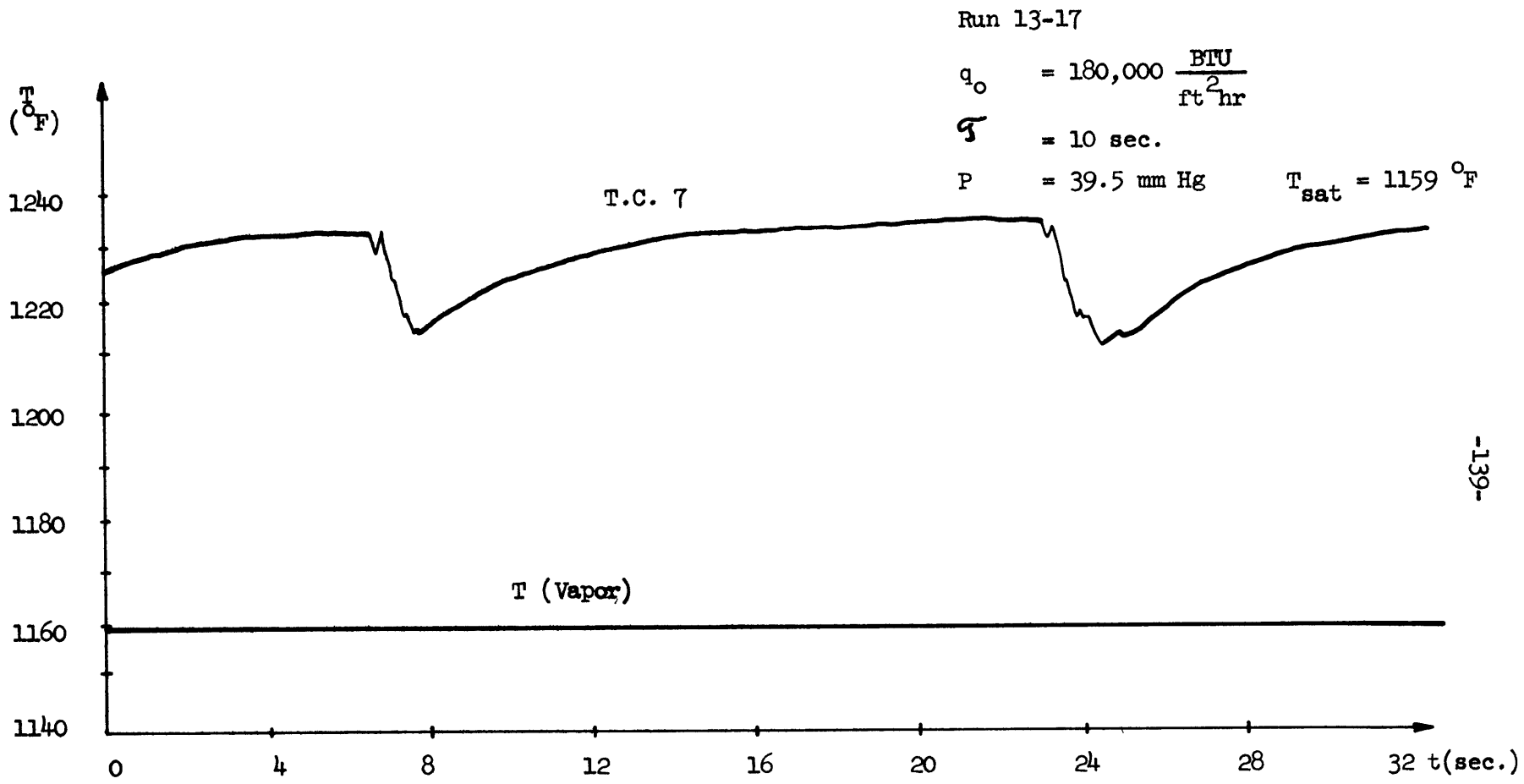

FIG. 25f: TRACES OF TEMPERATURE VARIATION DURING STABLE BOILING

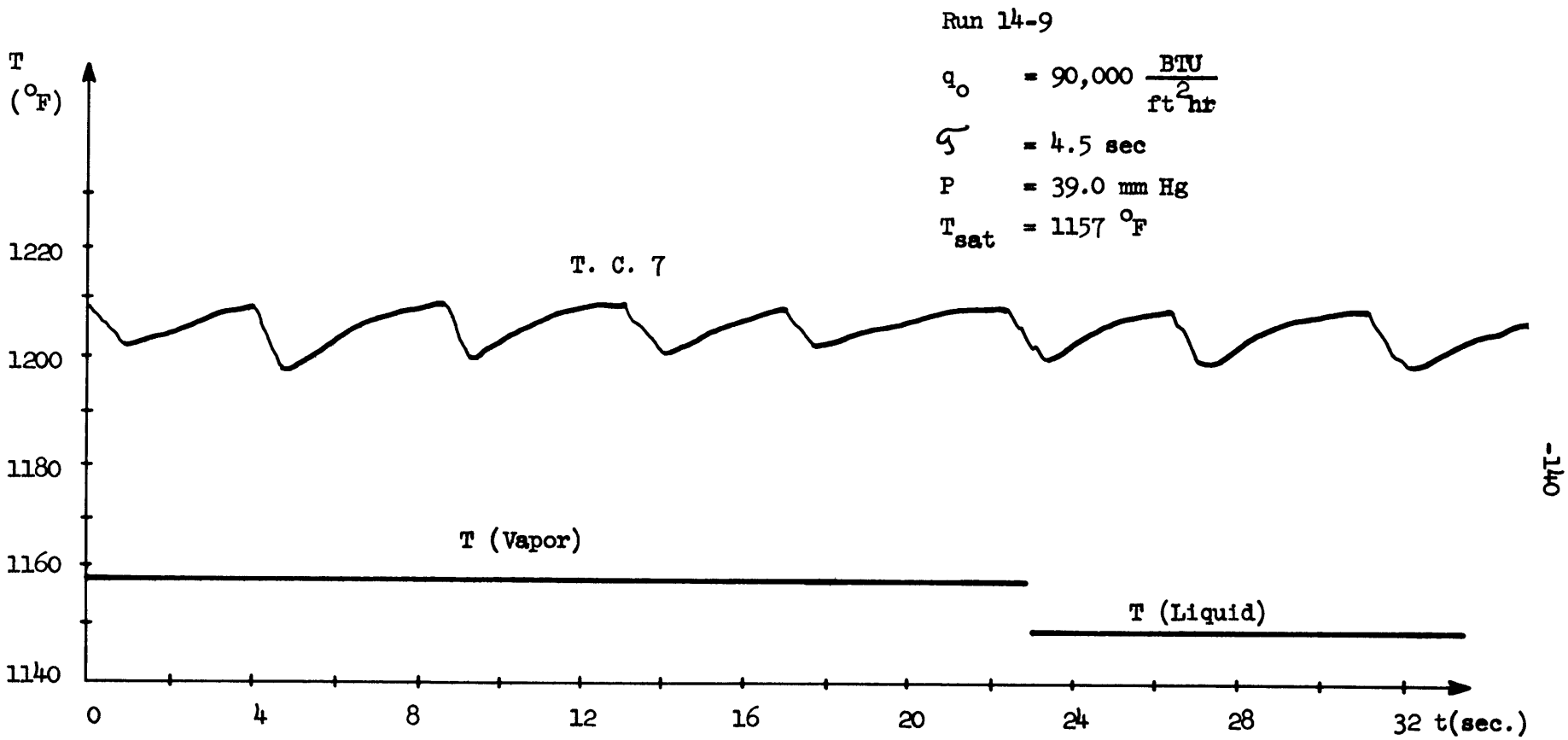

FIG. 26a: TRACES OF TEMPERATURE VARIATION DURING STABLE BOILING

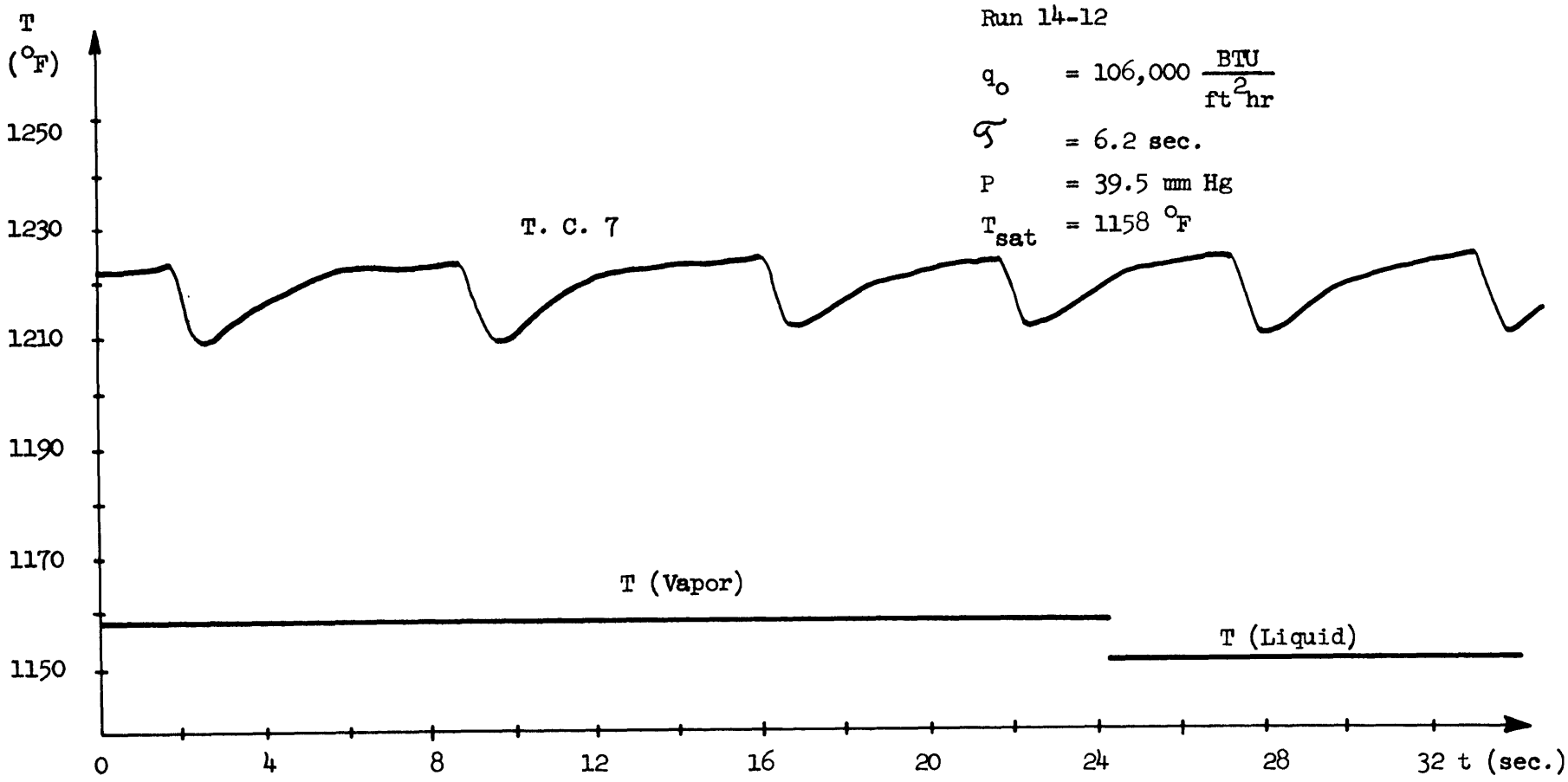

FIG. 26b: TRACES OF TEMPERATURE VARIATION DURING STABLE BOILING

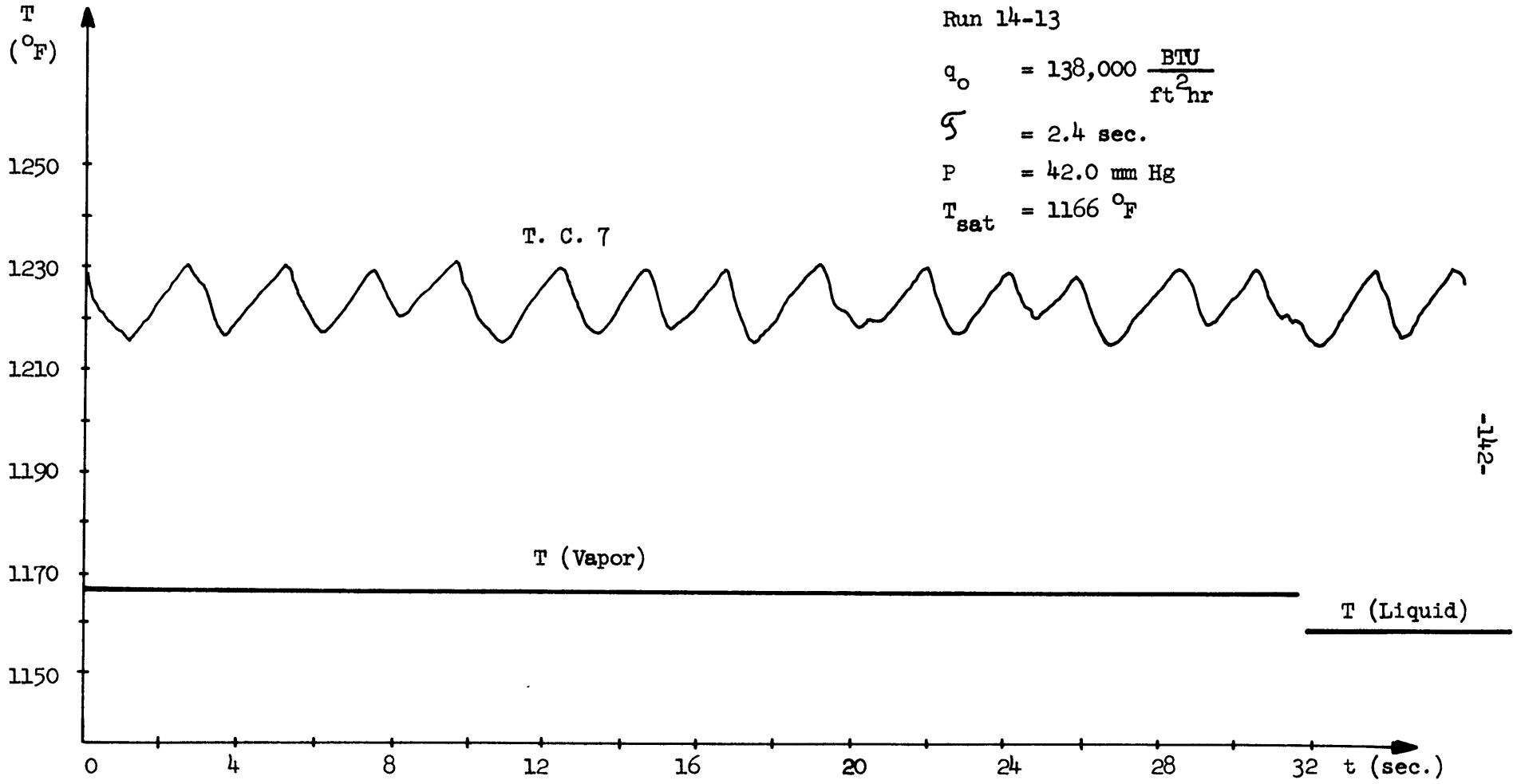

FIG. 26c: TRACES OF TEMPERATURE VARIATION DURING STABLE BOILING

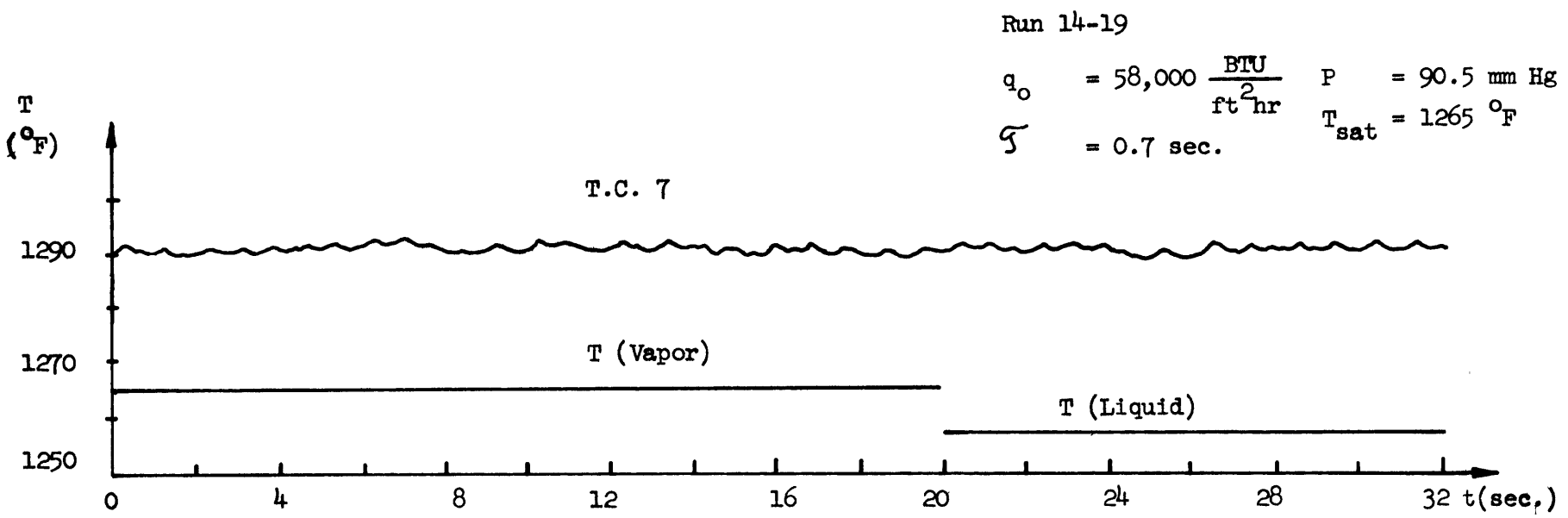

FIG. 26e

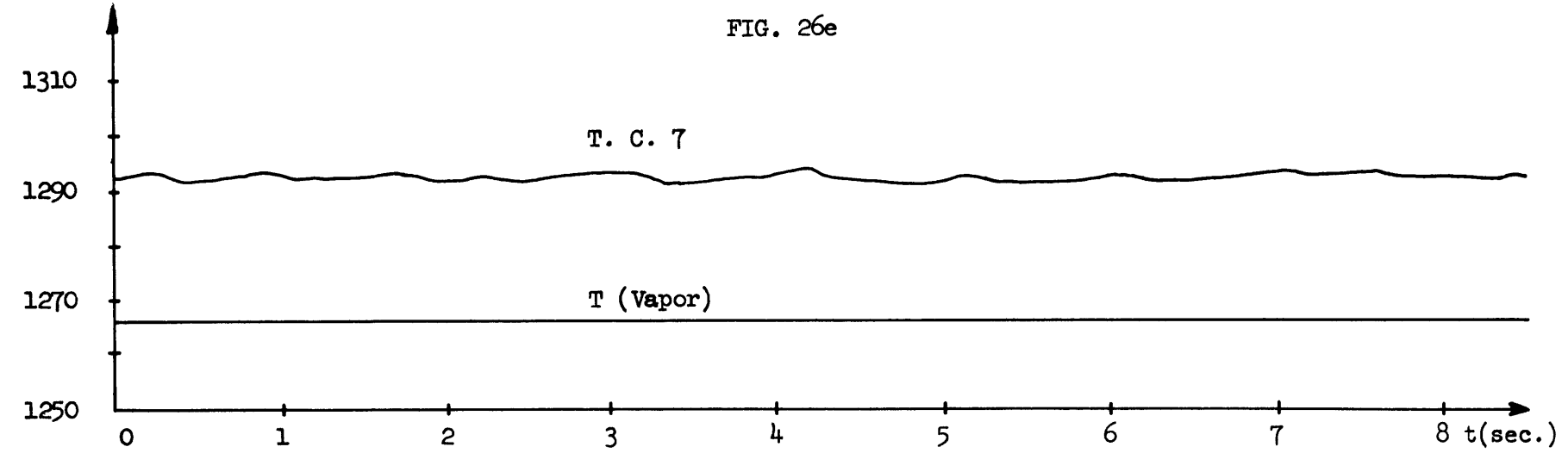

FIG. 26d

TRACES OF TEMPERATURE VARIATION DURING STABLE BOILING

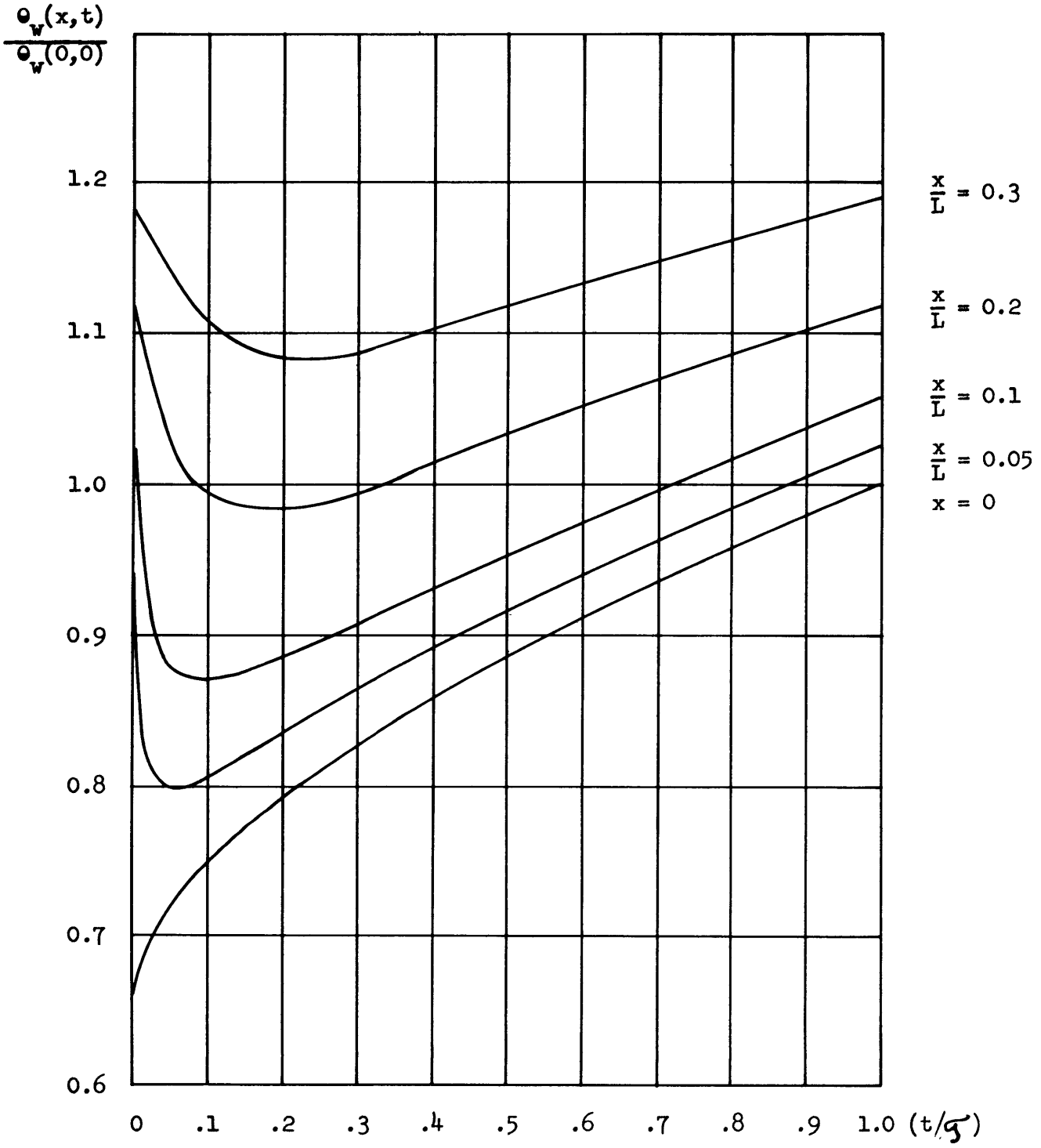

FIG. 27: TEMPERATURE VARIATIONS IN THE SOLID AS FUNCTION OF TIME (WITH THE POSITION AS A PARAMETER)

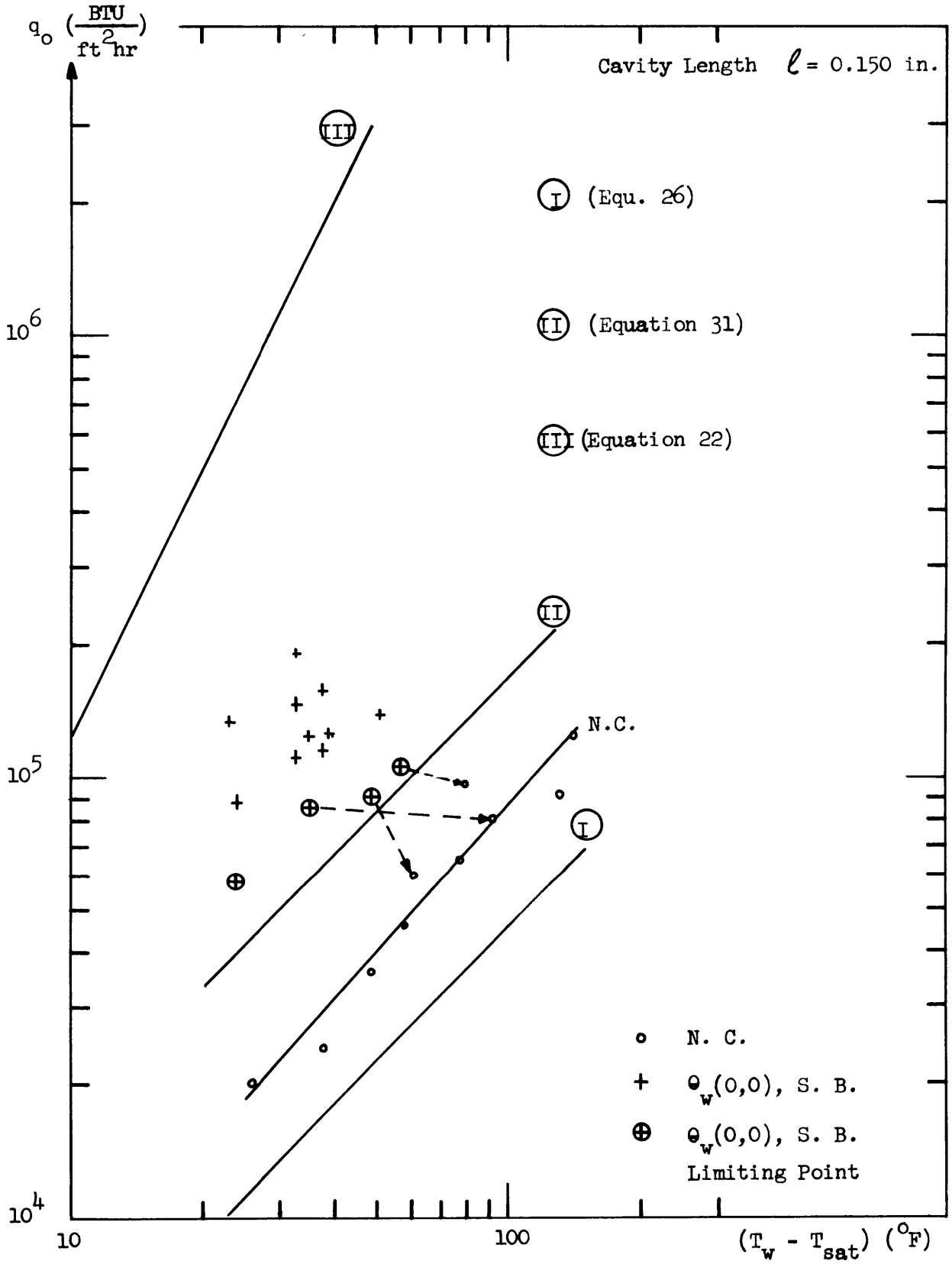

FIG. 28: MINIMUM HEAT FLUXES FOR STABLE BOILING

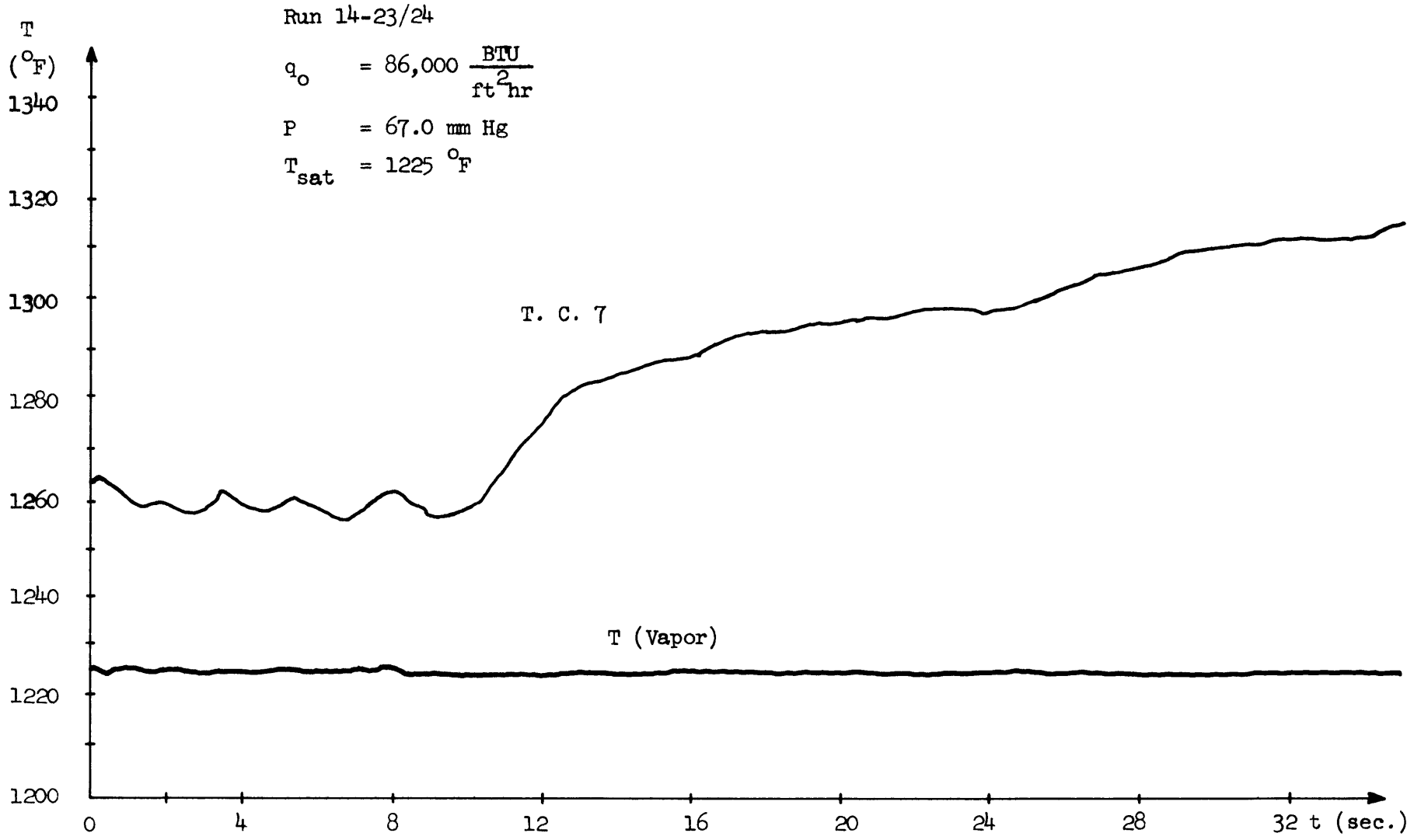

FIG. 29: TRANSITION FROM STABLE BOILING TO NATURAL CONVECTION

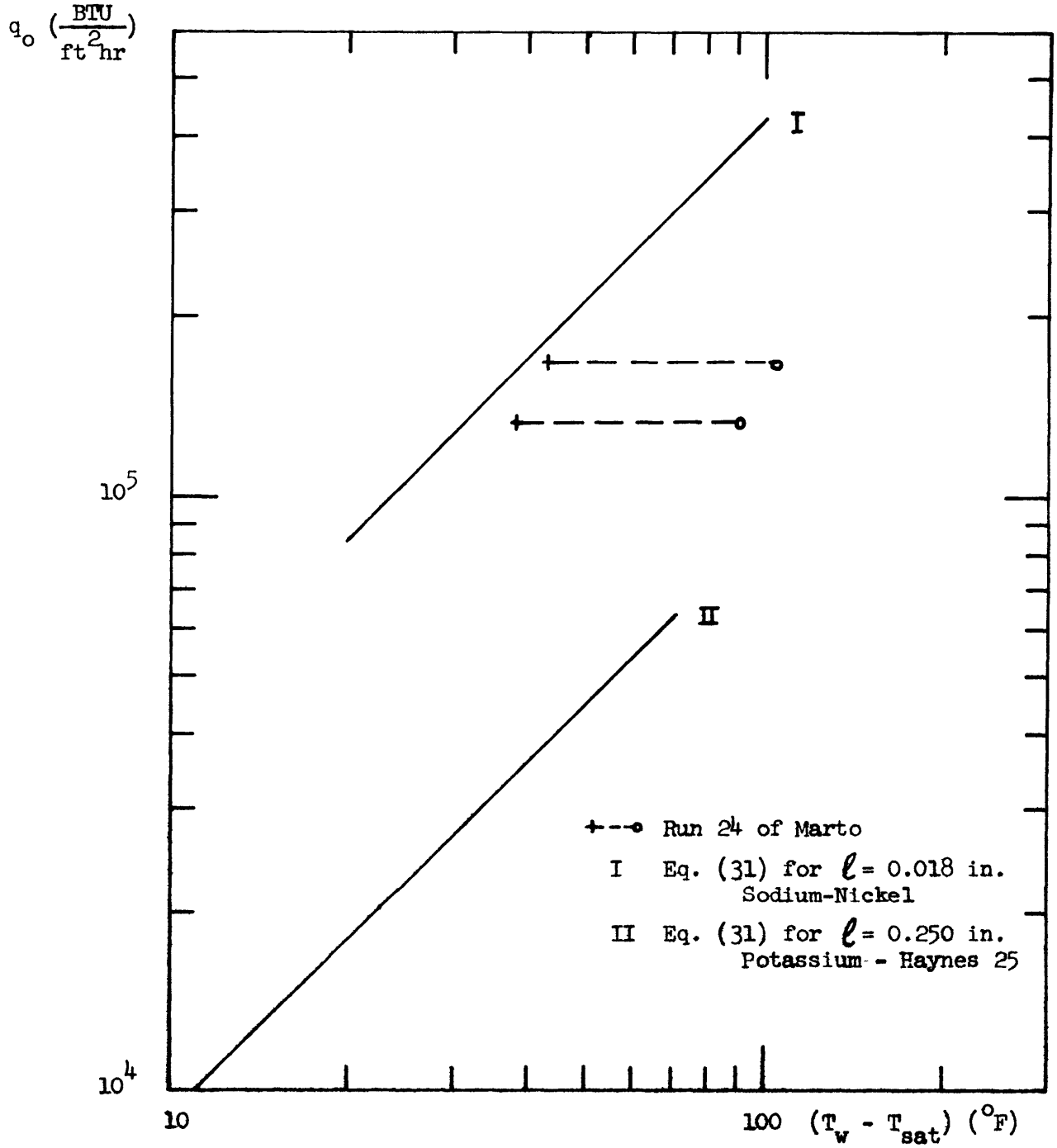

FIG. 30: MINIMUM HEAT FLUXES FOR STABLE BOILING FOR THE CASES OF MARTO (5) AND HOFFMAN (18)

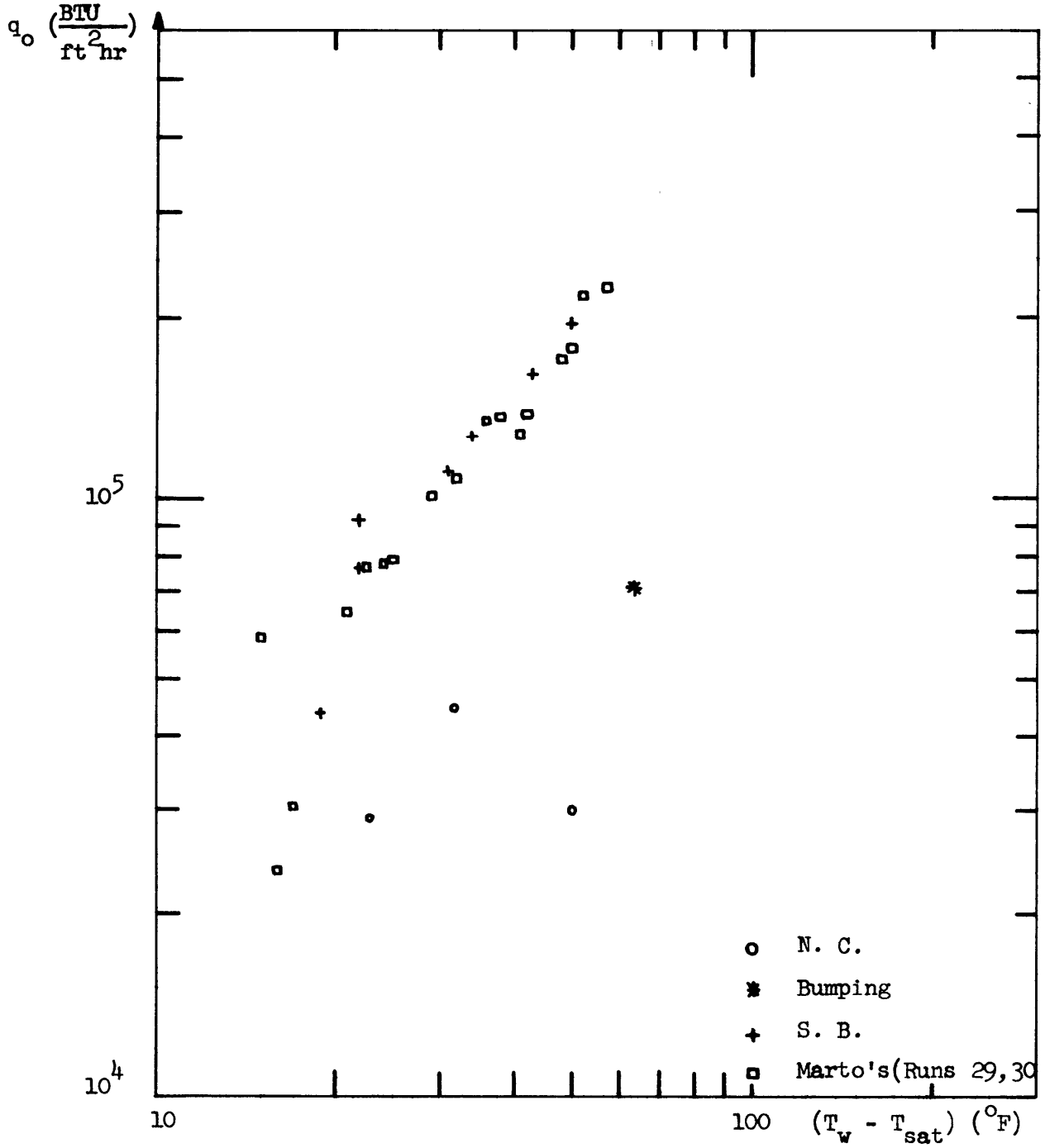

FIG. 31: RUN NO. 1

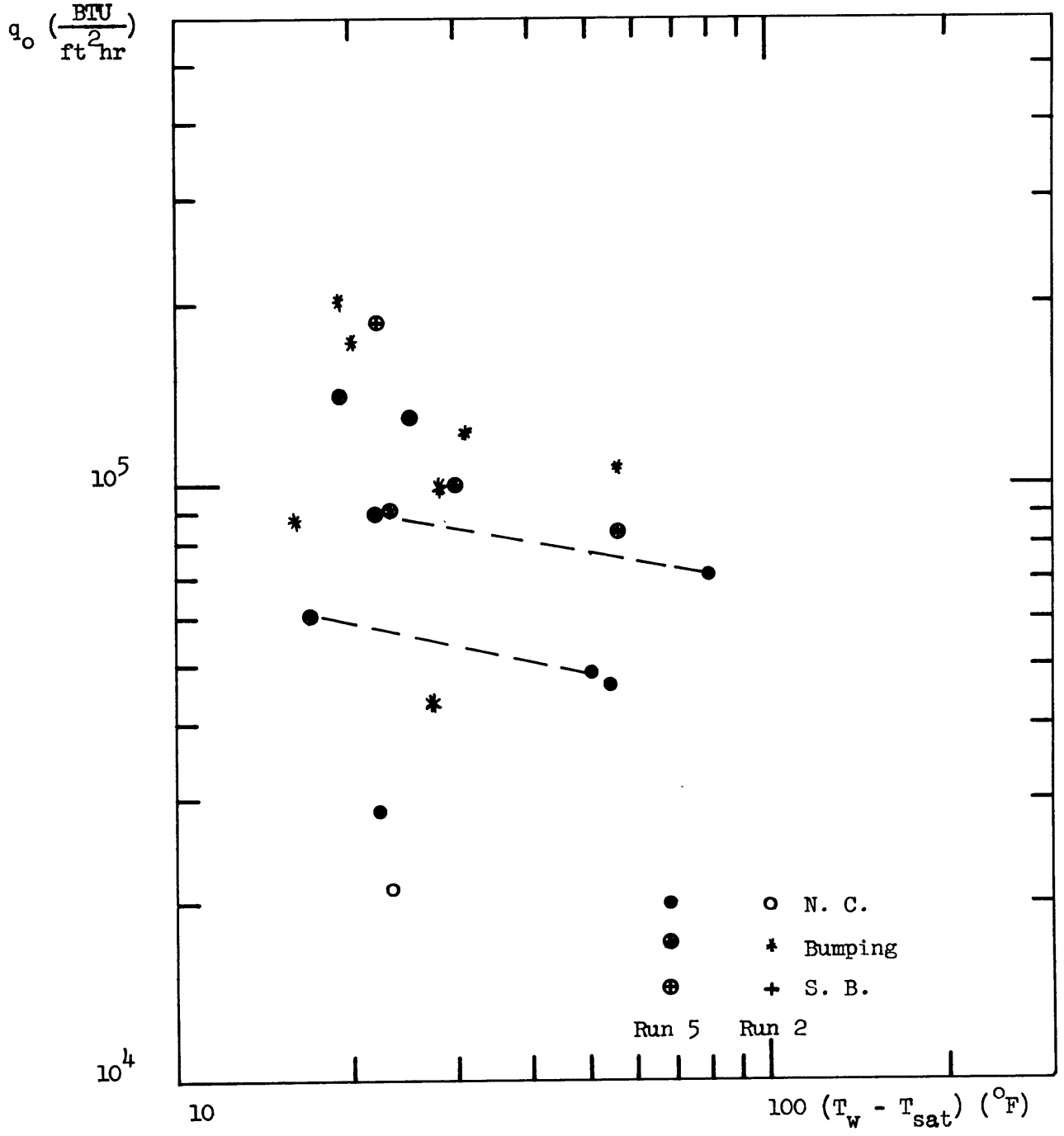

FIG. 32: RUNS NO. 2 AND 5

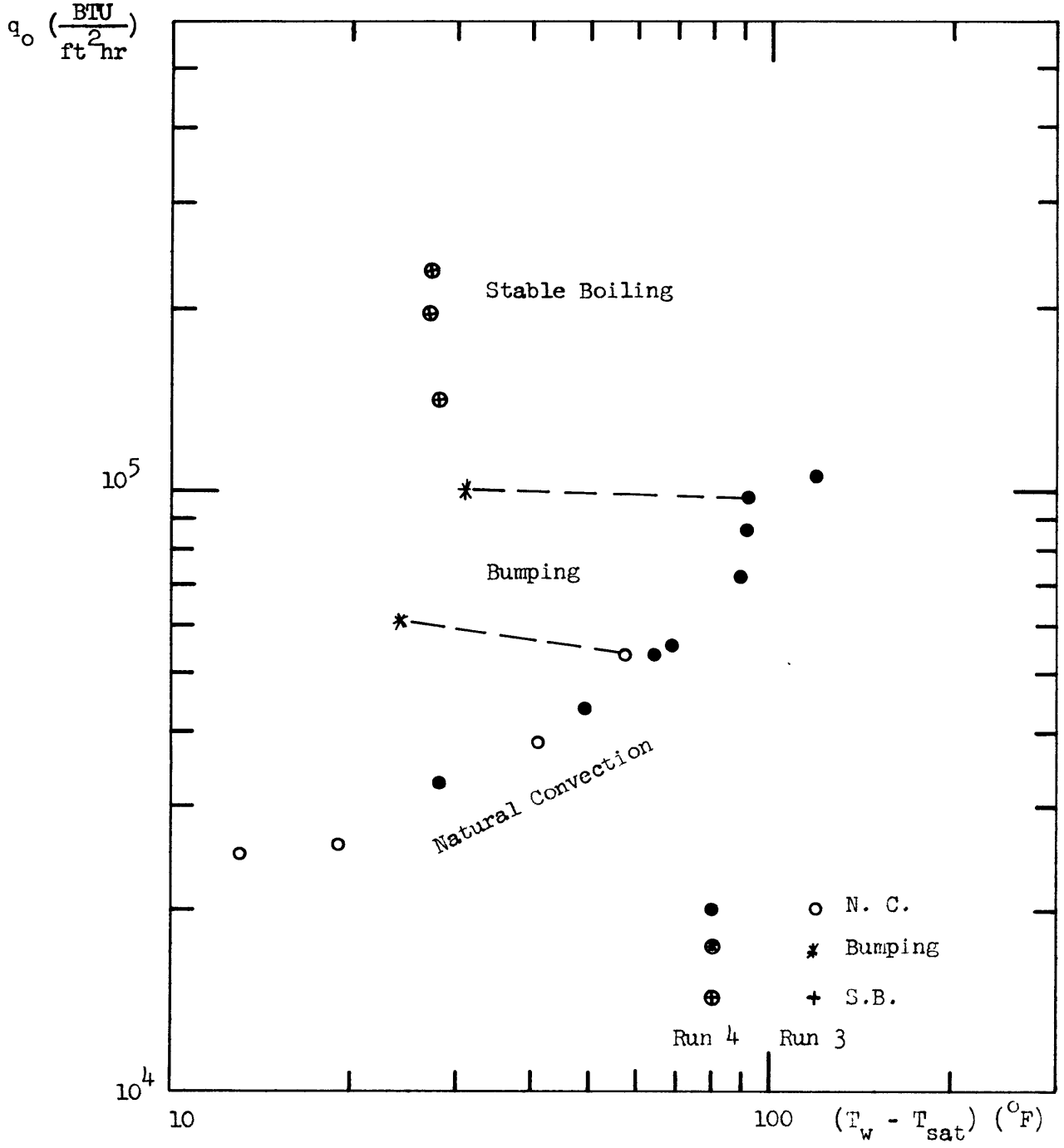

FIG. 33: RUNS NO. 3 AND 4

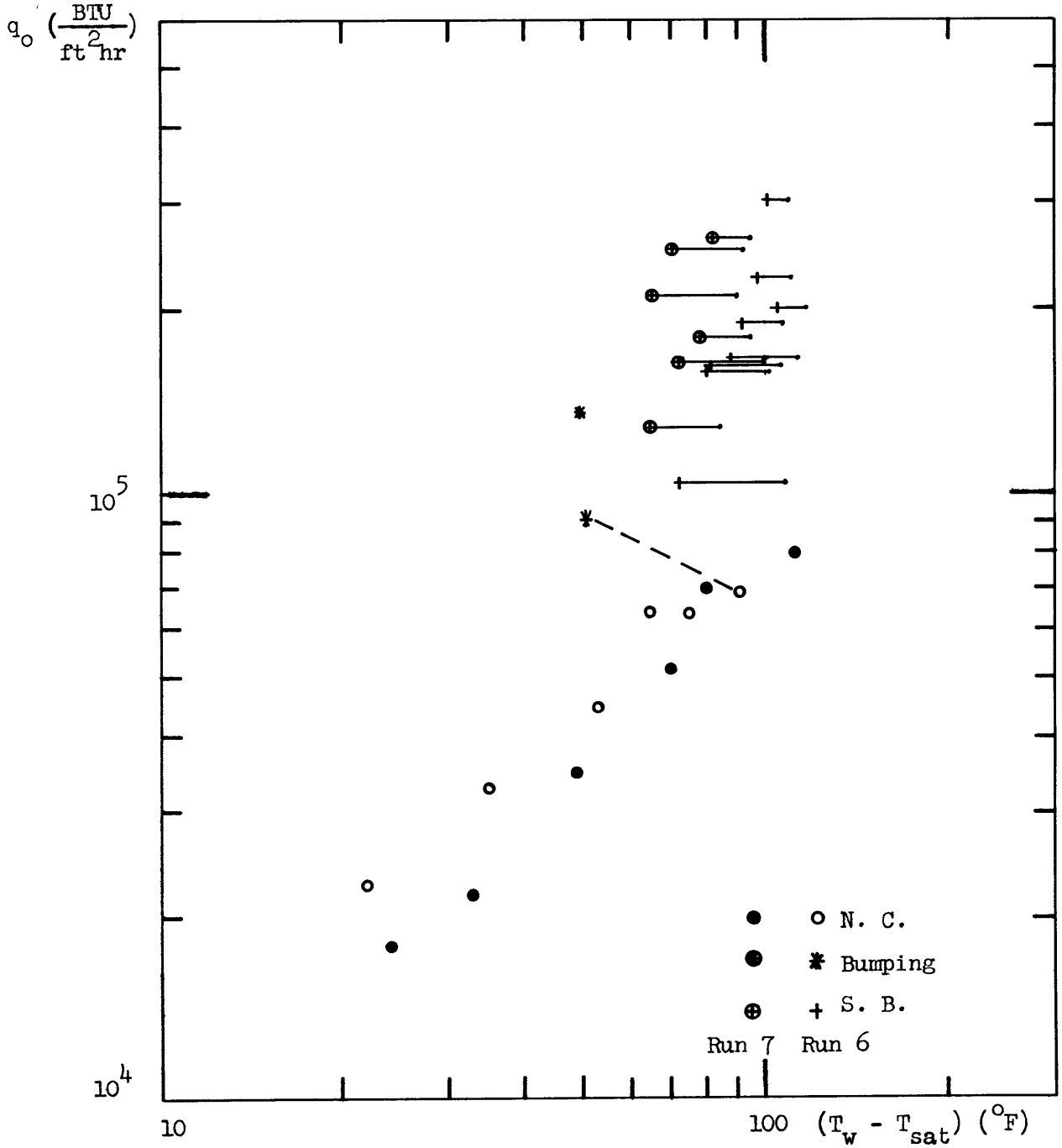

FIG. 34: RUNS NO. 6 AND 7

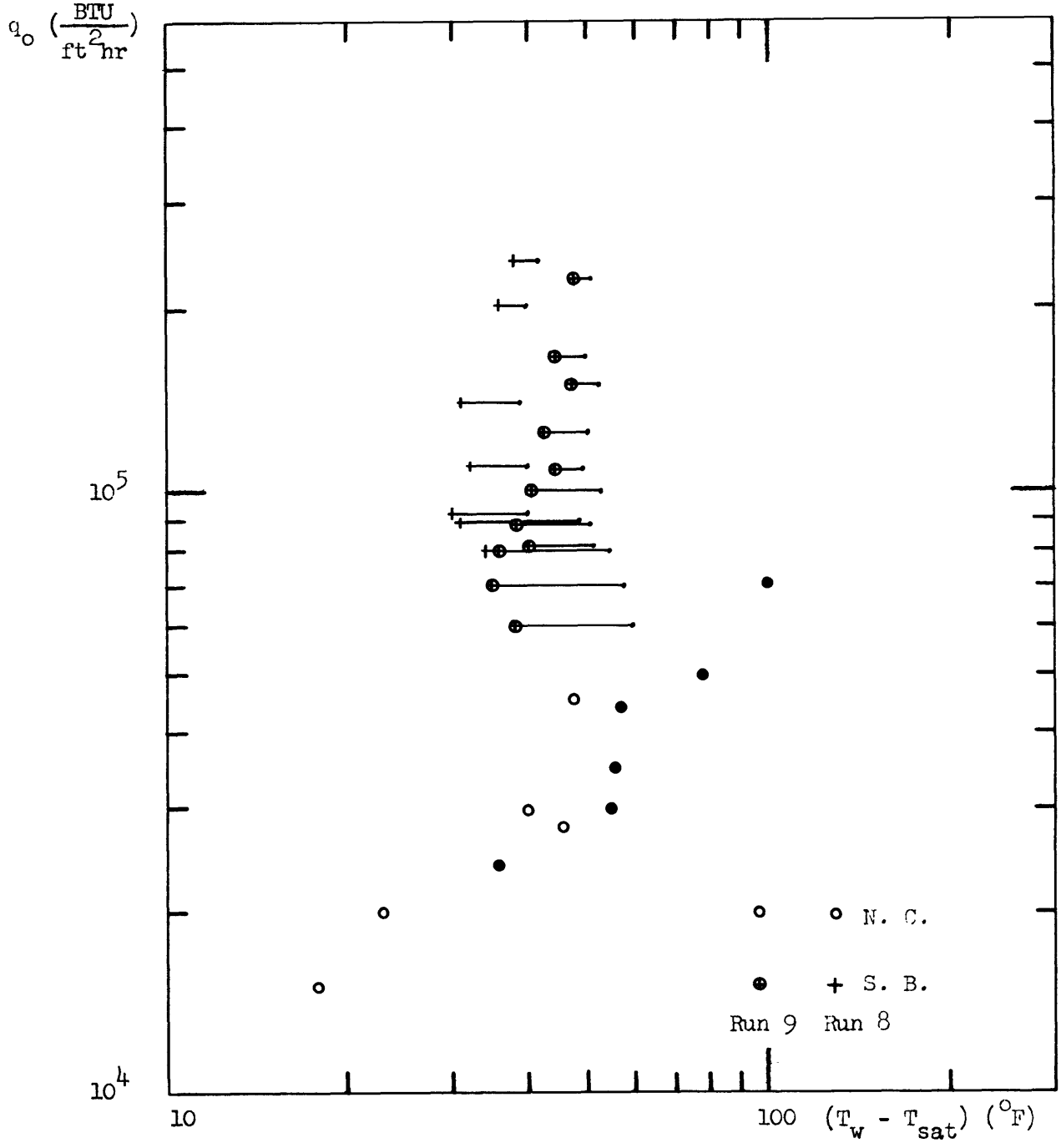

FIG. 35: RUNS NO. 8 AND 9

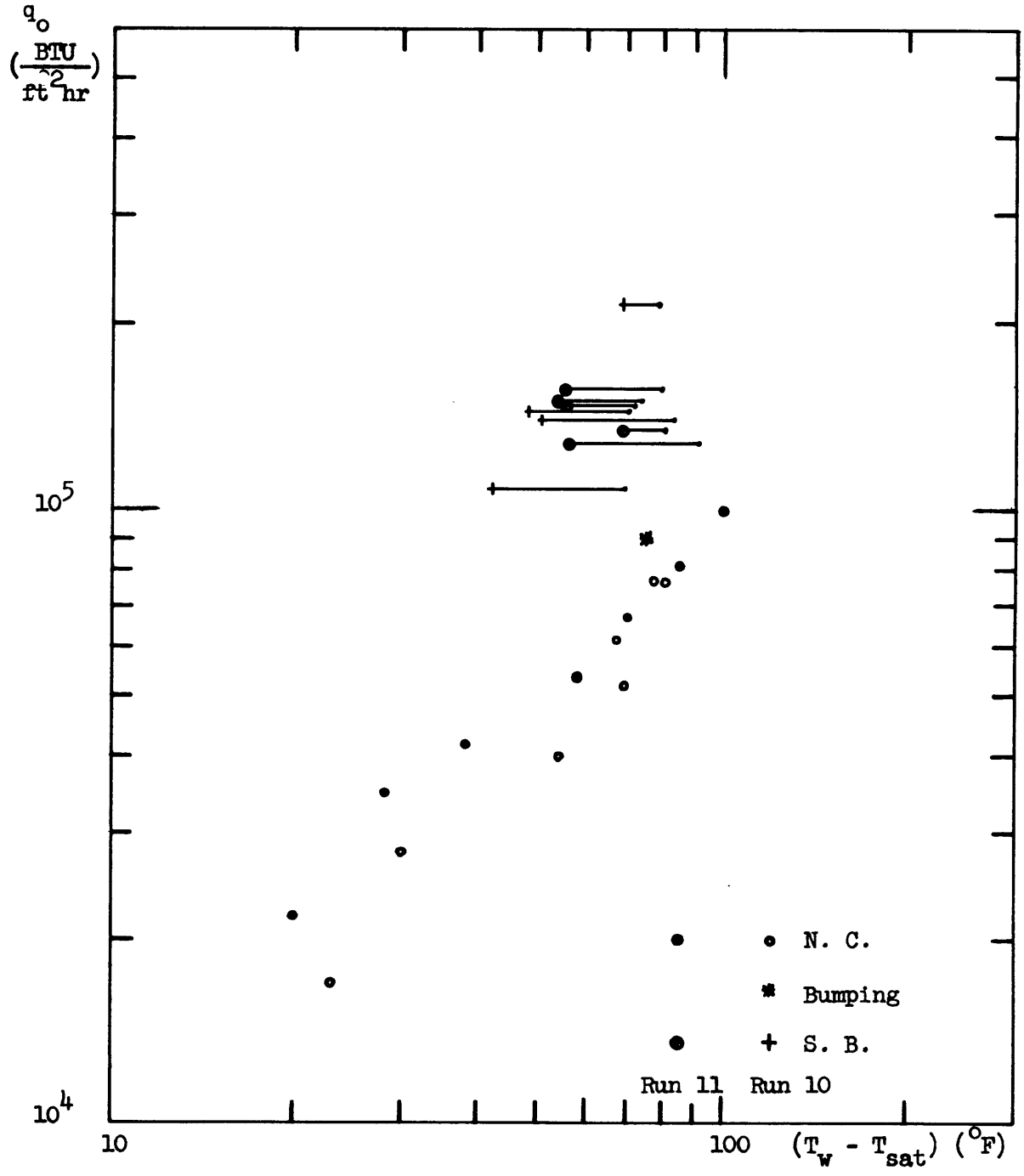

FIG. 36: RUNS NO. 10 AND 11

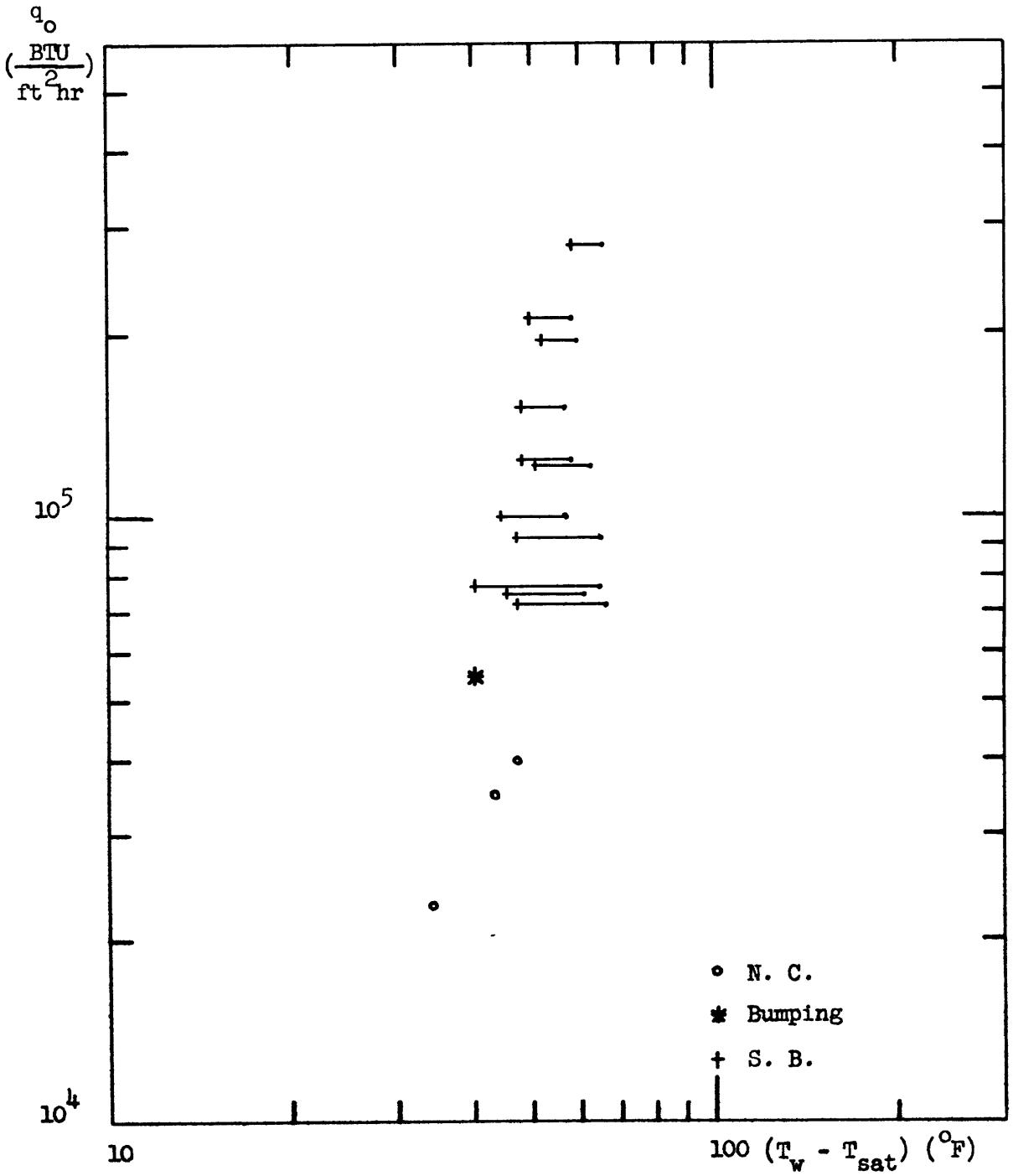

FIG. 37: RUN NO. 12

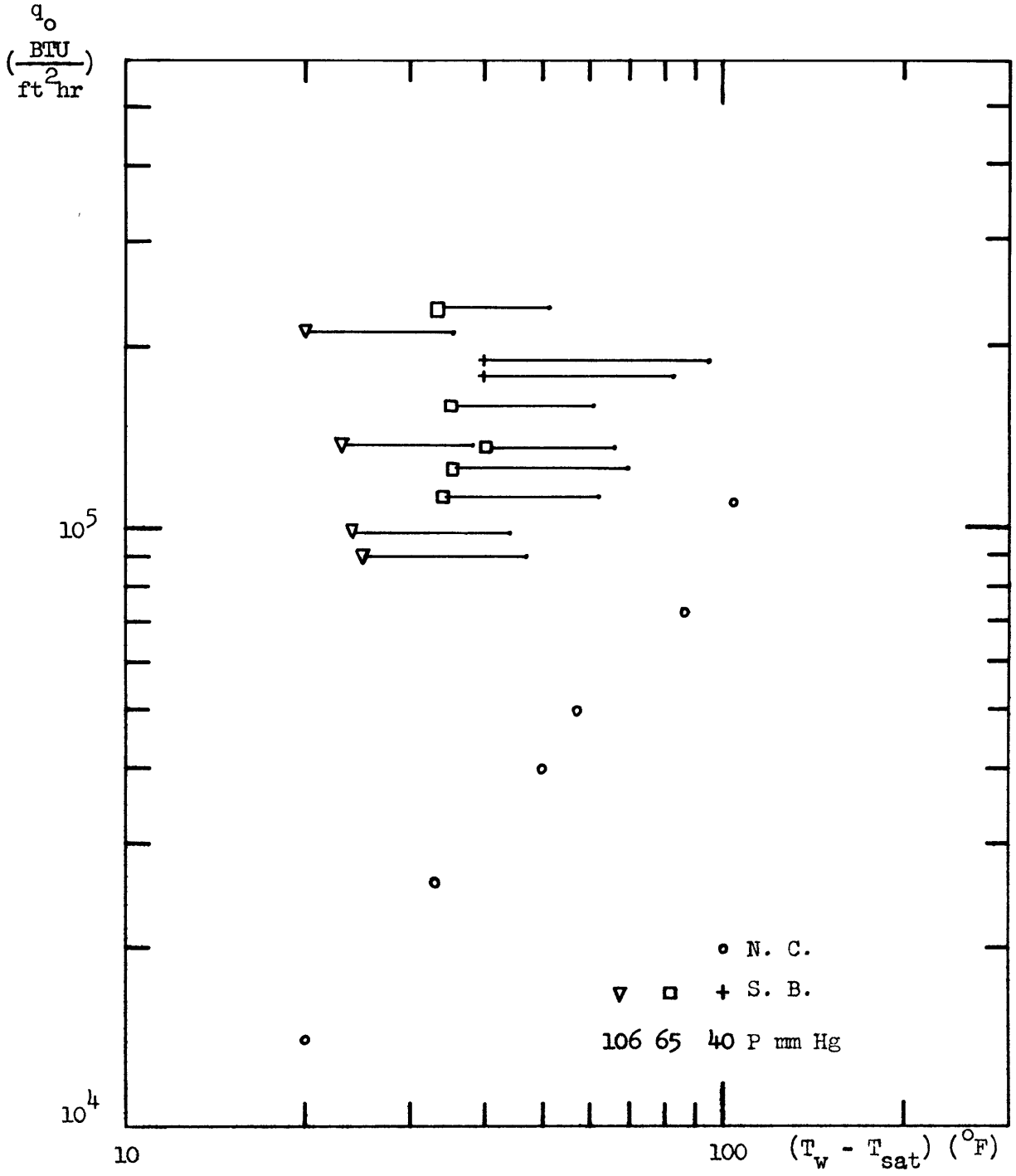

FIG. 38: RUN NO. 13

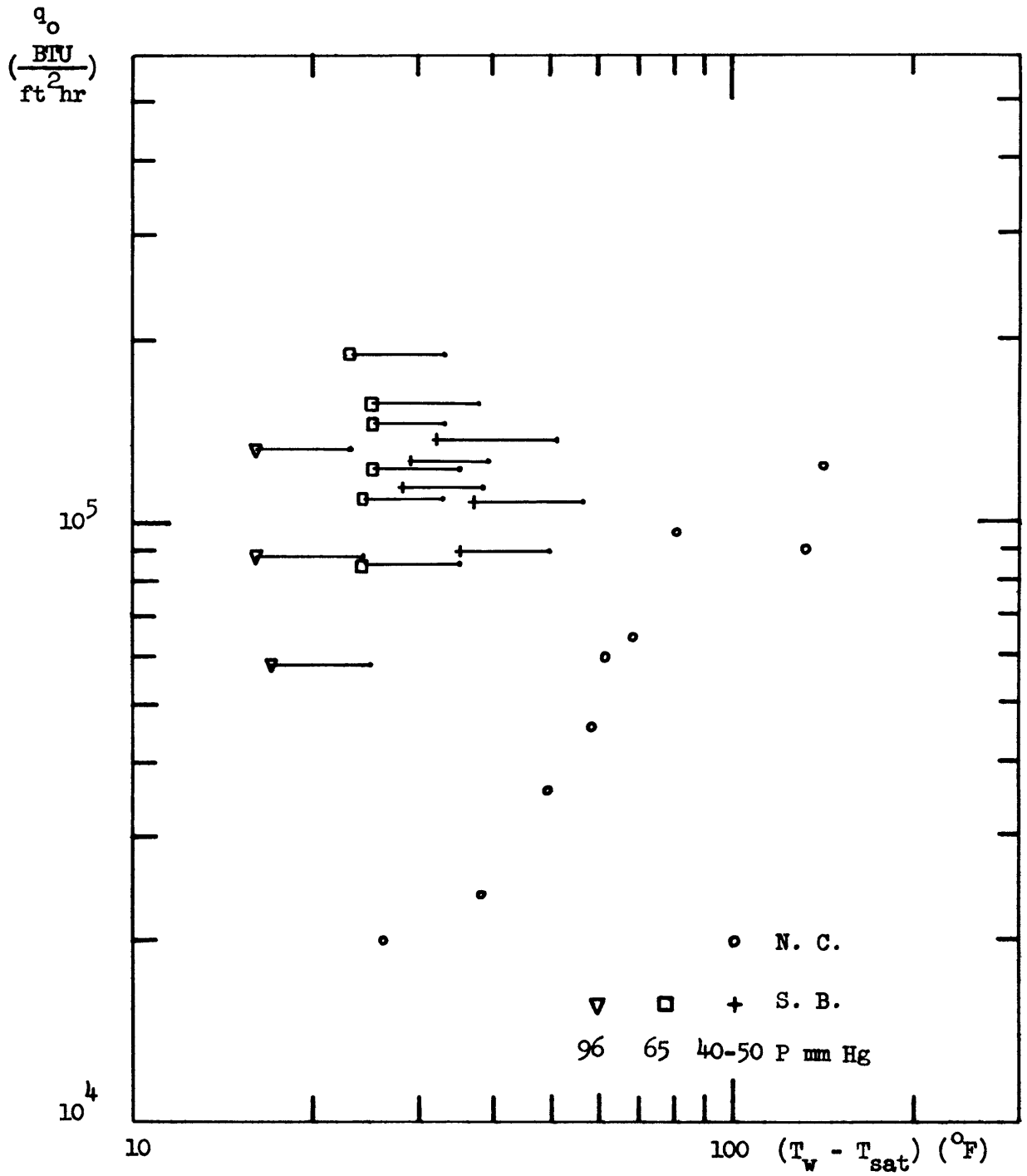

FIG. 39: RUN NO. 14

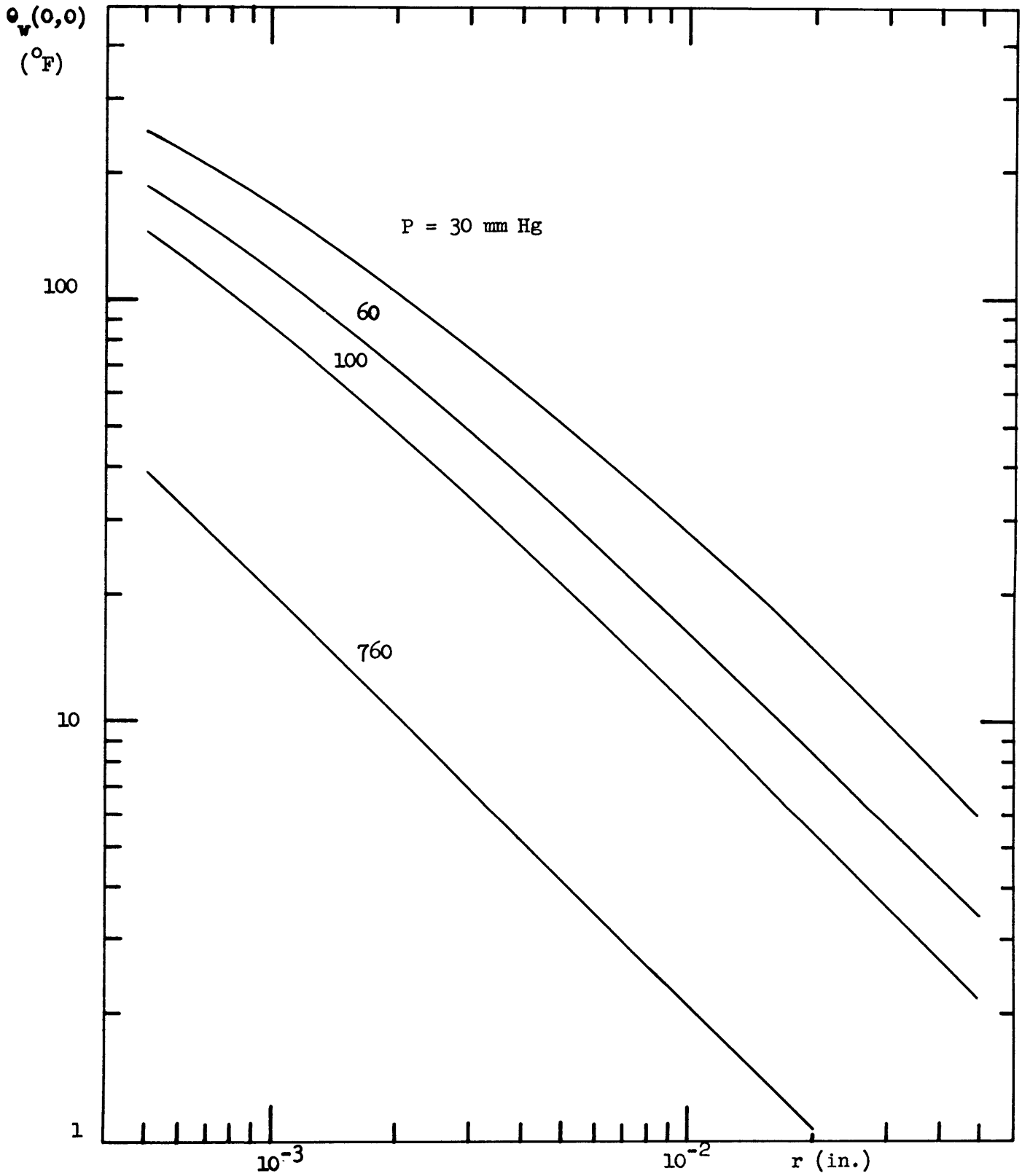

FIG. 40: SUPERHEAT IN LIQUID SODIUM

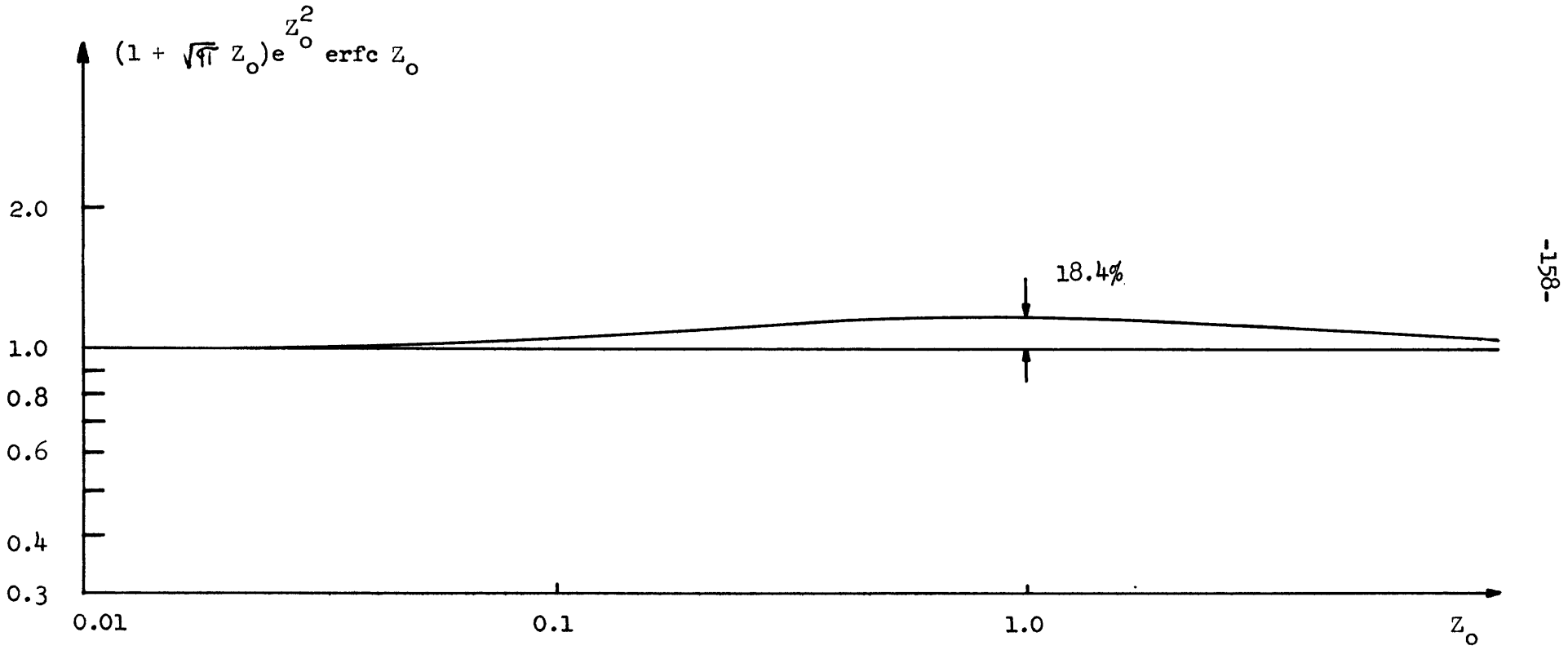

FIG. 41: THE APPROXIMATED EQUATION (E-10)

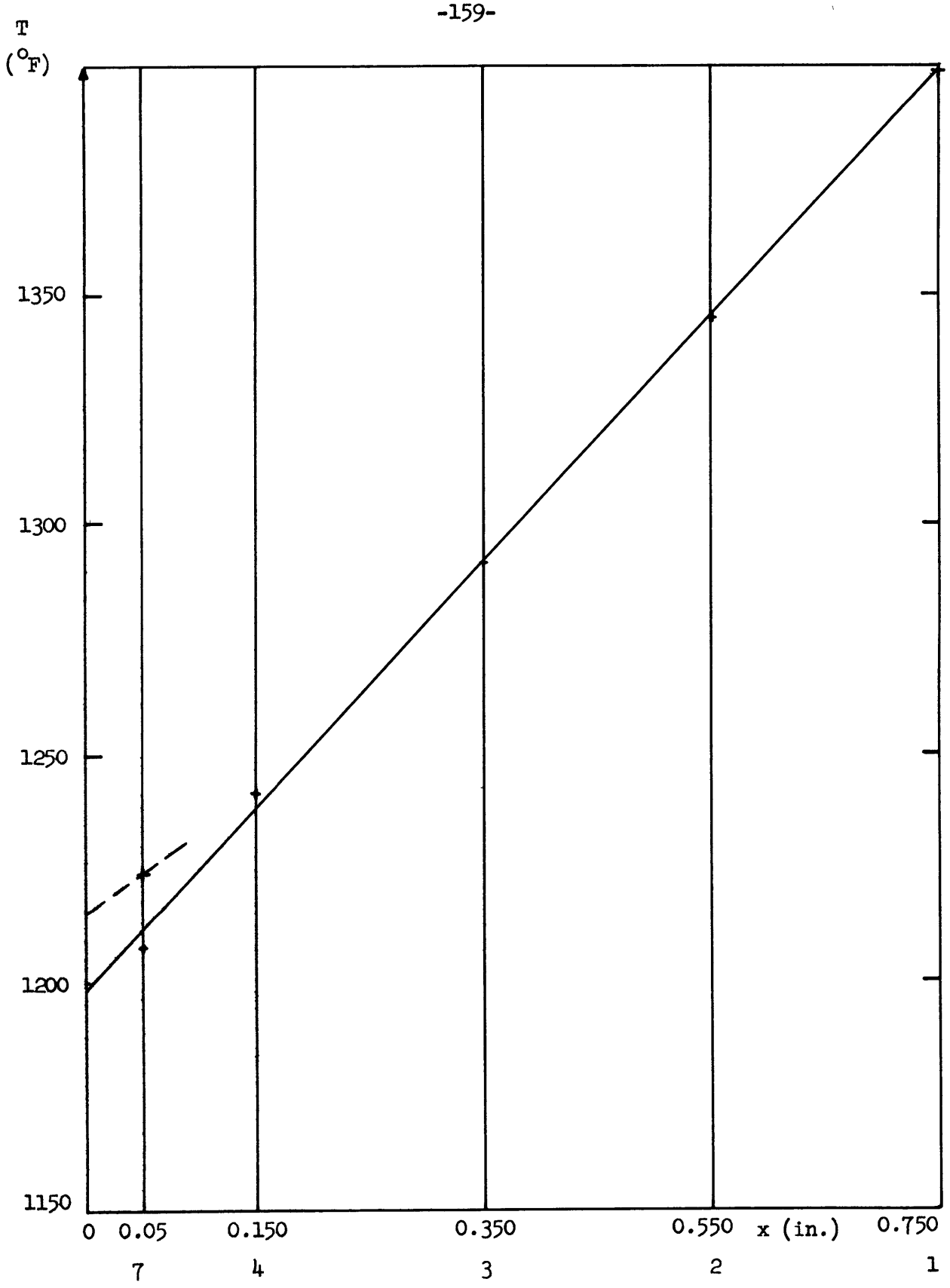

FIG. 42: CALICULATED EXAMPLE FOR REDUCING DATA